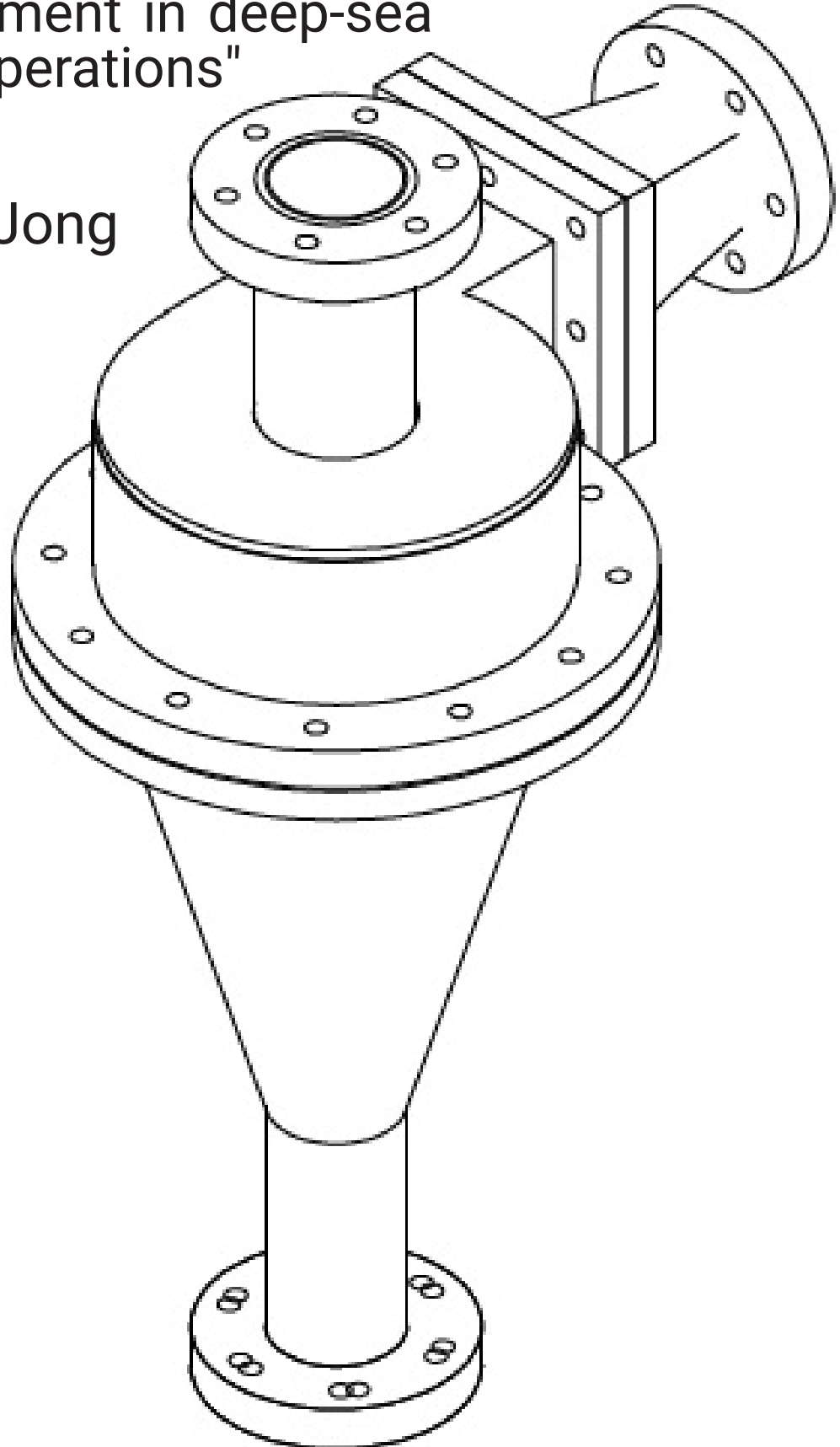


"Hydrocyclone separation of polymetallic nodules from surrounding water and sediment in deep-sea mining operations"

Thesis  
B.M. de Jong



# "Hydrocyclone separation of polymetallic nodules from surrounding water and sediment in deep-sea mining operations"

## Thesis

by

**B.M. de Jong**

to obtain the degree of Master of Offshore & Dredging Engineering  
at the Delft University of Technology,

Student number: 4263820  
Project duration: April 7, 2020 – July 5, 2021  
Thesis committee: Dr. ir. S.A. Miedema TU Delft, chair of committee  
Dr. ir. R.L.J. Helmons, TU Delft, supervisor  
Dr. ir. M.J. Mohajeri, TU Delft, committee member

# Preface

This report is the final deliverable of my graduation project in order to obtain my Offshore & Dredging master's degree, at the Delft University of Technology. Dr. ir. Rudy Helmons, prof. dr. ir Cees van Rhee, dr. ir. M.J. Mohajeri and Dr. ir. Sape Miedema from Delft University of Technology supervised the execution of this project.

*B.M. de Jong*  
*Delft, July 5, 2021*

# Abstract

Growing populations, high-technology applications and the energy transition raise the demand for rare earth elements. As a secure supply in the future is all but certain, opportunities arise for deep-sea mining. Polymetallic nodules that are located on the vast, sediment-covered ocean floors, are one of the more promising deep-sea mineral occurrences. Large amounts of unwanted surrounding water and sediment are collected along with the nodules in the harvesting process. Separating the sediment and excessive water from the nodules before transportation toward the surface could mitigate sediment plumes and be beneficial for energy consumption. In this research, the feasibility of a hydrocyclone inspired machine is investigated for this process. With model experimentation, the key performance parameters are studied using varying particle fractions, adjusting split ratio and conical angle. Timescale ratios are used for particle scaling, and to describe their behaviour. The cyclones' separation shows great potential. However, large particles can be problematic, and the energy consumption is too high for deep-sea operation. Therefore, topside utilisation is recommended.

Keywords: Polymetallic nodules, separation, hydrocyclone, performance parameters, topside.

# Contents

Abstract	ii
List of Figures	v
List of Tables	vii
1 Introduction	1
1.1 Background	1
1.2 Deep-sea mining	2
1.2.1 Regulation	2
1.2.2 Onshore vs offshore mining	3
1.2.3 Deposit compositions	3
1.3 Mining process	5
1.4 Problem statement	8
1.5 Research objective	8
2 Material properties	9
2.1 Polymetallic nodule data	9
2.1.1 Nodule characteristics	9
2.1.2 Sediment	10
2.1.3 Flow overview	11
3 State of the art hydrocyclone	14
3.1 Requirements separation methods & equipment	14
3.1.1 Restrictions	14
3.1.2 Preferences	14
3.2 Separation methods	15
3.3 Hydrocyclones	16
3.3.1 Components	16
3.3.2 Separation principles	17
3.3.3 Key performance parameters	18
3.4 Optimal geometry cyclone	19
4 Cyclone design	25
4.1 Conical angle	25
4.2 Design determination	27
4.2.1 Geometric dimensions	27
4.2.2 Alternative angle	28
4.3 Flow and particle behaviour	29
4.3.1 Mixture viscosity	29
4.3.2 Turbulence	30
4.3.3 Particle behaviour	30
4.3.4 Particle response	31
5 Experimental setup	35
5.1 Setup	35
5.2 Hydrocyclone separator	39
5.3 Particles	41
5.4 Experimental protocol	41
6 Experiments	42
6.1 Parameters	42
6.1.1 Particle diameter	42
6.1.2 Split ratio	42
6.1.3 Conical angle	42
6.1.4 Flow rate	43
6.1.5 Experimental matrix	43

6.2	Experimental observations . . . . .	44
6.2.1	Original model . . . . .	44
6.2.2	Partition curves original model . . . . .	47
6.2.3	Large angled model . . . . .	48
6.2.4	Partition curves large angled model . . . . .	51
7	Analysis . . . . .	52
7.1	Predicted performance . . . . .	52
7.1.1	Cut size . . . . .	52
7.1.2	Separation sharpness . . . . .	53
7.1.3	Bypass . . . . .	53
7.1.4	Split ratio . . . . .	54
7.2	Particle scaling . . . . .	54
7.2.1	Scaling $Stk$ . . . . .	55
7.2.2	Scaling $r$ . . . . .	55
7.2.3	Implementing scaling principles . . . . .	57
7.3	Performance . . . . .	58
7.3.1	Partition curve prototype cyclone . . . . .	58
7.3.2	Split ratio . . . . .	60
7.3.3	Capacity . . . . .	60
7.3.4	Energy consumption . . . . .	60
7.4	Conical angle . . . . .	61
8	Discussion . . . . .	62
8.1	Discussion . . . . .	62
8.2	Alternative use case . . . . .	63
9	Conclusion & Recommendations . . . . .	64
9.1	Conclusion . . . . .	64
9.2	Recommendations . . . . .	65
9.2.1	Theory . . . . .	65
9.2.2	Setup . . . . .	65
9.2.3	Experiments . . . . .	66
9.2.4	Future research . . . . .	66
	Bibliography . . . . .	67
A	Setup components . . . . .	70
A.1	Suggested bypass . . . . .	90
B	Particle tests . . . . .	91
B.1	Separation into compact fractions . . . . .	91
B.2	Density tests . . . . .	92
B.3	Settling tests . . . . .	93
B.4	Particles properties . . . . .	93
C	Operational protocol . . . . .	94
C.1	Preparation . . . . .	94
C.2	Operatation . . . . .	94
C.2.1	Large particles . . . . .	94
C.2.2	Small particles . . . . .	95
C.3	After operation . . . . .	95
C.3.1	Other occurrences . . . . .	95
C.4	Measurement protocol . . . . .	96

# List of Figures

1.1	Countries accounting for largest share of EU supply of CRM [8]	1
1.2	Critical Minerals: Global Production (2017) [10]	2
1.3	A world map showing the locations of the three main marine mineral deposits: polymetallic nodules (blue); polymetallic or seafloor massive sulfides (orange); cobalt-rich ferromanganese crusts (yellow); and including exclusive economic zones (white) [32]	3
1.4	Sulphide deposit [53]	4
1.5	Ferromanganese crust [53]	4
1.6	Nodule deposit [53]	5
1.7	Schematic overview of main deep-sea mining processes [53]	6
1.8	Schematic process flow. [27]	6
2.1	Schematic presentation of the nodule dimensions [27]	9
2.2	Nodule cumulative mass distribution [27]	10
2.3	Sediment particle size distribution of the GSR samples [27]	11
2.4	Relative settling velocity for a bi-modal mixture of particles [54]	12
3.1	Broad classification chart showing the forms of solid-liquid separators [51]	15
3.2	Particle size and concentration as guides in the selection of solid-liquid separation equipment [49]	16
3.3	Hydrocyclone	17
3.4	centrifugal sizing hydrocyclone. [31]	18
3.5	Partition curve hydrocyclone. [40]	18
3.6	5 inlet shapes [6]	20
3.7	Two cone combination [64]	22
3.8	5 Conical shapes [6]	22
3.9	Vortex-finder structures tested by Chu et al. [6]	24
4.1	Particle-wall interaction	25
4.2	Angles $\alpha$ and $\theta$	26
4.3	Hydrocyclone dimensions	28
4.4	Dimensions hydrocyclone with larger conical angle	29
4.5	Mixture viscosity [18]	29
4.6	Particle behaviour	33
4.7	Particle predicted response	33
5.1	Side view of the experimental setup	36
5.2	Top view of the experimental setup	36
5.3	Schematic design of a measuring container	38
5.4	Model dimensions	40
5.5	Topside dimensions	40
5.6	Assembled cyclone dimensions	40
6.1	Original cyclone separation of 8-12 mm particles	44
6.2	Original cyclone separation of 0.5-0.7 mm particles	45
6.3	Original cyclone separation 65-105 $\mu\text{m}$ particles	45
6.4	Original cyclone separation of 40-70 $\mu\text{m}$ particles	46
6.5	Partition curve original model with open underflow and low concentration	47
6.6	Partition curve original model with closed underflow and low concentration	47
6.7	Large angled cyclone separation of 8-12 mm particles	48
6.8	Large angled cyclone separation of 0.5-0.7 mm particles	49
6.9	Large angled cyclone separation of 65-105 $\mu\text{m}$ particles	49
6.10	Large angled cyclone separation of 40-70 $\mu\text{m}$ particles	50
6.11	Partition curve large angled cyclone with open underflow and low concentration	51
6.12	Partition curve large angled cyclone with closed underflow and low concentration	51

7.1	Ideal performance curves when sharpness of separation is neglected . . . . .	53
7.2	Sharpness curve . . . . .	53
7.3	Predicted 'actual' partition curves . . . . .	54
7.4	Scaling particle diameter from model to equivalent prototype diameter . . . . .	57
7.5	Alternative timescale curve . . . . .	59
7.6	Model & prototype partition curves . . . . .	60
A.1	Side view of setup in laboratory . . . . .	71
A.2	Side view of the experimental setup . . . . .	72
A.3	Top view of the experimental setup . . . . .	72
A.4	Topside of the centrifugal pump . . . . .	73
A.5	Centrifugal pump . . . . .	73
A.6	Frequency converter to control pump RPM . . . . .	74
A.7	Empty conveyor belt in position . . . . .	75
A.8	Partly filled conveyor belt in position . . . . .	75
A.9	Hopper used for guiding particles into stream . . . . .	76
A.10	Schematic design cyclone topside . . . . .	77
A.11	Schematic design conical section . . . . .	77
A.12	3D illustration conical section . . . . .	78
A.13	Schematic design of Large angle conical section . . . . .	78
A.14	Picture cone with large angle . . . . .	79
A.15	Schematic design assembled cyclone . . . . .	79
A.16	3D illustration assembled cyclone . . . . .	80
A.17	Pictures assembled cyclone . . . . .	80
A.18	Schematic design assembled large angle cyclone . . . . .	81
A.19	3D illustration of assembled cyclone with large conical angle . . . . .	81
A.20	Installed cyclone . . . . .	82
A.21	3D printed inlet transition piece design . . . . .	82
A.22	Photo's 3D printed transition piece for underflow to pipe . . . . .	83
A.23	3D printed underflow to pipe transition piece . . . . .	83
A.24	Photo's 3D printed inlet transition piece . . . . .	84
A.25	Empty settling tank . . . . .	85
A.26	Operating settling tank . . . . .	85
A.27	Large measuring tank . . . . .	86
A.28	Small measuring tank . . . . .	86
A.29	Valves used for altering split ratio of the cyclone. . . . .	87
A.30	Flow meter attached to underflow . . . . .	87
A.31	Flow meter attached to the inflow . . . . .	87
A.32	Scale used for mass partition measurements . . . . .	88
A.33	Drill used for mixing suspension . . . . .	88
A.34	Light panel used to illuminate the cyclone . . . . .	89
A.35	Ball valves . . . . .	89
A.36	Suggested redirected flow . . . . .	90
B.1	Particle sorting device . . . . .	91
B.2	Sorted particle fractions . . . . .	92
B.3	Sand used for density tests . . . . .	92
B.4	Scale used density tests . . . . .	92
B.5	Tank and timer used for settling tests . . . . .	93

# List of Tables

2.1	Nodule characteristics [27]	10
2.2	Sediment fractions [27]	11
2.3	GSR sediment characteristics [27]	11
2.4	Hydraulic collection characteristics [27]	12
2.5	Concentrations particles hydraulic collection [27]	12
2.6	Abbreviations equivalent liquid model	13
3.1	Hydrocyclone geometric symbols	17
3.2	Other geometric parameters capable of optimizing separation	24
4.1	Hydrocyclone dimensions & parameters	28
4.2	Hydrocyclone dimensions & parameters	29
4.3	Particle Reynolds numbers per fraction	31
4.4	Stk, r & $Re_p$ values per particle	34
5.1	Setup components	35
5.2	Particle properties and timescale ratios	41
6.1	Particle properties and timescale ratios selected for research	42
6.2	Experimental matrix	43
6.3	Parameters of original cyclone separation of 8-12 mm particles	44
6.4	Parameters of original cyclone separation of 0.5-0.7 mm particles	45
6.5	Parameters of original cyclone separation of 65-105 $\mu\text{m}$ particles	46
6.6	Parameters of original cyclone separation of 40-70 $\mu\text{m}$ particles	46
6.7	Original cyclone with closed underflow partition curve parameters	47
6.8	Original cyclone with closed underflow partition curve parameters	47
6.9	Parameters of large angled cyclone separation of 8-12 mm particles	48
6.10	Parameters of large angled cyclone separation of 0.5-0.7 mm particles	49
6.11	Parameters of large angled cyclone separation of 65-105 $\mu\text{m}$ particles	50
6.12	Parameters of large angled cyclone separation of 40-70 $\mu\text{m}$ particles	50
6.13	Large angled cyclone with open underflow partition curve parameters	51
6.14	Large angled cyclone with closed underflow partition curve parameters	51
7.1	Expected flows and velocities	54
7.2	Terminal settling velocities different fractions	54
7.3	r scaling units	56
7.4	r scaling values	57
7.5	Corresponding particle diameters	58
B.1	Particle properties and timescale ratios from sorted particles	93

# Nomenclature

## List of Abbreviations

<b>CCZ</b>	Clarion-Clipperton Zone
<b>CFC</b>	Cobalt-rich ferromanganese crusts
<b>CRC</b>	Cobalt-rich crusts
<b>CRM</b>	Critical raw materials
<b>DMD</b>	Deep-sea minerals deposits
<b>DRC</b>	Democratic Republic of Congo
<b>EEZ</b>	Exclusive economic zone
<b>EU</b>	European Union
<b>GSR</b>	Global Sea Mineral Resources (Belgian Company)
<b>ISA</b>	International Seabed Authority
<b>nmi</b>	Nautical miles
<b>NTNU</b>	Norwegian University of Science and Technology
<b>PMN</b>	Polymetallic manganese nodule
<b>PSD</b>	Particle size distribution
<b>PSV</b>	Production support vessel
<b>REE</b>	Rare earth elements
<b>SMS</b>	Seafloor massive sulphides
<b>SPTs</b>	Seafloor production tools
<b>SWOE</b>	Sediments, wastes, and other effluents
<b>UN</b>	United Nations
<b>USGS</b>	United States Geological Survey
<b>US</b>	United States of America
<b>VTS</b>	Vertical transport system

## List of Symbols

$\alpha_t$	Volume concentration of solids [-]
$\Delta$	Specific density[-]
$\Delta_m$	Specific density model[-]
$\Delta_p$	Specific density prototype[-]
$\eta$	Dynamic viscosity carrier fluid [ <i>Pa</i> s]
$\mu$	Original fluid dynamic viscosity [ <i>Pa</i> s]
$\mu_m$	Mixture dynamic viscosity [ <i>Pa</i> s]

$\mu_r$	Relative dynamic viscosity [-]
$\nu$	Kinematic viscosity [ $m^2/s$ ]
$\nu_m$	Kinematic viscosity model fluid [ $m^2/s$ ]
$\nu_p$	Kinematic viscosity prototype fluid [ $m^2/s$ ]
$\rho_f$	Fluid density [ $kg/m^3$ ]
$\rho_s$	Density solids [ $kg/m^3$ ]
$\rho_{dw}$	Density deep-sea water [ $kg/m^3$ ]
$\rho_{fm}$	Density model fluid [ $kg/m^3$ ]
$\rho_{fp}$	Density prototype fluid [ $kg/m^3$ ]
$\rho_{pm}$	Density model [ $kg/m^3$ ]
$\rho_{pp}$	Density prototype particles [ $kg/m^3$ ]
$\rho_{sw}$	Density sea water [ $kg/m^3$ ]
$\rho_w$	Density water [ $kg/m^3$ ]
$\tau_f$	Fluid response time [s]
$\tau_p$	Particle response time [s]
$\theta$	Conical angle cyclone [ $m$ ]
$a_c$	Centripetal acceleration [ $m/s^2$ ]
$a_{cm}$	Centripetal acceleration model [ $kg/m^3$ ]
$a_{cp}$	Centripetal acceleration prototype [ $kg/m^3$ ]
$A_p$	Surface of particle in flow direction [ $m^2$ ]
$A_u$	Apex surface area in flow direction [ $m^2$ ]
$A_{vf}$	Vortex-finder surface area in flow direction [ $m^2$ ]
$C_d$	Drag coefficient [-]
$c_m$	Mass concentration [-]
$c_v$	Volume concentration of solids [-]
$D_c$	Diameter cyclone [ $m$ ]
$D_i$	Inlet diameter [ $m$ ]
$D_o$	Vortex-finder diameter [ $m$ ]
$d_p$	Particle diameter [ $m$ ]
$D_u$	Apex diameter [ $m$ ]
$d_w$	Wet density [ $kg/m^3$ ]
$D_{10}$	Particle diameter where all smaller particles make up 10% of total mass [ $m$ ]
$D_{50}$	Particle diameter where all smaller particles make up 50% of total mass [ $m$ ]
$d_{50}$	Cutsizes [ $m$ ]
$D_{90}$	Particle diameter where all smaller particles make up 90% of total mass [ $m$ ]
$d_{pm}$	Particle diameter model [ $m$ ]
$d_{pp}$	Particle diameter prototype [ $m$ ]

$E$	Power [ $W$ ]
$F_B$	Buoyancy force [ $N$ ]
$F_c$	Centripetal force [ $N$ ]
$F_D$	Drag force [ $N$ ]
$F_g$	Gravitational force [ $N$ ]
$g$	Gravitational acceleration [ $m/s^2$ ]
$h_i$	Cyclone inlet height [ $m$ ]
$h_n$	Height nodule [ $m$ ]
$H_{barrier}$	Barrier height settling tank [ $m$ ]
$H_{inlet}$	Inlet height settling tank [ $m$ ]
$L$	Total length cyclone [ $m$ ]
$L_1$	Length cylindrical-section cyclone [ $m$ ]
$L_n$	Length nodule [ $m$ ]
$l_{vf}$	Vortex-finder length [ $m$ ]
$m_s$	Mass of particular solids [ $kg$ ]
$m_w$	Wet weight of nodules [ $kg$ ]
$m_{total}$	Total mass [ $kg$ ]
$m_{total}$	Total mass of all solids and fluid combined [ $kg$ ]
$P$	Pressure [ $Pa$ ]
$P_p$	Particle pressure [ $Pa$ -s]
$Q_i$	Flow rate inlet [ $m^3/s$ ]
$Q_{max}$	Maximal allowable flow rate [ $m^3/s$ ]
$Q_{pump}$	Flow rate created by pump [ $m^3/s$ ]
$Q_u$	Flow rate through underflow [ $m^3/s$ ]
$Q_{vf}$	Flow rate through vortex-finder [ $m^3/s$ ]
$r$	Stokes number independent of viscosity [-]
$r_c$	Radius cyclone [ $m$ ]
$r_m$	Model timescale ratio [-]
$r_p$	Prototype timescale ratio [-]
$Re$	Reynolds number [-]
$Re_p$	Particle Reynolds number [-]
$Stk$	Stokes number [-]
$t_{experiment}$	Allowable experiment length [ $s$ ]
$t_{micro}^{fall}$	Time it takes for a particle to travel one particle diameter [ $s$ ]
$t_{micro}^{inert}$	Inertial time scale [ $s$ ]
$t_{micro}^{visc}$	Viscous micro time scale [ $s$ ]
$T_{res}$	Average residence time fluid in cyclone [ $m/s$ ]

---

$V$	Volume [ $m^3$ ]
$V_c$	Volume hydrocyclone [ $m^3$ ]
$v_i$	Inlet flow velocity [ $m/s$ ]
$V_s$	Solids volume [ $m^3/s$ ]
$V_s$	Volume particular solids [ $m^3$ ]
$v_u$	Apex flow velocity [ $m/s$ ]
$V_{nod}$	Nodule volume [ $m^3$ ]
$v_{rel}$	Relative velocity [ $m/s$ ]
$V_{total}$	Total volume of all solids and fluid combined [ $m^3$ ]
$v_{vf}$	Vortex-finder flow velocity [ $m/s$ ]
$w_0$	Particle settling velocity [ $m/s$ ]
$w_i$	Cyclone inlet width [ $m$ ]
$w_n$	Width nodule [ $m$ ]
$\bar{c}$	Total volume concentration [-]
$A_{container}$	Surface area container [ $m^2$ ]
$v_{watercolumn}$	Water level velocity in the settling tank [ $m/s$ ]
$w_s$	Settling velocity [ $m/s$ ]

# Introduction

## 1.1. Background

The growing world population in combination with urbanization, high-technology applications, economic growth and the energy transition toward a green-energy economy are the main reasons for an increasing demand for rare earth metals. Metals that are essential for mobile phones batteries, solar panels and other low-carbon applications, are needed more than ever[21].

As of 2020, the European Union (EU) has a list of 30 Critical Raw Materials (CRM) that are said to be vital for the EU economy and sustainable development [7]. Figure 1.1 shows where these CRM are produced. The United States Geological Survey (USGS) constructed its own list of 35 Rare Earth Elements (REE) essential for the economy and its national security[10]. Figure 1.2 indicates where these materials are produced. Deep-sea mining is a potential way of being less dependant on those producers and securing a constant and sufficient supply of CRM.

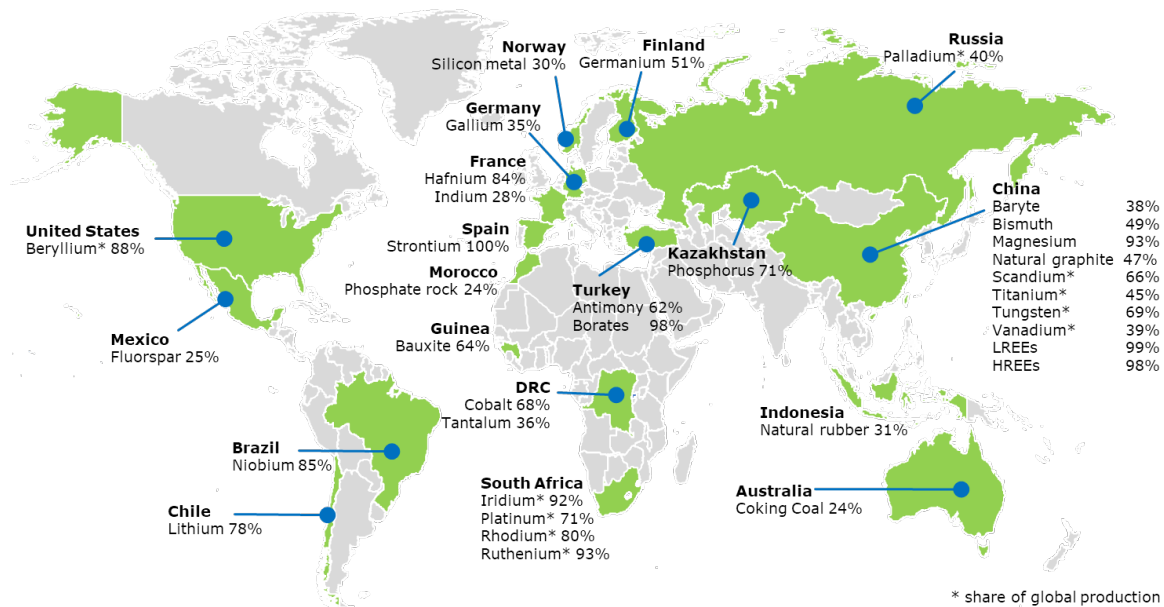


Figure 1.1: Countries accounting for largest share of EU supply of CRM [8]

Because many of the metals that can be mined on the bottom of the oceans are found in few selected areas on the earth's surface, interruption of the supply is a real threat. For example, onshore mines located in the Democratic Republic of Congo (DRC) produce 60% of all the Cobalt on earth. Refined cobalt is an essential element for the lithium battery and 81% of the global market share of refined cobalt is supplied by China.[4] This example shows that a secure future for low-carbon applications requires a more diverse production to reduce dependency on limited number of suppliers. Mining CRMs on the ocean floors could provide a solution.



Figure 1.2: Critical Minerals: Global Production (2017) [10]

## 1.2. Deep-sea mining

During a two year expedition of the H.M.S. Challenger in 1873, the first deep-sea minerals were discovered by expedition leader C.W. Thomson. The dredge haul of polymetallic nodules were described as 'peculiar black oval bodies about 1 inch long'. The location of this discovery was the western end of the Clarion-Clipperton Zone (CCZ) shown in Figure 1.3. Economic interest was developed in the 1960's, which led to consortia of different countries to develop resource assessments and extraction technologies for polymetallic nodules[30]. In the early 1980's most commercial activities ceased due to low metals prices globally[12]. However, the demand has increased in recent years, due to an unstable and potentially insufficient supply and advanced technologies available for the extraction of deep-sea minerals deposits (DMD) from the ocean floors. In 2010, private companies became involved resulting in a mining industry. Exploration activities are ongoing and the mid 2020's will likely see the beginning of polymetallic nodule mining[21]. These exploration activities primarily take place in the CCZ. The main reason expeditions target the CCZ for exploration and exploitation is the massive potential of DMDs it contains. The nodules located in the CCZ contain a higher tonnage of Mn, Ni, Co, Ti and Y than the entire global terrestrial reserve[21].

### 1.2.1. Regulation

Oceanic zones around the globe have different mining regulations. In 1982 the United Nations Convention on the Law of the Sea prescribed exclusive economic zones (EEZ), stretching 200 nmi from the coast, over which the right of exploitation and the use of marine resources can be claimed by a sovereign state only. [35]. Figure 1.3 shows these EEZ in white. Areas located outside EEZs fall under International Seabed Authority, ISA jurisdiction. The ISA consists of the EU and 167 individual member states, and is mandated by the Law of the Sea to regulate, organize and control all activities related to minerals in the international seabed area for the benefit of the whole of mankind[1]. ISA's main commitment is to ensure the effective protection of the marine environment from harmful effects that can result from deep-seabed related activities is ISA's main commitment. The ISA decides if and where commercial exploration and future mining operations take place.

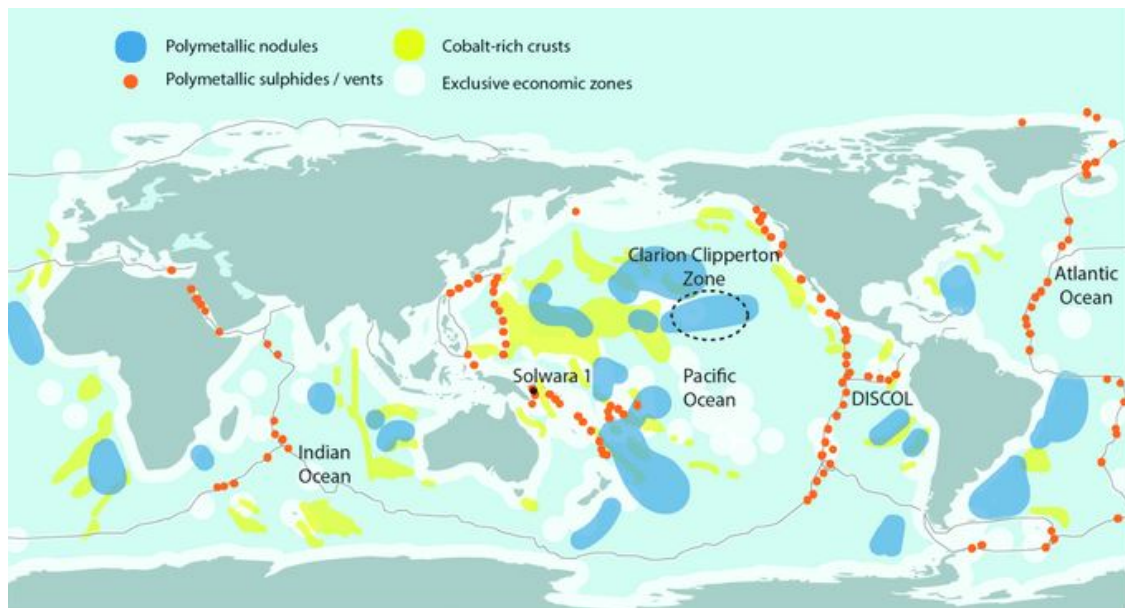


Figure 1.3: A world map showing the locations of the three main marine mineral deposits: polymetallic nodules (blue); polymetallic or seafloor massive sulfides (orange); cobalt-rich ferromanganese crusts (yellow); and including exclusive economic zones (white) [32]

### 1.2.2. Onshore vs offshore mining

Deep-sea mining is a complex operation. However, there are favourable incentives to develop marine based mine sites. They do not require water-transportation or electrical-transport systems, roads, ocean floor ore-transport systems, buildings, waste dumps and other terrestrial mine infrastructure. Many marine sites contain at least three metals of economic interest and less ore is required to provide the same amount of metal as terrestrial mines.[9].

Many challenges faced by onshore mining will be avoided when mining the deep seas. Acid mine drainage and soil or river contamination will not occur. Furthermore, deforestation, large scale lowering of ground water table and relocation of towns and villages is not needed[26]. Additionally, reduced risk to on-site workers and the absence of child labour are incentives for deep-sea mining.

However, deep-sea mining could encounter opposition as extraction of marine minerals and the environmental and ecological impacts are a concern to many countries, even in those not directly affected[43]. There are numerous ways in which deep-sea mining can be harmful to the environment. The main concerns are altering the geochemical composition of seafloor surface releasing toxic metals into the water column, crushing organisms and their habitat, or sediment plumes disrupting tardy ocean life over large areas. Therefore, it is important to create an understanding of these possible impacts and research mitigation measures before commercial mining is initiated.

### 1.2.3. Deposit compositions

Besides polymetallic nodules, two more considerable DMD compositions exist on the ocean floors. This section will give a concise explanation on the DMD locations, compositions and the difference in mining techniques.

#### Polymetallic sulphides

One of the three main DMD occurrences are polymetallic sulphides, also known as seafloor massive sulphides(SMS). SMS were the last DMDs to be discovered in the late 1970's. These deposits are found at hydro-thermal vents located at mid-ocean ridges and near island or volcanic arcs[45]. These vents occur at depths varying from 350 to 5000 meters [3]. An estimate indicate that between 1000 and 5000 large sulfide deposits may exist on the seafloor. The inactive vents will most likely become subject to mining activity in the future. One of the environmental advantages is only small amounts of sediment is covering the vents, therefore almost none is released during the mining process. On the other hand, these vents have to be crushed so the minerals can be collected. This results in an increased potential of heavy metal release into the ocean[13]. Figure 1.4 illustrates active hydro-thermal vents where sulphide deposits occur.



Figure 1.4: Sulphide deposit [53]

### Cobalt-rich ferromanganese crusts

Locations where hard substrate rock exists, e.g. volcanic hyaloclastites, are ideal for the formation of hydrated mineral crusts. These layers can be up to 25 cm thick and are formed by direct precipitation from cold seawater under oxic conditions. Sediment coverage of hard surfaces prevents these crusts to form. Therefore the main geomorphological areas are locations where ocean currents keep the seafloor relatively free of sediment[45].

Generally areas between 800 and 3000m water depth have economically interesting crust deposits because of higher Nickel and Cobalt concentrations. Figure 1.3 shows where ferromanganese crusts can be found. The western regions of the Pacific Ocean show the highest potential for mining operations. Ferromanganese crusts grow at approximately 1-7 mm/Ma depending on the conditions and contain, besides mainly Iron and Manganese oxides, high concentrations of economically and strategically important metals (e.g. Co, Ti, Ce, Zr, Ni, Pt, Mo, Te, Cu, W) and high amounts of REE[2]. The formed crusts are often m- to dm- sized plates and always in their highest state of oxidation [45].



Figure 1.5: Ferromanganese crust [53]

Cobalt-rich ferromanganese crusts can be mined by crushing the layers and collecting the debris. Figure 1.5 illustrates these crusts. After the shattered crust is collected by the bulldozer, it is sent upwards through the VTS to the PSV. Similar environmental issues arise with crust mining as with SMS mining. Besides relative low quantities of sediment being released into the ocean currents, heavy metal release into the environment is a major concern.

### Polymetallic Nodules

Polymetallic nodules, also known as ferromanganese nodules or simply manganese nodules, consist of concentrically banded zones of micro-layers around a nucleus. Metal precipitation from pore water in the sediments (diagenetic) or from ambient seawater (hydrogenetic) causes them to form around a nucleus[45]. Manganese nodules are composed of alternating Fe-rich and Mn-rich laminae and are formed at water depths of 3,500m to 6,500m [21] on sediment covered ocean floors globally. They can be found on, or just below, the sediment surface on the bottom of the abyssal

ocean. Figure 1.3 shows the locations around the world where polymetallic nodules have been discovered, indicated by the blue areas.

Manganese nodules can have different sizes, surface morphology and shapes. Figure 1.6 shows the nodules on the ocean floor. Extremely large specimens have been found of 21cm in diameter[59], however, these are exceptions and in most areas they can reach up to 15cm. Nodules exist in numerous shapes, of which discoidal is the most common. But this differs depending on the area. The seafloor density of the nodules varies widely from 10 per square meter up to thousands[45]. This is an important parameter when predicting economical feasibility for a mining operation. Determining the nodule seafloor density of the entire mining area is impossible which makes the predicted collection uncertain.

Because the polymetallic nodules lie on or just below the sediment surface they can be harvested similar to a potato field. No crushing is needed, only a mechanical, hydraulic or hybrid uptake mechanisms are to be used to collect the nodules[23]. When collecting mechanically, fork-like tools mounted on drums guide the nodules toward the collector. Hydraulic collection will use water jets to lift the nodules, together with ambient sediments, which are subsequently sucked into the nodule collector[23]. From the collector, the sediment, surrounding water and nodules are pumped toward the VTS. As collecting nodules can be done with relative ease, it is expected that 300 to 500 tons of ore per hour can be gathered by one collector. Flow-rate control and handling density waves will be a difficult objective for present-day technologies[23].



Figure 1.6: Nodule deposit [53]

### 1.3. Mining process

Mining the ocean floor is a complex operation which is being developed continuously. First, a seafloor production tool(SPT) specifically designed for that type of mining operation collects the deep-sea minerals. These minerals together with surrounding sediment and seawater are transported upwards through a vertical transport system (VTS) to the production support vessel(PSV) on the ocean surface. The PSV separates the deep-sea minerals from the remaining slurry in order to prepare it for transport. When ready, the minerals are transferred to a transport vessel which ships them to their on-shore destination. Figure 1.7 illustrates the processes of mining the 3 types DMDs.

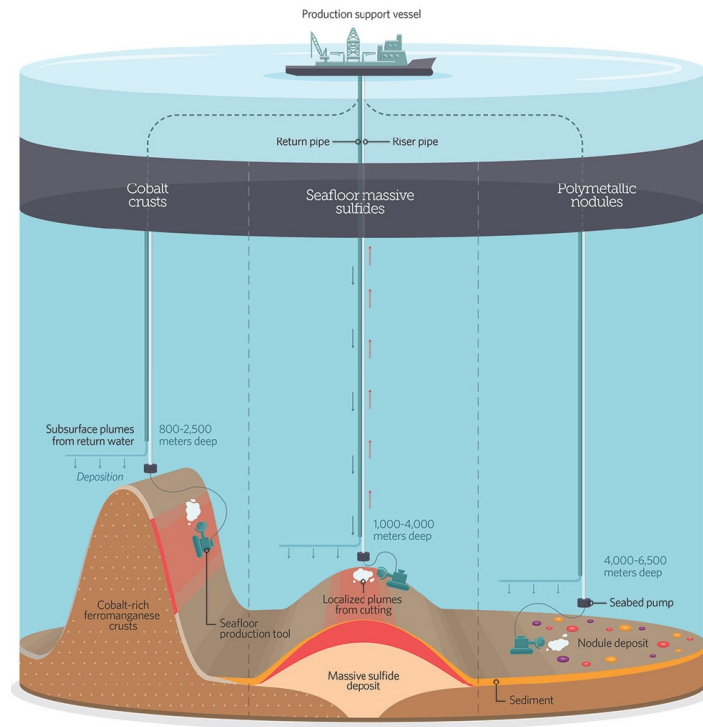


Figure 1.7: Schematic overview of main deep-sea mining processes [53]

Of the three deposits, commercial mining of poly-metallic nodule is the most promising for the near future. However, nodule collection from the ocean floor brings its own operational and environmental challenges. Figure 1.8 schematically shows the proposed process flow for nodule harvesting [27]. The solid lines represent the main flow (nodules) and the dashed lines represent secondary flow (SWOE). The blue arrows indicate the general direction of the flow.

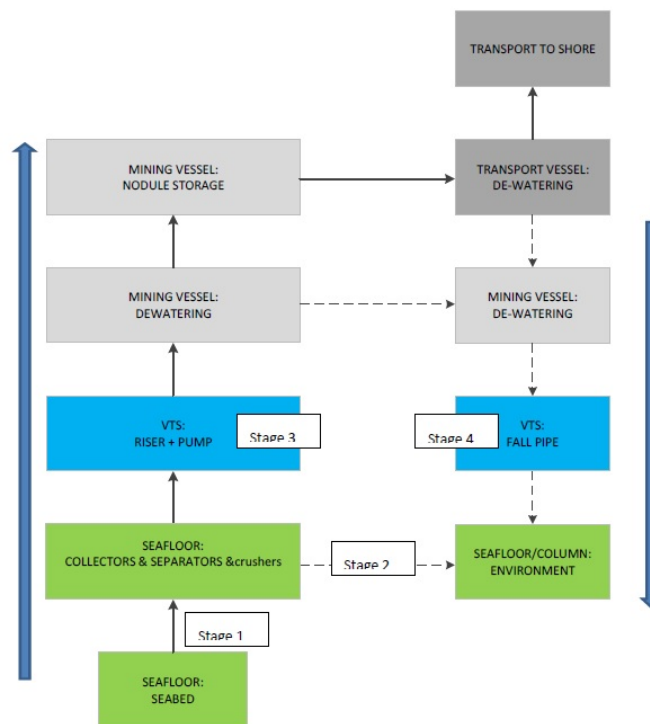


Figure 1.8: Schematic process flow. [27]

During harvesting, sediment and surrounding water will inevitably be collected with the nodules because nodules lie either on top or just below the sediment surface. The sediment and unnecessary water transport is unwanted. Separation at the ocean floor is required to minimize mass transport to the sea surface, and thereby reducing energy

consumption and impact to the marine environment[27]. Sediments that are collected along with the nodules should ideally be removed and disposed at the ocean floor immediately after the pick-up. The three main environmental challenges are: mitigating the formation of near bottom plumes, separating the sediments from the nodules and minimizing the seabed disturbance[27].

Figure 1.8 clearly indicates that when sediment and unnecessary amounts of water are separated from the nodules at seafloor level (stage 2), the other processes will require less energy. Sediment would not have to be transported through the VTS (stage 3) to the mining vessel. The mining and transport vessels would not have to separate large amounts of sediment and water. And the transportation of dispensable material back into the ocean (stage 4) causing environmental harm would be limited.

## 1.4. Problem statement

The following can describe the problem statement: When mining for poly-metallic nodules in deep sea conditions large amounts of sediment and water will be sucked into the suction pipes together with the manganese nodules. This slurry consisting of sediment and water is undesirable when transporting the nodules to the surface for financial and ecological reasons. If unnecessary amounts of mass is transported towards the ocean surface, large amounts of energy and power are required. This needs to be avoided if possible.

When large quantities of sediment are deposited back into the ocean after separation, large plumes of suspended sediment can cause environmental harm to life at the ocean floor which lives at a glacial pace. Normally sediment would accumulate around 1 millimeter every thousand years. The slurry that is separated from the nodules becomes the discharge plume when deposited back into the ocean. When this process happens high above the ocean floor, this sediment plume can cover large distances and great areas [16]. When disturbing large areas with sediment plumes, they would be unlikely to recover in a reasonable timescale.

It would be desirable for unnecessary sediment and water to be removed from the flow before it is transported toward the surface as much as possible in order to save energy and minimizing sediment plumes by discharging sediment as close to the ocean floor as possible.

## 1.5. Research objective

A better understanding of solid-solid and liquid-solid separation methods needs to be created and the underlying physical phenomena need to be researched when designing a device that can be used to separate nodules from the surrounding carrier fluid.

The aim of this project is to design a separation device inspired by a classic hydrocyclone that can separate poly-metallic nodules from the surrounding carrier fluid and sediment as efficient as possible. This will be done by answering the following research question:

**'What is the feasibility of a hydrocyclone inspired machine designed to separate polymetallic nodules from surrounding water and sediment in deep sea mining operations.'**

In order to substantiate the conclusion several questions need to be answered:

1. When will the design be feasible?
2. What is the best method for this separation?
3. What principles of a hydrocyclone can be used for separation of the nodules?
4. What is the separation efficiency of this technique for the proposed operation?

# 2

## Material properties

### 2.1. Polymetallic nodule data

Nodule and sediment characteristics, collector type and parameters and process flow overview are all needed when designing a device capable of separating the ambient fluid from the required nodules. This information provided by the Blue Nodules report, and consists of two sets of data. The first data set is provided by GSR (Global Sea mineral Resources). This data was gathered from 25 box-cores during two sampling campaigns to the CCZ license area in 2017. The contents of these box-core samples were measured on the vessel immediately after recovery. The second set gathered from just two box-cores examined by NTNU(Norwegian University of Science and Technology). These box-cores where provided to NTNU by GSR and where examined in semi-dry state at in-house conditions[27].

The following section will make a selection of valuable data for the proposed separation process and explain why this information is required for the design of a separation device. It must be said that the data gathered by GSR is based on a limited sample volume compared to the area's extent.

#### 2.1.1. Nodule characteristics

The whole mining operation is based on extracting the manganese nodules from the ocean floor. Therefore it is important to understand the valuable nodule characteristics. Figure 2.1 and table 2.1 show the nodule characteristics compiled from the GSR measurements. The GSR samples are more relevant than the NTNU samples in this situation because GSR based their results on 25 box-cores and gathered data from the wet samples. As the separation process will happen under wet conditions and nodule weight and density vary under wet and dry conditions due to their porosity, the GSR results give an accurate representation of the insitu nodule characteristics.

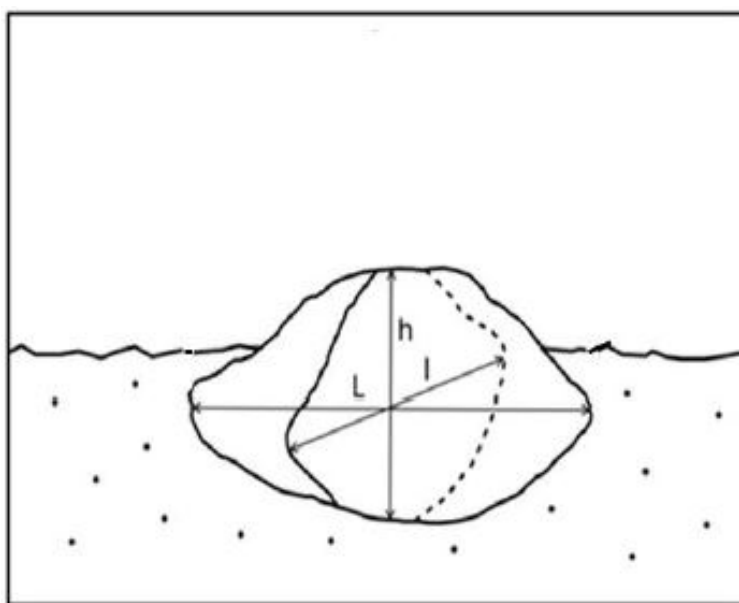


Figure 2.1: Schematic presentation of the nodule dimensions [27]

	Length $L_n$	Width $w_n$	Height $h_n$	$(L_n+w_n)/2$	Wet weight $M_w$	Volume $V$	Wet density $d_w$
	[mm]	[mm]	[mm]	[mm]	[g]	[ml]	$\text{kg}/\text{m}^3$
Average	71.8	57.3	34.4	64.5	168.3	85.1	2000
Max	140.0	120.0	92.0	130.0	2636.0	1300.0	5800
Min	11.0	9.0	5.0	10.0	0.6	1.0	100

Table 2.1: Nodule characteristics [27]

When looking at the wet densities from table 2.1. The first observation is that the average density of the nodules is lower than ordinary sediment. This is most likely due to the porous nature of the nodules.

The second observation is the minimum wet density. With a density of  $100 \text{ kg}/\text{m}^3$  it is 10 times less dense than water which would mean the nodules should float. This cannot be possible and therefore this is considered a measurement error.

The GSR data does not explain if there is a physical difference in economically interesting or non-interesting nodules. As it is unknown if low density or very small nodules have economic value, nodules of all sizes and densities larger than  $\rho_f$  are considered desirable for harvesting.

Table 2.1 indicates a minimal nodule diameter of 10 mm, which raises some questions. As nodules are formed around a very small nucleus, it would be expected that nodules with economic value exist with a smaller diameter than the minimum measured 1 cm. Accordingly, for this research the smallest nodules diameter desired for collection is 1 mm [22].

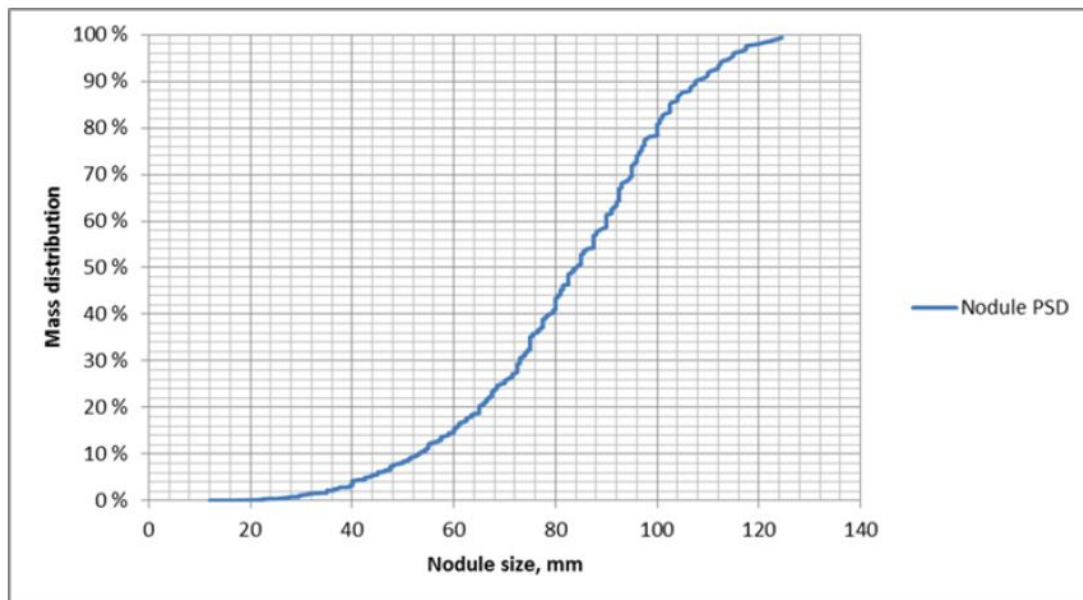


Figure 2.2: Nodule cumulative mass distribution [27]

Determination of the maximum nodule diameter is also required. As different harvesting locations can have different maximum nodule sizes [59], a maximum size for separation needs to be determined. The Blue nodule report indicates that nodules with diameters larger than 120 mm are not collected. They will be discarded or rejected before entering the harvester. As a result a maximum of 120 mm in diameter is established as the maximum nodule size entering the separation device. Figure 2.2 indicates an estimation of only 2% of the total mass consists of nodules larger than 120 mm.

### 2.1.2. Sediment

In order to design a device capable of separating nodules from the surrounding slurry, more knowledge about the slurry is needed. The sediment carried by the incoming flow consists of different grain sizes. Table 2.2 shows the distribution of sediment characteristics found by GSR from their 25 box cores.

An overview of the slurry composition is important as it can have an effect on the flow behaviour. In order to determine a separation technique the sizes and distribution of the particles in the mixture-flow need to be known.

	Diameter limits [ $\mu\text{m}$ ]	Average %	Min %	Max %
Clay	Less than 2	12.0	2.5	18.4
Silt	2 - 63	76.2	44.8	89.8
Very fine sand	63 - 125	11.8	0	52.7

Table 2.2: Sediment fractions [27]

Tables 2.2 and figure 2.3 show the grain size distribution found by GSR.

GSR data	PSD - $D_{10}$ [ $\mu\text{m}$ ]	PSD - $D_{50}$ [ $\mu\text{m}$ ]	PSD - $D_{90}$ [ $\mu\text{m}$ ]
Average	1.8	8.7	66
Max	4.7	67.7	185
Min	1.3	4.3	18

Table 2.3: GSR sediment characteristics [27]

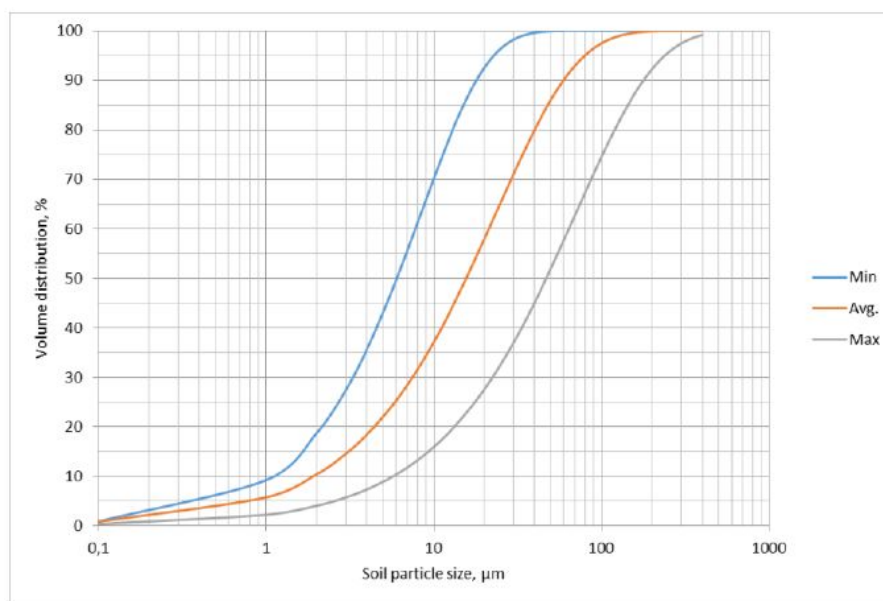


Figure 2.3: Sediment particle size distribution of the GSR samples [27]

The largest sediment fraction,  $D_{90}$ , will require the most attention when researching separation possibilities. The largest grains will have the most similarities with the manganese nodules in terms of behaviour to the surrounding flow.

### 2.1.3. Flow overview

After determining the solid characteristics, an overview of the flow into the separator can be constructed. This overview needs to be formulated in order to predict the flow and particle behavior. For a successful separation this information is essential.

#### Collector type

As stated in the previous section, nodules can be picked up in two different ways depending on the collector type. This research will focus on hydraulic harvesting[22]. The difference is crucial for the separation device as the flow mass and volume vary widely from mechanical collection. Hydraulic harvesting creates a volume flow rate almost seven times larger than that of mechanical collection. Larger volumes of water sucked into the collector also results in lower concentrations of solids. This can have an affect in separation efficiency. The following section will illustrate important expected flow values of sediment, nodules and water collection from the CCZ when harvested hydraulically.

Table 2.4 indicates the prediction of mass and volume collection of sediment, nodules and ambient water during the hydraulic collection process.

Parameter	Nodule	Sediment	Water	Total
Mass [kg/s]	136.67	223.61	6399.17	6759.72
Volume [ $m^3/s$ ]	0.0668	0.0894	6.243	6.400

Table 2.4: Hydraulic collection characteristics [27]

From table 2.4 the concentrations can be determined with equations 2.1 & 2.2.

The mass concentrations:

$$c_m = \frac{m_s}{m_{total}} \quad (2.1)$$

Where  $m_s$  represents the total mass of the particular solids and  $m_{total}$  represents the total mass of all the solids and water combined.

The volume concentration:

$$c_v = \frac{V_s}{V_{total}} \quad (2.2)$$

Where  $V_s$  represents the total volume of the particular solids and  $V_{total}$  represents the total volume of all the solids and water combined.

The concentration of solids can have a significance influence on particle interaction and flow behaviour. The settling velocity of individual particles is reduced when a large number of particles is settling in a confined space[54]. Particle settling velocity is assumed to be one of the key parameters for determining the separation efficiency. Table 2.5 shows low concentrations of solids are predicted for hydraulic pick-up.

Particles	Mass concentration $c_m$	Volume concentration $c_v$
Nodules (wet)	0.02022	0.01044
Sediment (dry)	0.03308	0.01397
Total	0.05329	0.02441

Table 2.5: Concentrations particles hydraulic collection [27]

The particle terminal settling velocity,  $w_o$ , is the maximum velocity a particle reaches relative to the surrounding fluid. However, in reality the particle settling velocity,  $w_s$ , is often less than the theoretical terminal velocity. One of the reasons for this difference is the influence of the volume concentration of solids. Higher concentrations lead to more particle settling interference, resulting in a hindered settling. Figure 2.4 shows the settling velocity divided by the terminal settling velocity of the particles as a function of the total volume concentration of solids  $\bar{c}$ . The reaction of the nodules to the surrounding solids is important to understand. Figure 2.4 illustrates a bimodal mixture, which shows that different particle sizes have different reactions to higher concentrations.

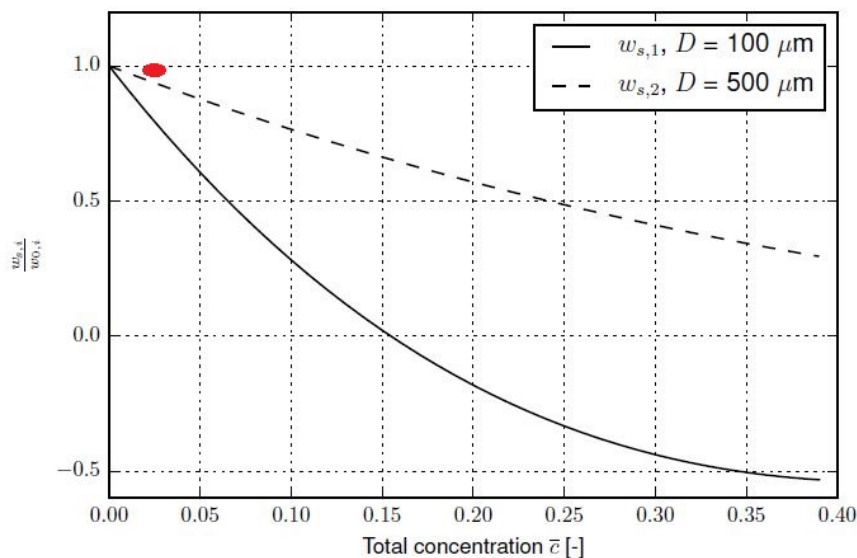


Figure 2.4: Relative settling velocity for a bi-modal mixture of particles [54]

Table 2.5 shows a total volume concentration of solids of only 0.02441. The smallest nodules considered in this research have a diameter of 1mm. This is twice the size of the solids indicated with the dotted line in figure 2.4. Nodules with larger diameters would experience even less hindered settling. Therefore it can be concluded that the nodules do not experience any interaction with other present solids. However, this does not mean nothing changes due to the present solids. According to the liquid equivalent model, a pseudo-homogeneous flow with a low concentration of solids behaves as a single phase fluid with a density equal to the slurry. All other properties remain equal to that of the fluid[29]. Derivation of the liquid equivalent model gives the following equation indicating the relative density change of the fluid due to the presence of the particles.

$$c_{vs}(S_s - 1) + c_{vn}(S_n - 1) = S_m - 1 \quad (2.3)$$

With:

Abbreviation	Definition
$c_{vs}$	Volume concentration of sediment
$c_{vn}$	Volume concentration of nodules
$S_s$	Relative density of the present sediment
$S_n$	Relative density of the present nodules
$S_m$	Relative density of the fluid

Table 2.6: Abbreviations equivalent liquid model

This equals a 3.07% percent increase in density.

# 3

## State of the art hydrocyclone

This research focuses on a device that is inspired by a conventional hydrocyclone in order to separate the polymetallic nodules from the surrounding fluid and sediment as efficiently as possible. However, before doing so, it should still be determined if a hydrocyclone is indeed the best option.

There are numerous separation methods and devices available that could help design a device for nodule separation. Therefore, existing separation methods and devices are examined based on the conditions, restrictions & preferences of the operation in order to determine if their separation principles can support the design. Reviewing separation techniques should also confirm that a hydrocyclone is a correct piece of equipment to inspire the nodules separation device. When a hydrocyclone is considered to have suitable qualities that can be used for nodule separation, it will be examined thoroughly and every geometric variable is analysed for optimal separation efficiency of manganese nodules.

### 3.1. Requirements separation methods & equipment

The conditions under which the separation process will take place are shown in chapter 1 & 2. These conditions lead to several criteria for the separation device. Together with some additional criteria [22], they are be divided into restrictions and preferences.

#### 3.1.1. Restrictions

The vital requirements for the proposed device are shown under restrictions. The device should:

1. be able to separate solids from other solids and liquids.
2. be able to collect nodules with diameters ranging from 0.1 cm to 12 cm should all be collected.
3. have no moving parts (can cause blockage, or maintenance).
4. have a continuous separation process.
5. be unable to get blocked.
6. be low maintenance.
7. have a low pressure drop.

#### 3.1.2. Preferences

The requirements that do not immediately cause the device to be a failure are named in this section. However these requirements are still important[22].

1. Volume of device should be around  $1 m^3$
2. Device can handle high flow rates of  $0.5 m^3/s$

The reason for the division of restrictions and preferences is established as they have different consequences for the feasibility of the proposed separation device. If a restriction is not met, the project can be defined as non-feasible. Failing to comply with a single restriction would make the cyclone unsuitable for application in polymetallic nodule separation in deep-sea conditions.

As the separation device is intended to separate nodules on the the ocean floor, the idea is to integrate the cyclone into the harvesting equipment. This harvester has certain dimensions and a designed flow rate. Therefore, the cyclone should comply with those dimensions, and be able to handle the required flow rate to be applied. Not complying with these conditions means the separation device cannot be used for this operation. However, this does not necessarily mean it fails with other dimensions or flow rates and could possibly be a suitable device under different conditions. Thus, the flow rate and the dimensions are categorized as preferences.

### 3.2. Separation methods

Besides complying with as many restrictions and preferences as possible, to be the best method, it must also be the most effective at separating sediment and water from the nodules. The following section investigates the known separation methods to find the technique with the highest potential.

For this research, only solid-liquid separation techniques are considered . It is not desirable to focus on other separation types according to type of medium as there would be an excess of options. For solid-liquid or solid-solid separation, chemical methods are often used. This is not a possibility for deep sea mining operations. Therefore, these options are neglected as well. Tarleton & Wakeman describe a large number of possible separation methods in their book: 'Solid/liquid separation: equipment selection and process design'. Figure 3.1 shows a large number of devices capable of separating solids from liquids and solids from solids.

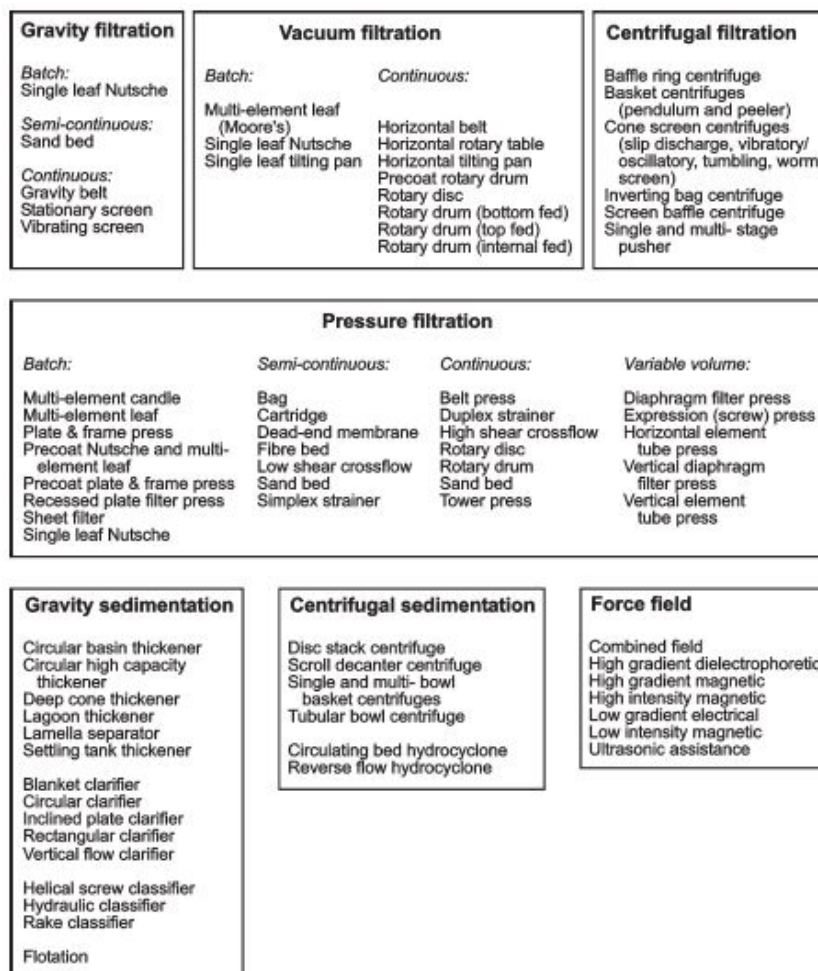


Figure 3.1: Broad classification chart showing the forms of solid-liquid separators [51]

The preferences and restrictions indicate that the separation process needs to have a low resistance, be a continuous process and, if possible, moving parts need to be avoided. This narrows down the possibilities considerably. Figure 3.1 shows, in the section centrifugal sedimentation, that hydrocyclones are indeed a potential equipment and can possibly accomplish the proposed separation .

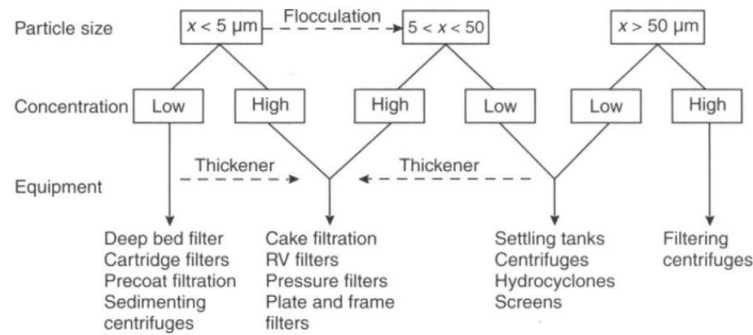


Figure 3.2: Particle size and concentration as guides in the selection of solid-liquid separation equipment [49]

Figure 3.2 illustrates a guide created by Ladislav Svarovsky in his book *Solid-liquid separation*. This shows recommended solid-liquid separation equipment guided by particle size and concentration. Svarovsky explains that for low concentrations seen in chapter 2 and larger particle sizes, the main options are settling tanks, centrifuges, screens and hydrocyclones. It should be noted that the graph above does not indicate a maximum size limit but is focused on particle sizes much smaller than manganese nodules.

Blockage during operation would result in serious consequences, as mining must be stopped temporarily. Maintenance or repair of a mining vehicle located at 6000 meters water depth causes large delays and high costs. In order to avoid these consequences moving parts and screens are recommended to be avoided. Moving parts can break down or jam and screens or filters can get blocked. Simple and robust devices have a preference for this particular application.

Guided by figure 3.2, settling tanks and hydrocyclones are the best options. However, with limited available space and high flow rates, hydrocyclones show the highest potential. Hydrocyclones are primarily designed for separation of particles up to several micrometers. However, there is no evidence that larger particles cannot be separated by a hydrocyclone. Therefore, researching hydrocyclone separation of manganese nodules from sediment in water is justified.

### 3.3. Hydrocyclones

For more than a 100 years hydrocyclones have been used for a wide variety of separation purposes. Cyclones designed for use with liquids are referred to as hydrocyclones [51]. Besides mineral processing as the traditional role of hydrocyclones, they now attract a lot of attention in numerous industries like biotechnology, chemical engineering and the oil and gas industry [48]. Figure 3.3 shows a hydrocyclone in its basic form.

The hydrocyclone is a relatively compact, cheap and versatile device as the basic unit has no moving parts and comprises an inverted conical bottom section attached to a cylinder containing a tangential inlet [51]. A feed enters this tangential inlet at a high velocity near the top of the cylindrical section. The fluid is pushed toward the bottom in a spiralling fashion where it experiences a flow reversal and passes up as a central core. This central core actually flows toward a central outlet in a reverse spiral [60]. This can clearly be seen in figure 3.3b.

Apart from compact, cheap and versatile other properties are advantageous for hydrocyclone compared to other separation technologies with similar principles. Unlike centrifuges and filtering equipment, the application of hydrocyclones offers low energy consumption, wide operating range, convenient installation and operation, low maintenance cost, low energy consumption, small cut sizes, high separation efficiency and absence of moving parts [39].

Hydrocyclones are categorized as classification devices. Classification is a process of dividing a particle-laden stream into two, ideally at a particular particle size, known as the cut size. [60]. A wide variety of classifier types are available, which can be categorized according to their operation principles. An important distinction is made between classifiers in which a partition of the particle size distribution is sought and gas cleaning equipment, in which removal of all solids from the gas stream is the aim [60]. This particular operation requires separation based on both, as sediment and fluid are unwanted

#### 3.3.1. Components

Before the working principle is discussed, the individual components of a basic hydrocyclone are explained. Figure 3.3a and table 3.1 illustrate a schematic overview of the components found in a hydrocyclone.

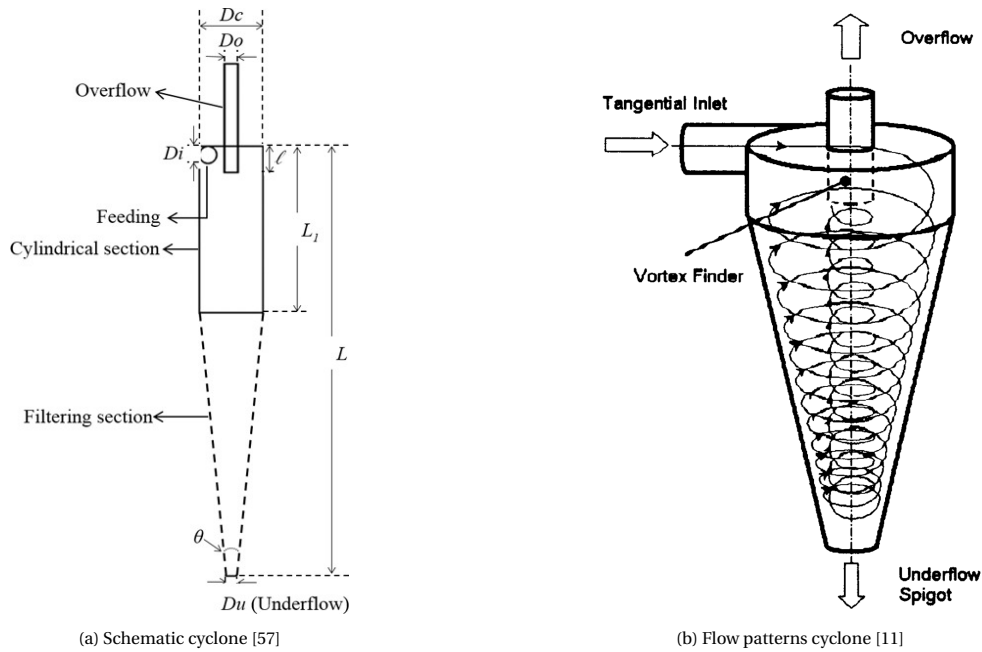


Figure 3.3: Hydrocyclone

Symbol	Definition
$D_i$	Inlet diameter
$D_c$	Diameter cyclone
$D_o$	Vortex-finder/overflow diameter
$D_u$	Apex/underflow diameter
$L$	Total length cyclone
$L_1$	Length cylindrical section
$l_{vf}$	Length vortex finder
$\theta$	Conical angle

Table 3.1: Hydrocyclone geometric symbols

A basic hydrocyclone consists of five main parts. Following the path of the flow these parts are : tangential inlet ,cylindrical section, conical section, underflow pipe and the vortex-finder. The inlet is where the fluid enters the cyclone tangentially. The cylindrical section is the section where the fluid arrives and where the swirling motion is created that is needed for the separation. When the fluid flows in a circular motion in the direction of the underflow spigot it passes through the conical section. This section is where the main separation process takes place. As not all of the fluid passes through the underflow, the rest escapes through the overflow pipe called the vortex-finder. Due to the spiralling fluid column a central vortex is created at the centre of the cyclone travelling in the opposite direction toward a pipe at the top of the cylindrical section. This explains why this pipe section is called the vortex finder. As heavy material is transported toward the edges, this exits through the underflow. Finer material that does not have the time to travel toward the edges is carried by the central vortex toward the vortex-finder. In figure 3.3b the flow path can clearly be seen.

### 3.3.2. Separation principles

The basic separation principle in a hydrocyclone is centrifugal sedimentation. This is a more efficient and faster way of gravitational sedimentation. Combining the two accelerations results in a rapid removal of particles from a fluid. The main difference between centrifuges and hydrocyclones is the absence of moving components[39] as the necessary vortex motion is only performed by the fluid itself which is favorable when maintenance and repair are costly.

The inlet of the cyclone is designed to guide an incoming feed that generates the spiral path that creates the swirl needed for centrifugal sizing [31]. The main hydrocyclone working principle is based on this centrifugal force that is generated by the spin created by the spiral path. This centrifugal sizing is illustrated in figure 3.4. The direction of larger and smaller particles can clearly be seen.

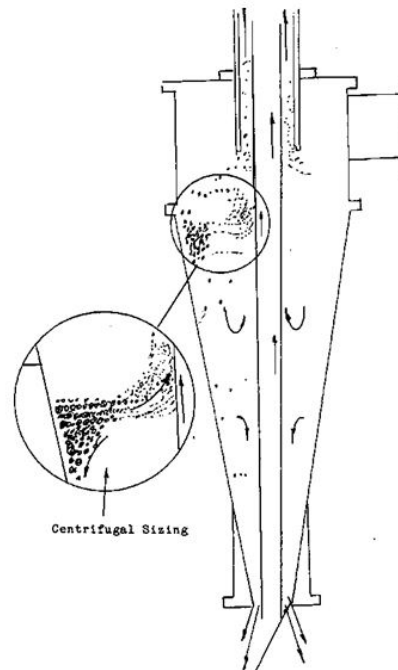


Figure 3.4: centrifugal sizing hydrocyclone. [31]

### 3.3.3. Key performance parameters

By analysing the key performance parameters of a hydrocyclone, its separation efficiency can be determined. These performance parameters consist of the partition curve, split ratio, capacity and energy consumption. The efficiency of particle separation can be obtained from the partition curve and the efficiency of the separation of the fluid is described by the split ratio.

#### Partition curve

The feed to a hydrocyclone contains unsorted particles of different sizes and shapes. A perfect hydrocyclone would guide all coarse particles toward one stream, the underflow, and all fine particles in the direction of the other stream, the overflow. The cut size of the cyclone,  $d_{50}$ , is defined as the point at which the particles are equally affected by the forces and where particles have a 50% chance of either flowing to the underflow or overflow streams[40].

During operation some fine particles will get in the underflow and some coarse particles get in the overflow. It is said that the sharpness of separation decreases if more of the fine particle report to the underflow and coarse particles report to the overflow. The complexity of the flow process in a hydrocyclone leads to empirical equations for prediction the actual cyclones performance[34]. This makes an accurate prediction of the cyclones' performance difficult when no resembling experimental data is available.

In reality fine particles also get bypassed to the underflow as they remain suspended in the carrying fluid. Therefore the underflow will contain both fine and coarse particles. This does not occur in the opposite direction. Large particles travel toward the wall more freely. Therefore they are not likely to be collected by the vortex-finder.

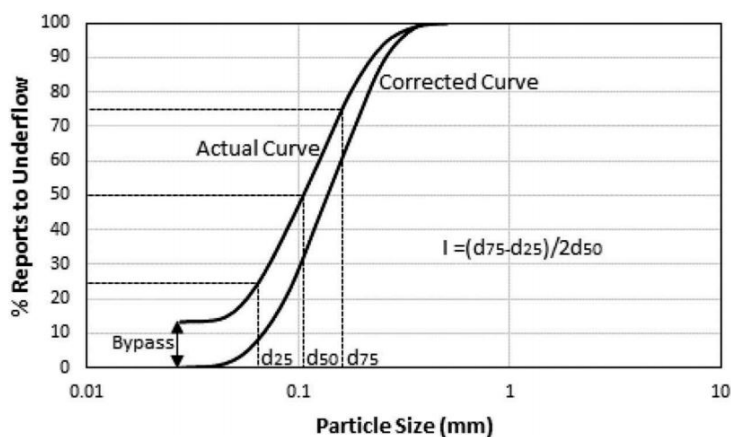


Figure 3.5: Partition curve hydrocyclone. [40]

Figure 3.5 illustrates a partition curve of a hydrocyclone. Particles below the curve are collected in the underflow and the particles above the curve are collected in the overflow. A perfect hydrocyclone would have a straight vertical line with all particles on the right reporting to the underflow and all particles on the left reporting to the overflow. When implementing the imperfections and the sharpness of separation you get the corrected curve. The actual curve shown in figure 3.5 is obtained when implementing the bypass effect.

#### **Split ratio**

The ratio between the volume flow through the apex and the volume flow through the vortex-finder,  $Q_u/Q_{vf}$  is called the split ratio. The main goal of this hydrocyclone is separating the coarse particles from the rest of the slurry. This means that when large amount of the surrounding fluid exits through the underflow pipe with the coarse particles is unwanted. The bypass effect described above will also increase as the flow through the apex increases. Therefore a low split ratio is beneficial for high separation performance[39].

#### **Capacity**

A high capacity is almost always beneficial for any separation activity. Hydrocyclones have a relative high capacity compared to their size. However, just like all other separation techniques, it is limited. This capacity depends on the size, shape, flow characteristics and requested separation. Larger influx of slurry results in higher velocities inside the cyclone. This adjusts the direction of forced sedimentation, shorter residence times, higher turbulence and increased pressure. To counter these effects, the shape and size of the cyclone must be adjusted. Therefore, shape, size and capacity are all connected. When available space is restricted the capacity will be restricted as well. For higher capacity, larger cyclones are required[39].

#### **Energy consumption**

The final key separation-performance is energy consumption. Hydrocyclones are known for their low energy consumption. But this depends on a lot of factors. The energy consumption depends on the size, shape, volume flow and flow composition.

It is expected that many low split ratio, low energy consumption, and low costs cyclone separation technologies will be developed and applied successfully in the near future. Long Ni, et al. claim that the application scope of hydrocyclones can be expanded greatly[39].

### **3.4. Optimal geometry cyclone**

Standard classical hydrocyclones performances have been investigated. E.g. Rietema [42] and Bradley [5] both researched the performance of hydrocyclones. They investigated cyclones with standard dimensional ratios. As a result of their research, hydrocyclone performance can be predicted relative accurate. However, these standard cyclones are not designed for separation of large poly metallic nodules. These cyclones are designed to separate particles of a few micrometers. Thus unfortunately, their findings cannot be used for the design and performance prediction of a cyclone than required for this operational purpose.

Figure 3.3 shows a schematic overview of a basic hydrocyclone. The cyclone can be divided into 5 primary parts that need investigating for optimization of the proposed separation. The following section will elaborate on these parts individually and elaborate on how they can be modified for enhanced separation. Appart from the 5 primary parts a wide variety of extensions exist. However, for this project focusing on all extensions is not possible as there would be too many parameters to research. Therefore, the focus lies primarily on the 5 standard parts.

#### **Tangential inlet**

The inlet pipe is attached tangential to the cylindrical section. This is where the feed enters the cyclone. Three different types of alterations are known to have an effect on separation efficiency: inlet size, angle and shape.

##### *Inlet size*

For circular inlets the size is inversely proportional to energy consumption[58] [56]. This is logical as the energy consumption is directly proportional to the inlet velocity which is inversely proportional to the square of the inlet diameter. With the decrease of inlet diameter, the separation efficiency first increases and then decreases. This can be appointed to the following: When the inlet size is extremely large, the flow velocity will decrease which decreases the centrifugal force. But when the inlet size is extremely small, the velocity increases drastically, resulting in a high centrifugal force that can result in break-up problems, where particles reduce in size. [39]

Where available space is limited the inlet size can play a crucial role for the separation efficiency. When low flow velocities are desired, a squared inlet is recommended. As a square inlet has the largest surface area, lower average

velocities can be obtained. This makes a squared cross section the preferred shape for this research.

#### *Inlet angle*

The inlet angle is another parameter affecting the separation performance of cyclones and is capable of eliminating the bypass effect. However this only has a significant effect for small particles in the 4-7  $\mu\text{m}$  range. [14]. Separation efficiency was not affected for particles larger than 15  $\mu\text{m}$ . This research was done on mini hydrocyclones. So these findings are not representative for the large cyclone proposed for this design. Therefore, it is not ruled out that an inlet angle can have an effect on separation performance. However due to lack of supporting information an angle is not recommended.

#### *Inlet shape*

Several shapes have been investigated for separation enhancement. Chu et al. researched 5 different inlet shapes seen in figure 3.6. These investigations included: involute type, A1, tangent type, A2, arc type, A3, slanting type, A4, and spiral type, A5.

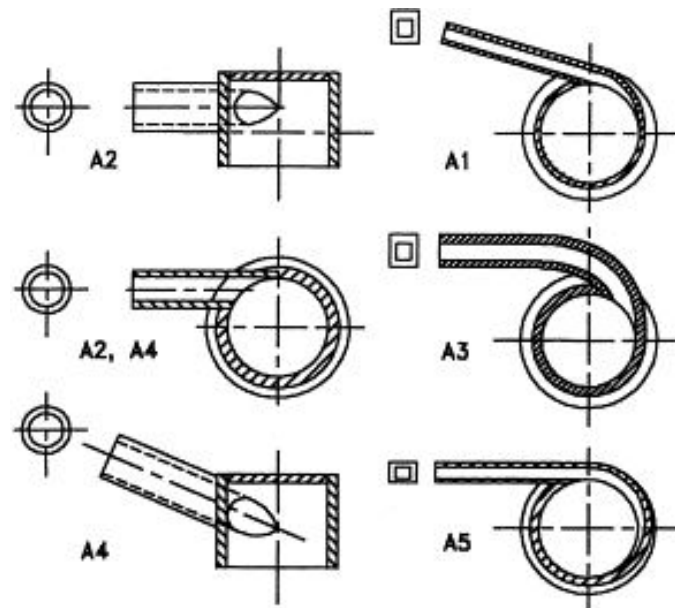


Figure 3.6: 5 inlet shapes [6]

Chu et al. concluded that only the spiral type was capable of reducing the corrected cut size. A reduced corrected cut size is not interesting for this research at this moment, as a relative large cut size is desired compared to traditional hydrocyclone operations.

The shape and direction outside the cyclone will also have an effect. If the pipe attached to the inlet is curved the particles in the flow will be located more to the outside of the flow. The angle of the pipe outside the inlet can also have a significant effect. When the pipe attached to the inlet has an inclined angle, particles will move slower than the average flow velocity. If the angle is declined, particles will move faster than the incoming flow. When there is a horizontal angle, particles will enter the cyclone more in the direction of the edge or center depending on direction due to their inertia. These factors lie beyond the scope of this research.

#### **Cylindrical section**

When the feed enters the cyclone, it arrives in the cylindrical section. Due to the tangential inlet, this is where the 'swirl' is created. As the fluid containing the particles is pressed against the cylinder wall, the fluid is pushed into a circular motion creating a swirl. This swirl is essential for effective classification.

#### *Diameter*

This section generally ranges from 10mm to 2.5m [39], and plays an important role in the separation process. The cut size, which is explained in the previous section, is proportional to the cylindrical-section diameter of the cyclone[5]. Several studies show that decreasing the cylindrical section diameter is an essential approach toward enhancing separation efficiency[39]. However these researches focus on cut sizes up to several micrometers. This is not close to the

cut size needed when separating polymetallic nodules from the carrier fluid.

The application of large hydrocyclones is increasing due to their high capacity and low energy consumption. The use of large hydrocyclone is generally limited by its low efficiency of separation of fine particles and that of material with small marginal density difference[39]. However, this does not need to be a problem in this situation and could possibly work as an advantage for the proposed application. Therefore, the maximum possible diameter is recommended to be implemented into the proposed hydrocyclones' design.

#### *Length*

With an increased length of the cylindrical section, separation efficiency and capacity can increase[15]. This results from a larger space inside the cyclone and a longer residence time of the fluid[46]. An increased cylinder length is not always an improving feature. In some cases hydrocyclones are even made without a cylindrical section [5]. In a situation where space is limited, it should be questioned if an increased cylinder has any added value. For separation of large particles from sediment, an unknown application for a commonly used cyclone, there probably is a negative effect when extending its cylindrical section length. This can cause sediment to move toward the wall as well, which is not desirable. Only the nodules need to travel completely toward the outer wall.

#### **Conical section**

The main separation area in hydrocyclones is the conical section. Differences in conical angle and shape can largely affect the separation efficiency and performance. Therefore, the effects of various conical shapes and sizes must be understood in order to optimize the performance of the hydrocyclone.

#### *Cone angle*

An enhanced separation efficiency for hydrocyclones is found when decreasing the cone angle [48]. The circulation flow in the conical section is fundamentally influenced by the cone angle. When cyclones have small cone angles up to approximately 25°, they can be employed to obtain relative low cut sizes. This is because the circulation flow is suppressed which leads to a fine particle separation. Svarovsky et al.[49] describe that cyclones with cone angles between 25° and 180° show high classification sharpness, specifically for separation of fine particles of a similar size by particle density.

As shown in chapter 4, the nodules that need to be guided toward the underflow vary between 1 mm and 12 cm in diameter. This range is far from any available study with significant information. Therefore, from literature only, it is not clear what phenomena will occur for different cone angles when separating the nodules. Chapter 4 introduces a theorem constructed for the required cone angle.

#### *Shape*

Various conical sections were developed to enhance hydrocyclone separation as this is the main separation space. Yang et al. [64] devised several cyclones with two cone combinations in order to enhance solid-liquid separation for solids up to 70 $\mu$ m in diameter. Figure 3.7 illustrates a cyclone with a two cone combination.

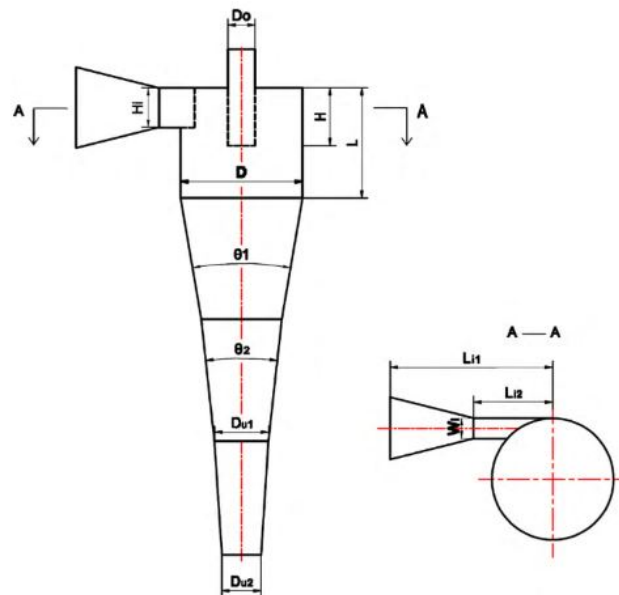


Figure 3.7: Two cone combination [64]

They observed three phenomena. The first observation was when the second conical angle is maintained constant, the separation efficiency is proportional to the first conical angle. The second observation involved that the variation between the two conical angles is inversely proportional to the sharpness of the grade efficiency curve. The last observation was when the conical angle of the second section was considerably smaller than the first, the separation efficiency of small particles increased significantly.

Chu et al.[6] compared five types of cone sections for separation performance. Figure 3.8 shows these types of cone sections. From C1 to C5 the types are : parabola type, hyperbola type, spiral type, one with a smooth surface and a ringed type. The cone with a smooth surface showed to be capable of obtaining the smallest corrected cut size.

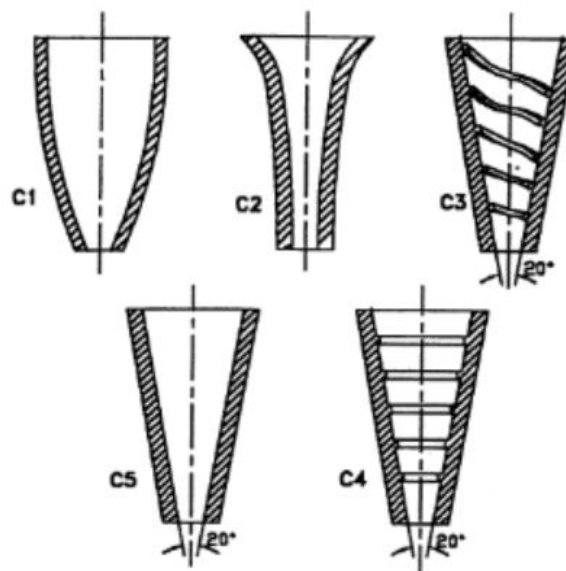


Figure 3.8: 5 Conical shapes [6]

Conical sections composed of two cone combinations found a higher separation efficiency for smaller particles, which is not required when sediment needs to leave through the vortex-finder as much as possible. And implementing a special conical shape from figure 3.8 is risky as these have not been tested on large scale cyclones. However, the smooth surface cone obtained the smallest cut size. This means the other shape might be more promising when larger cut sizes are wanted.

**Underflow pipe**

The underflow pipe, also known as spigot or apex has a large influence on the performance of a hydrocyclone [39]. Experimentation and simulations have shown that when increasing the spigot diameter caused both the split ratio and separation efficiency to increase ([36],[17]). On the other hand, an extremely narrow underflow-pipe resulted in a very low separation efficiency and a small split ratio. Therefore, an optimum underflow-pipe diameter exists depending on its operation [36].

A variable spigot diameter is used by most commercial hydrocyclones. In order to obtain the optimum separation performance, the spigot diameter is highly critical, but it is a challenge to reliably predict [39]. In traditional hydrocyclones blockage is not an issue when working with low concentrations. The diameter of the particles that need to be separated normally vary around a couple of  $\mu\text{m}$ . As it is of extreme importance that the underflow is not blocked when mining at depths around 6000 meters, a wide enough underflow diameter needs to be implemented into the design of the prototype. An well-considered apex diameter should be selected with a minimal size but is large enough to be certain it is not obstructed during operation.

**Vortex-finder**

The vortex-finder can be described as a pipe section entering the cylindrical section of the hydrocyclone designed to prevent particles to directly escape into the overflow and induces the separated fluid to flow upward in an axial direction [28].

*Length*

The separation performance of a cyclone is strongly effected by the vortex-finder length. Numerous studies ([28], [24], [47], ) found the vortex-finder length should be shorter than length of the cylindrical section  $L_1$ . Generally the optimal length of the vortex finder is described as a ratio between the vortex-finders' length to a specified dimension of a hydrocyclones' component. Specifically the diameter or length of the cylindrical-section or the total length of of the vortex-finder and the conical section. From these ratio's for optimum vortex-finder length, the ratio vortex-finder length to cylindrical-section length is found the most appropriate [20].

This is the result of research done with narrow or small hydrocyclones. And it is difficult to determine if a optimum ratio for vortex-finder lengths exists as it is a function of geometric dimensions, flow rate, feed-particle concentration, particle size [37] particle density [38] etc. An interesting research of separating nodules from sea water and sediment, is done by Wand et al. The model created for the research shows that separation efficiency decreases for fine particles but increases for relative coarse particles as vortex-finder length decreases [61]. Therefore, a vortex-finder that is longer than the cylindrical section is not recommended.

*Diameter*

In the same model where they studied optimal vortex-finder length, Wang et al. [61] also find that a thin vortex finder is helpful to high separation efficiency for coarse particles. This comes with a downside, however. It would result in a larger pressure drop and a higher split ratio [61].

The cone ratio (ratio of apex diameter and vortex-finder diameter) is often used as one of the variables used to design hydrocyclones. However, Shah et al. [44] explain that the use of cone ratio can be misleading. As the underflow diameter and vortex-finder diameter are considered independent variables, the ratios between them are not suitable to be employed as variables [44].

In this case it is best to use ratios that have been implemented in the past. For example, Bradley and Rietema cyclones use  $D_{vf}/D_c$  as a standard ratio. Both ratios have values around 0.3. Because these ratios have proven to obtain low split ratios, a  $D_{vf}/D_c$  of 0.3 is found to be satisfying.

*Thickness*

The degree of influence on separation sharpness can be arranged in the following order: The diameter of the vortex-finder has a larger influence than its length, which in turn has a greater influence than the thickness of the walls [50]. This does not mean thickness has no influence at all. Research suggests ([6], [61]) that by decreasing the thickness of the vortex-finder walls, the separation efficiency will increase. Therefore a thin-walled vortex-finder is recommended. It should however be able to handle the wear and forces that are involved in the separation process.

### Shape

In the search for an optimum separation efficiency several shapes and structures have been tested for vortex-finders[6]. Figure 3.9 shows the vortex-finder shapes that were researched by Chu et al. They determined that the conventional thin walled straight pipe (on the left) had the smallest cut size.

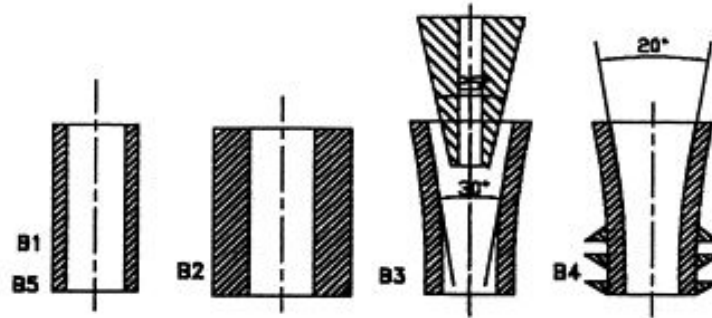


Figure 3.9: Vortex-finder structures tested by Chu et al. [6]

Besides different shapes, other structures have also been tested. E.g Wang et al.[62], changed the standard solid straight rod with a porous filter that allowed fluid to pass through but keep the particles out of the overflow. This significantly reduced short circuit flow and the turbulence surrounding the overflow pipe.

Many sizes, shapes and structures have been researched for the optimum vortex-finder. However, it cannot be determined if any of these shapes and sizes benefit separation efficiency for this particular hydrocyclone. The research done for these varying vortex-finder shapes was done with the purpose of separating extremely small particles with small cyclones. Accordingly the vortex-finder implemented into the design is recommended to be a standard, thin walled pipe that doesn't exceed the cylindrical section length  $L_1$ .

### Other parameters

As stated in the beginning of this section, the following geometric parameters can not be implemented into the design:

Separation technology	Definition
Inclination angle	Angle under which hydrocyclone is used
Insertion	Addition of objects influencing flow
Water injection	Water is injected into cyclone in conical section, flushing lighter particles toward the core
Reflux device	Device designed to reroute the exiting flows
Multi hydrocyclone arrangement	Combining cyclones in series and/or parallel to obtain higher efficiency

Table 3.2: Other geometric parameters capable of optimizing separation

It must be noted that these parameters have been examined in this research if they can help the separation of the nodules and if they can easily be implemented into the design. However, due to the restrictions caused by this research these parameters cannot be adjusted or implemented in the design of a prototype. That is why they are not reviewed or implemented in this research.

# 4

## Cyclone design

Now that it is established that cyclones can potentially separate nodules from the surrounding fluid and sediment under the proposed circumstances, a design can be constructed. The following section will illustrate the design process and shows a prediction of how this design is expected to perform. First a theorem is explained that determines the conical angle of the hydrocyclone. Secondly a design can be constructed with this angle and the information from the previous chapters. After this design is put together its performance is predicted by assessing individual particle behaviour. If the predicted performance is insufficient, the design has to be altered.

### 4.1. Conical angle

When designing a separation device inspired by a hydrocyclone the first thing that needs to be done is assessing the internal process. One of the main requirements is the continuous flow through the cyclone of both water and particles. This requirement restricts particles from remaining inside the cyclone. Otherwise the cyclone would act like a bag-less vacuum cleaner. Vacuum cleaners require emptying from time to time. This needs to be avoided.

In order to be certain of a constant flow of nodules and sediment a maximum conical angle  $\theta$  is constructed. When  $\theta$  becomes too large, the suspended particles would not be transported downwards. A holdup at the edge between the cylindrical and conical section is expected. A similar situation is where a roulette ball does not slide down towards the spinning wheel when the velocity is too high. It remains at the edge until its velocity is reduced. This situation is illustrated in the 2D figure 4.1a and gives the following theorem for the maximum conical angle  $\theta$ :

When the direction of the force vector created by, gravity, centripetal force and drag is perpendicular to the conical wall the particle does not move parallel along the wall in the illustrated 2D plain. Because the illustration is only meant to illustrate the direction of the force vector of the particle on the wall, the reaction force of the wall on the particle is left out.

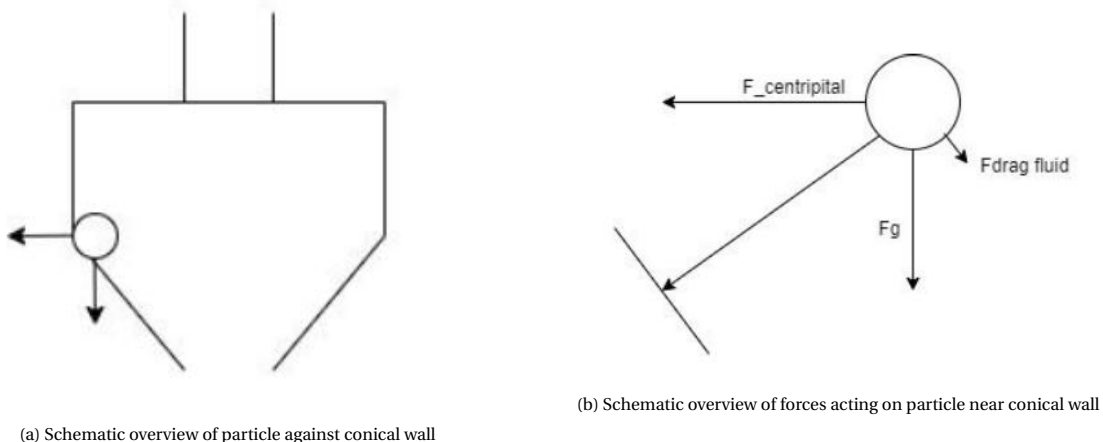


Figure 4.1: Particle-wall interaction

Figure 4.1b illustrates the the vectors of the centripetal, gravitational and drag forces. For the calculation of the resulting vector, several assumptions are made. As there is very little information about the processes outside the cyclone, the nodule velocity in axial direction is equal to the inflow velocity. The second assumption is that there is no drag

force created by wall-particle interaction. This is because little is known about the flow regime and the particle behaviour at this point. There is a chance particles bounce off the inner walls and do not slide along them. The third assumption for this calculation is that the smallest particles are the most crucial. As smaller particles are more likely to be influenced by the surrounding fluid and particles they are the ones the force calculation should focus on. Larger nodules are more likely to move down toward the apex. The last assumption is that the flow inside the cyclone is highly turbulent. It is reasonable to assume this before the final flow velocities and cyclone dimensions have been determined as it is known that the cyclone's size is approximately  $1 m^3$  and the flow is  $0.5 m^3/s$ .

From the three forces needed to obtain the direction of the total force vector, the drag force is considered first. The drag force,  $F_{drag}$ , acts in the direction of the apex and is dependent on the relative velocity,  $v_{rel}$  and the surface of the particle in the flow direction,  $A_p$ . Therefore the drag force on the particle is expected to be very low.

$$F_{drag} = 0.5A_p C_D \rho_{dw} v_{rel}^2 \quad (4.1)$$

The drag coefficient  $C_D$  is considered 0.4 for turbulent regimes[54].  $\rho_{dw}$  represents the deep-sea water density. This is equal to 1050 for depths around 4000 - 6000 meters[63]. This gives  $F_d = 1.65 \cdot 10^{-4} \cdot v_{rel}^2$  for the smallest nodules with 1mm diameter. For this case  $v_{rel}$  is assumed as a low as the nodule will have a velocity close to that of the surrounding current in the vertical direction.

This leaves a negligible low value for the drag force. Therefore, the direction of the total vector will be a combination of just the centripetal force and the gravity force. The masses in equations 4.2 & 4.3 must be adjusted to submerged weight according to Archimedes' principle.

$$F_g = mg \quad (4.2)$$

$$F_{centripetal} = \frac{mv_i^2}{r_{cylinder}} \quad (4.3)$$

Figure 4.2 illustrates the positions of  $\alpha$  and  $\theta$  that are needed for the determination of the conical shape. When  $\alpha$  is known, the conical angle can be found in the following way:

$$\theta = 180^\circ - 2 \cdot \alpha \quad (4.4)$$

Where  $\alpha$  is determined by:

$$\alpha = \tan^{-1}\left(\frac{F_{centripetal}}{F_g}\right) = \tan^{-1}\left(\frac{v_{nod}^2}{g \cdot r_{cyclone}}\right) \quad (4.5)$$

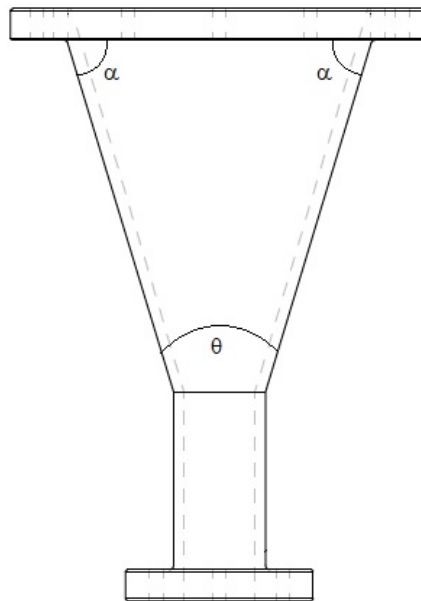


Figure 4.2: Angles  $\alpha$  and  $\theta$

A design can be constructed for the whole separation device not that it is possible to determine the maximum conical angle. This will be done by programming the cyclone geometric characteristics in Matlab. Together with the geometric suggestions made in chapter 3 and the theorem shown above, inputs are determined for the construction of the design.

## 4.2. Design determination

For the design of the separation device Matlab has been used. Matlab has been selected as the preferred tool as changing parameters will automatically adjust the design. One of the goals of the design is to minimize the volume of the cyclone. Therefore, minimization of the volume is always kept in mind.

### 4.2.1. Geometric dimensions

Some inputs are values that are not adjustable. The values like gravitational acceleration and water density are all set. However, these are not the only values that are set in the beginning. Nodule and sediment characteristics together with the incoming volume flow are all values that are not influenced by the design. These values are documented in the script before determining the geometric characteristics.

The first geometric parameter input is the cyclone diameter. The cyclone diameter is kept at a constant maximum value of 1 meter. The goal is to keep the volume below a maximum of  $1 \text{ m}^3$ . When the diameter is reduced, a smaller inlet is the result. A smaller maximum inlet surface would cause an increase in inflow velocity which causes the conical section to extend heavily as described in the theorem in the previous section. Therefore, the maximum allowable cyclone diameter of 1 meter is chosen.

The second parameter input is the apex diameter. This diameter must be chosen as small as possible. A large underflow diameter would cause large amounts of carrier fluid and sediment to escape through the underflow reducing the efficiency of the cyclone. However, this cannot be taken too small as blockage would be disastrous. Normally a pipe would be recommended to have at least 3 times the diameter of that of the largest particles passing through. But for this case this is unnecessarily large. According to table 2.5 the volume concentration of solids is only 0.0024. Also, the weight fraction of nodules exceeding 10 cm is only 20% of the nodules, which indicates an even lower chance of large particles being at the exit at the same time. Thus 2 times the diameter of the largest nodules is found to be sufficient[22].

For the following parameters compromises need to be made. As the cylindrical section diameter is limited, the inlet and the vortex-finder needs to fit next to each other, as the incoming slurry should not be pushed against the vortex-finder. This would result in higher velocities due to narrowing space, disturbed flows and probable particle - vortex-finder interaction. As classical Rietema and Bradly cyclones use a vortex-finder width to cyclone diameter ratio  $\frac{D_a}{D_c}$  of around 0.3 [42] this is implemented into the design. This leaves  $0.35 D_c$  for the inlet diameter.

The previous chapter explained that several hydrocyclones use a square inlet. For a short cyclone, the conical angle  $\theta$  needs to be large.  $\theta$  increases with a lower velocity of the stream. A larger inlet surface reduces the inlet flow velocity when the volume flow is constant.

$$V_{inlet} = \frac{Q_{inlet}}{A_{inlet}} \quad (4.6)$$

Taking a square inlet gives the maximum surface and therefore a lower average flow velocity. This results in a fixed inlet of 35cm ( $w_i$ ) by 35cm ( $h_i$ ). This 35 cm inlet height,  $h_i$ , is also chosen to be the height of the cylindrical section in order to minimization of the cyclone. Like the previous chapter explained, a cylindrical section is not always necessary and sometimes totally absent. Due to the inlet size and the simplicity of the design however, it is implemented here.

The vortex-finder length  $L_{vf}$  is the last dimension to be determined.  $L_{vf}$  has been subject to numerous researches with optimum length differing per objective as a result. This complicates defining a preferred length for this type of separation. However, as explained in the previous chapter, a vortex-finder length equal or shorter than the cylindrical section length is recommended. Because removing length is easier than adding it, the vortex-finder length will be equal to the cylindrical section length.

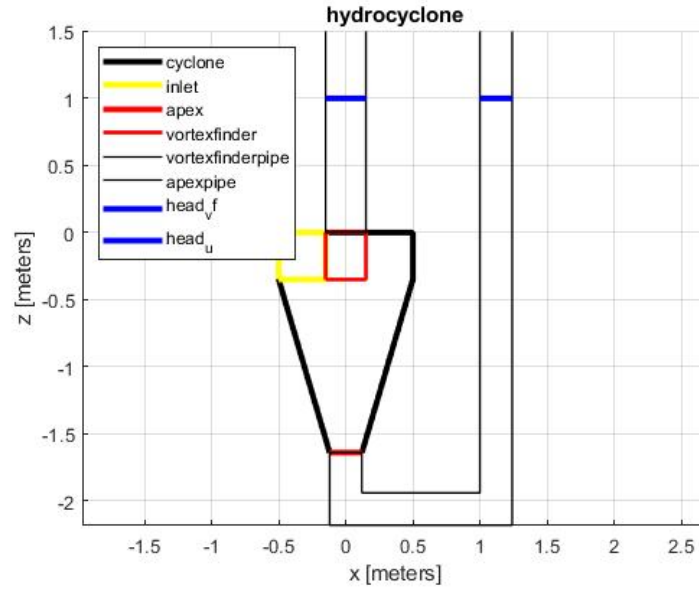


Figure 4.3: Hydrocyclone dimensions

With these values the prototype cyclone is designed. The calculated dimensions and parameters are illustrated in figure 4.3 and table 4.1. The resulting average inlet flow velocity is 4.08 m/s with these inlet dimensions. Implementation of equations 4.4 & 4.5 result in a conical angle  $\theta$  of  $32.8^\circ$ . Unfortunately, this results in a total cyclone length ( $L_{cycl}$ ) of 1.64 meters. Which indicates that if the theorem of the conical angle is correct, the cyclone would exceed its' preferred dimensions. However, because the conical angle theory is constructed with very conservative assumptions, it is likely  $\theta$  is too small in reality and the cyclone can probably be shorter.

$Q_i$	$D_c$	$w_i$	$L_i$	$D_{vf}$	$l_{vf}$	$D_u$	$L$	$\theta$	$V_{cycl}$	$T_{res}$	$v_i$
$0.5 m^3/s$	1m	0.35m	0.35m	0.3m	0.35m	0.24m	1.641m	$32.81^\circ$	$0.71 m^3$	1.43s	4.08m/s

Table 4.1: Hydrocyclone dimensions &amp; parameters

#### 4.2.2. Alternative angle

Because the conical angle design of the cyclone is conservative, a larger conical angle is researched. When testing a wider cone, the theory of circulating particles from section 4.1 can be investigated. The design with the conical angle of  $33.2^\circ$  is taller than 1m, which is undesirable due to the maximum dimensions introduced in section 3.1.2.

The velocity and direction of the arriving particles through the inlet depends on factors outside of the cyclone. Incoming angle of the inlet pipe, shape and flow velocity among others, all affect the way particles are introduced into the swirl. Not all factors can be take into account for the determination of a large conical angle. Therefore the second angle is determined with the assumption of particles arrive at  $0.5 v_i$  [22]. Implementing this velocity into equation 4.5 and 4.4 the cyclone with the larger conical angle has the following dimensions:

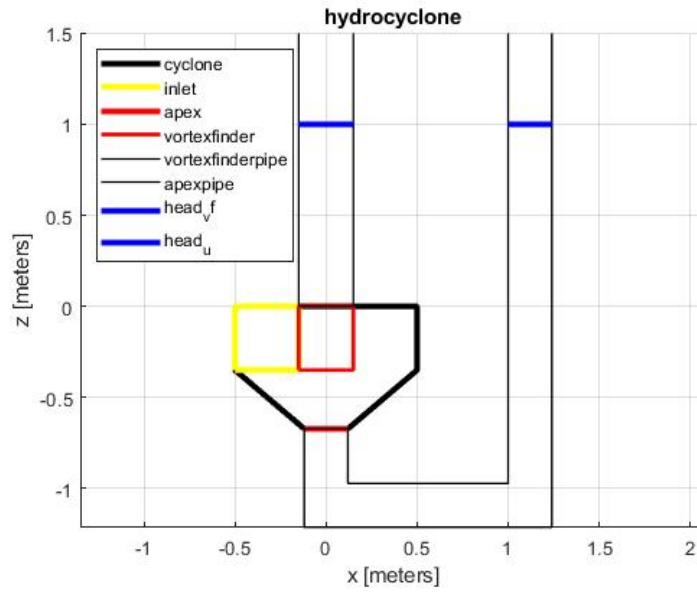


Figure 4.4: Dimensions hydrocyclone with larger conical angle

$Q_i$	$D_c$	$w_i$	$L_i$	$D_{vf}$	$l_{vf}$	$D_u$	$L$	$\theta$	$V_{cycl}$	$T_{res}$	$v_i$
$0.5m^3/s$	1m	0.35m	0.35m	0.3m	0.35m	0.24m	0.67m	$99.33^\circ$	$0.38m^3$	0.769s	2.04m/s

Table 4.2: Hydrocyclone dimensions &amp; parameters

The new conical angle is a lot larger than the original. This proves that the conical angle is very responsive to the velocity of the flow. Further investigation can provide further insight of the impact of the conical angle on the separation process.

### 4.3. Flow and particle behaviour

A prediction should be constructed of the performance of the designed cyclone. If the prediction is unfavourable, the design must be adjusted on order to enhance the cyclones performance. If no satisfying outcome is found, any future research is not recommended.

#### 4.3.1. Mixture viscosity

The viscosity of a slurry or mixture depends, amongst others, on the total volume concentration of solids[18]. A relation was proposed by Einstein (1906) describing the relative viscosity as a function of the volume concentration of solids. After Einstein described this relation three more researches have been conducted adjusting this theory. These adjustments prove to be more accurate for higher concentrations. Nonetheless, as figure 4.5 shows, for a low concentration of 0.024, Einsteins theorem proves to be sufficiently accurate.

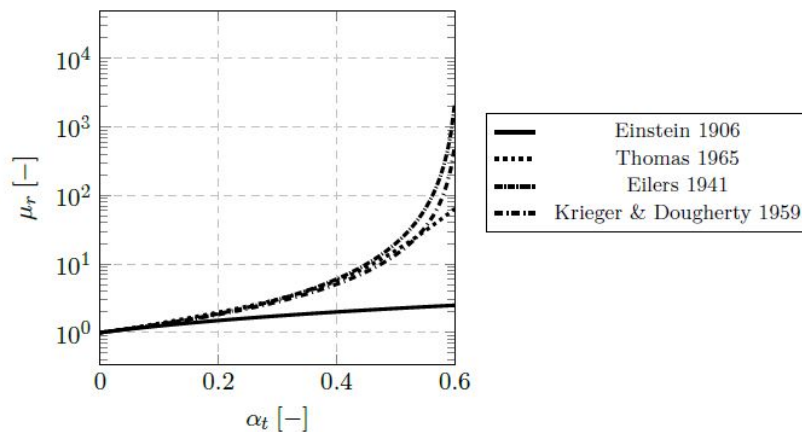


Figure 4.5: Mixture viscosity [18]

Einstein's function 4.7 describes relative mixture viscosity. This relative mixture viscosity is the ratio between the dynamic viscosity of the fluid and the dynamic viscosity of the mixture.

$$\mu_r = 1 + 2.5\alpha_t \quad (4.7)$$

Where  $\mu_r = \mu_m / \mu$  with  $\mu_r$  and  $\mu_m$  the relative mixture viscosity and mixture dynamic viscosity respectively. With a concentration,  $\alpha_t$  of 0.024,  $\mu_r$  has a value of 1.06. This indicates a very low change in viscosity due to the present solids. Einstein's relation only holds for dilute suspensions. As it has the same outcome as the other three relations, it can be concluded this mixture acts as a dilute suspension[18]. This means the solids in the flow do not have a significant effect on the rheology of the flow.

The presence of suspended particles is not the only factor that is different from normal sea water that largely influences the viscosity of the fluid. A fluid's viscosity is strongly a function of temperature. At depths varying from 4000 to 6000 meters the water temperature varies between 1 °C and 3 °C [41]. At these temperatures dynamic viscosity would roughly be 0.0017 Pa, which is 1.7 times higher than water at 20°[52].

### 4.3.2. Turbulence

Before investigating the behaviours of varying particles, the flow itself needs to be described. To be more precise, the turbulence of the flow inside the cyclone must be established.

$$Re = \frac{\rho_f v_i D_c}{\mu} \quad (4.8)$$

Equation 4.8 shows how the turbulence is calculated. Here  $D_c$  is chosen as the characteristic length scale and  $v_i$  as the fluid's velocity. All the necessary values are indicated in previous sections, and result in a Reynolds number of  $2.46 \cdot 10^6$ . This indicates a high turbulent flow regime inside the cyclone.

### 4.3.3. Particle behaviour

With the constructed design of a prototype, a prediction of the separation process is made. When the prediction does not indicate a proper functioning design, testing is irrelevant. Therefore a prediction is constructed for the different particle behaviours inside the hydrocyclone. The suspension contains a large variety in particle sizes and weight that all react uniquely to the surrounding fluid flow.

A hydrocyclone's separation method relies on centrifugal sedimentation. Particles can react in three categorized ways inside the cyclone:

1. Particles move toward the centre of the swirl.
2. Particles remain spread out in the flow.
3. Particles move toward the cyclone wall.

For particles to fall under the first category, their buoyancy,  $F_B$  should be positive. They must have a lower density than that of the surrounding fluid,  $\rho_s < \rho_f$ , in order to 'float' and move toward the centre of the vortex. It can be assumed that all particles collected from the ocean floor have a density higher than sea water. This option is therefore ignored and only options 2 & 3 remain.

If particles would circle for an infinite time, they will all move toward the cyclone wall if their density is higher than that of the fluid. However, the time a particle has for it to move toward the outside of the swirling flow is limited. An approximation of this time can be made by constructing the residence time of the fluid inside the cyclone. This residence time of the fluid can be approximated by dividing the volume of the cyclone by the volume flow.

$$\frac{V_{cyclone}}{Q_i} = T_{residence} \quad (4.9)$$

The geometry of the preliminary design above and a flow of  $0.5 \text{ m}^3/\text{s}$  result in an estimated average residence time of the fluid of 1.42 seconds. For a cyclone with a larger  $\theta$ , and thus a smaller size, this residence time will decrease even further. Therefore the following assumption is made: If a particle holds its original trajectory when entering the cyclone toward the cyclone wall, it can be separated from the rest of the fluid in time for it to leave through the underflow. If a particle does not follow its original trajectory coming out of the inflow pipe and gets carried by the surrounding flow it can be assumed this particle remains suspended for the time it spends inside the cyclone.

#### 4.3.4. Particle response

Chapter 2.1.3 indicates the nodules do not experience the presence of the sediment due to the size differences, weight differences and low concentrations. This only leaves the particle-fluid interaction to be investigated. The Stokes number is an inertia parameter characterizing the particle motion that is often used for prediction of a particles reaction in a flow. [25]. This number is the ratio between the adjustment time of a particle to its surrounding compared to the timescale of adjustments in this surrounding.

$$Stk = \frac{\tau_p}{\tau_f} \quad (4.10)$$

Where  $Stk$  is the particle Stokes number with  $\tau_p$  and  $\tau_f$  the particle and the fluid response time respectively. For the prediction of the individual particle behavior in the cyclone, the rotation time of the fluid in the cyclone can be used for  $\tau_f$ . The particle adjustment time  $\tau_p$  however, is more difficult to predict. This is because the governing force determining the adjustment time of the particle is the drag force  $F_d$ .

The determination of this  $F_d$  differs depending on the flow regime.  $F_d$  is dependent on the drag coefficient  $C_d$ . Equation 4.13 indicates that for the laminar ( $Re_p < 1$ ) and transition regimes ( $1 < Re_p < 2000$ ),  $C_d$  is a function of the particle Reynolds number defined as  $Re_p = \frac{w_0 d}{\nu}$ . Where  $\nu$  is the kinetic viscosity of the fluid and  $w_{0c}$  is the terminal settling velocity of the particle in the cyclone. The terminal settling velocity is found with equation 4.11.

$$w_{0c} = \frac{\Delta d^2 \sqrt{g^2 + a_c^2}}{18\nu + \sqrt{0.75\Delta d^3 \sqrt{g^2 + a_c^2}}} \quad (4.11)$$

Where  $\sqrt{g^2 + a_c^2}$  is the total acceleration due to centripetal force and gravity, and  $\Delta$  is the specific density, defined as:

$$\Delta = \frac{\rho_s - \rho_w}{\rho_w} \quad (4.12)$$

Equation 4.13 shows that for all flow regimes different relations apply for  $Re_p$  and  $C_d$ . However, for  $Re_p > 2000$  the  $C_d$  becomes independent from  $Re_p$  [54].

$$C_d = \begin{cases} \frac{24}{Re_p} & \text{for } 0 < Re_p < 1 \\ \frac{24}{Re_p} + \frac{3}{\sqrt{Re_p}} + 0.34 & \text{for } 1 < Re_p < 2000 \\ 0.4 & \text{for } 2000 < Re_p \end{cases} \quad (4.13)$$

This indicates that larger particles with higher  $w_0$  and larger diameters have a  $C_d$  independent of the  $Re_p$  and their particle motion can be considered independent of the viscosity of the surrounding flow. Table 4.3 shows the particle Reynolds number of the different individual particles.

Particle	Diameter [m]	$Re_p$
$D_{10}$	$1.80 \cdot 10^{-6}$	$6.17 \cdot 10^{-6}$
$D_{50}$	$8.70 \cdot 10^{-6}$	$6.93 \cdot 10^{-4}$
$D_{90}$	$6060 \cdot 10^{-5}$	$2.74 \cdot 10^{-1}$
Smallest nodules	$1.00 \cdot 10^{-3}$	$8.31 \cdot 10^1$
Average nodules	$6.45 \cdot 10^{-2}$	$4.95 \cdot 10^4$
Largest nodules	$1.20 \cdot 10^{-1}$	$1.26 \cdot 10^5$

Table 4.3: Particle Reynolds numbers per fraction

Table 4.3 clearly indicates that the nodules all have a  $Re_p$  value higher than unity. Depending on the regime a suiting parameter should be implemented for a successful prediction of the particle response. Therefore, two parameters,  $Stk$  and  $r$ , are proposed to predict the particle behaviour in the swirl in the cyclone. Depending on the combination of  $Stk$  and  $r$  a more accurate particle behaviour can be projected by determining the different regimes. Just like equation 4.10  $Stk$  and  $r$  both ratios of particle and fluid timescales. In order obtain  $Stk$  and timescale ratio  $r$ , three regimes are defined depending on the timescale at which particles move.

## 1. Free fall regime:

For this regime, the drag force caused by the fluid is completely neglected. This would be the case for dry granular flows. The corresponding micro timescale is equal to the time it takes for a particle to travel one particle diameter:

$$t = t_{micro}^{fall} = \frac{d_p}{\sqrt{\frac{P_p}{\rho_p}}} \quad (4.14)$$

## 2. Inertial regime:

In this regime, the range of motion is governed by the inertial drag force  $F_d$ .  $F_d$  for a circular fluid motion is given by  $F_d = C_d \rho_f d_p \sqrt{g^2 + a_c^2}$ . Where  $C_d$  is independent of  $Re_p$  for  $Re_p > 2000$ . The inertial micro time scale is equal to :

$$t = t_{micro}^{inert} = \frac{d_p}{\sqrt{\frac{P_p}{\rho_f C_d}}} \quad (4.15)$$

## 3. Viscous regime:

The motion of the particle is governed by the viscous drag and pressure in this regime. This results in a terminal settling velocity that is quickly reached. The drag force is dependent on the viscosity of the fluid. The viscous micro time scale is represented by:

$$t = t_{micro}^{visc} = \frac{\eta}{P_p} \quad (4.16)$$

Timescale ratio  $r$  corresponds to the ratio of the free fall timescale and the inertial timescale. The number  $r$  is obtained from equation 4.17.

$$r = \frac{t_{micro}^{fall}}{t_{micro}^{inert}} = \frac{\rho_p}{\rho_f C_d} \quad (4.17)$$

Combining equations 4.13 and 4.17 clearly indicates that  $r$  is independent from the fluids dynamic viscosity  $\eta$  for particles with high  $Re_p$  values.

$$r = \begin{cases} \frac{\rho_p}{\rho_f} \cdot \left( \frac{24}{Re_p} + \frac{3}{\sqrt{Re_p}} + 0.34 \right)^{-1} & \text{for } 1 < Re_p < 2000 \\ \frac{\rho_p}{0.4 \rho_f} & \text{for } 2000 < Re_p \end{cases} \quad (4.18)$$

The Stokes number in equation 4.19 is the ratio between the free fall time scale and the viscous time-scale. Not only is the  $Stk$  dependent on the fluid viscosity, it is also dependent on the particle pressure  $P_p$ . Equation 4.19 will be used in this research as the timescale ratio for particles with lower  $Re_p$  values.

$$Stk = \frac{t_{micro}^{fall}}{t_{micro}^{visc}} = \frac{d_p \sqrt{\rho_p P_p}}{\eta} \quad (4.19)$$

Where the Particle pressure is found with equation 4.20. Here the acceleration parameter is adjusted for the presence of centripetal acceleration indicated by  $a_c$ . The centripetal acceleration is calculated with inlet velocity and the radius of the cyclone in the following way:  $a_c = \frac{v_i^2}{r_c}$ .

$$P_p = \frac{2}{3} (\rho_p - \rho_f) d_p \sqrt{g_z^2 + a_c^2} \quad (4.20)$$

For the estimation of the governing flow regime the numbers  $r$  and Stokes can be used in the following way. For dry granular flows, which can be compared to free fall, the longest time scale is  $t_{micro}^{fall}$ . When  $r \gg 1$  and  $Stk \gg 1$  the effect of the interstitial fluid can be neglected. When the longest time scale is  $t_{micro}^{inert}$ , the regime is said to be inertial. This is the case when  $r \ll Stk$  and  $r \ll 1$ . For the viscous regime the longest time scale is equal to  $t_{micro}^{visc}$  and for this case the following applies,  $r \gg Stk$  and  $Stk \ll 1$  [18]. Figure 4.6a indicates when a particle finds itself in a specified regime.

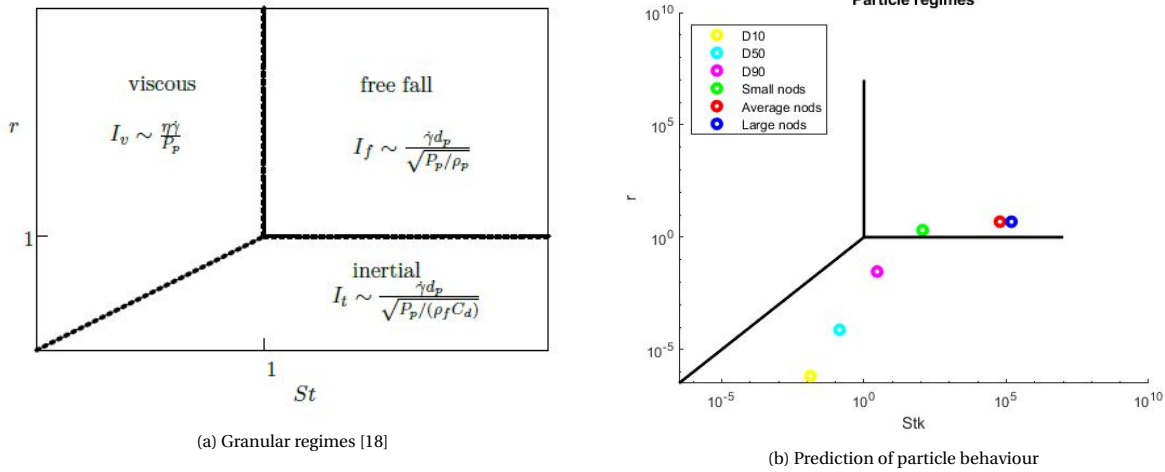


Figure 4.6: Particle behaviour

With the particle and flow characteristics, graph 4.6b is constructed. The particles that have been used for the construction of these graphs are the sediment fractions  $D_{10}, D_{50}, D_{90}$  and the smallest, average, and largest nodules. This graph helps predicting the particle behaviour in different flows. However, this prediction is not extremely accurate as  $Stk$  and  $r$  both utilize a specific aspect of the  $C_d$  behaviour relative to the  $Re_p$ . For turbulent  $Re_p$ ,  $Stk$  is an overestimate and for laminar  $Re_p$ ,  $r$  is very inaccurate. For turbulent and laminar particle Reynolds numbers this would not be a problem because for high particle Reynolds numbers  $r$  can be selected as the correct parameter. For low  $Re_p$  values  $Stk$  gives a reasonable prediction. However, for particles with  $Re_p$  values between 1 and 2000 a suitable solution needs to be found.

In order to find the appropriate particle responses graphs 4.7a and 4.7b are created. These graphs show the  $Stk$  and  $r$  values as a function of the  $Re_p$  of the sediment and nodules respectively. Matlab has been used for the creation of these graphs. The timescale ratios are easily obtained when the particle diameter is known, and the same counts for the  $Re_p$  values. However, obtaining the corresponding Stokes value from a particle Reynolds number is difficult. With Matlab, an array of diameters is generated, which is programmed to obtain both the corresponding timescale ratio values and  $Re_p$  values. Plotting these timescale ratio values against the  $Re_p$  values, results in graphs 4.7a and 4.7b. Besides the curves, the individual particle fractions are indicated on the graph. Two graphs are created separately because nodules and sediment have different densities.

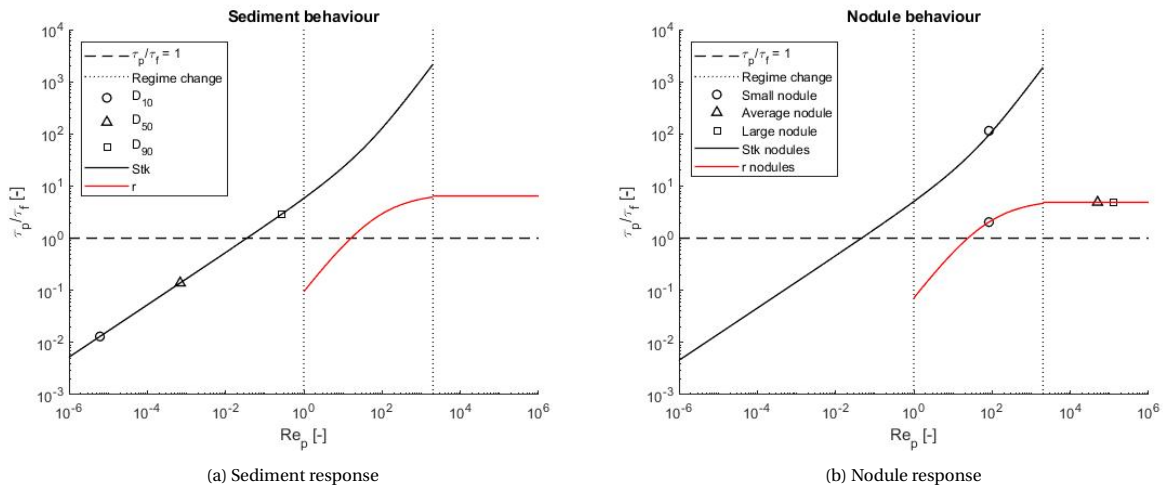


Figure 4.7: Particle predicted response

Particle	Stk	r	$Re_p$
$D_{10}$	$1.31 \cdot 10^{-2}$	$6.65 \cdot 10^{-7}$	$6.17 \cdot 10^{-6}$
$D_{50}$	$1.39 \cdot 10^{-1}$	$7.47 \cdot 10^{-5}$	$6.93 \cdot 10^{-4}$
$D_{90}$	2.89	0.03	$2.74 \cdot 10^{-1}$
Smallest nodules [1mm]	115	2.04	$8.31 \cdot 10^1$
Average nodules [64.5mm]	$5.96 \cdot 10^4$	4.88	$4.95 \cdot 10^4$
Largest nodules [120mm]	$1.51 \cdot 10^5$	4.88	$1.26 \cdot 10^5$

Table 4.4: Stk, r &  $Re_p$  values per particle

Table 4.4 shows the values from figure 4.7 of for the individual sediment and nodule fractions. Figure 4.7a and table 4.4 clearly show the  $Re_p$  values of the sediment are far below 1. Which makes the r value very inaccurate. The Stk values are more accurate when determining the sediment behaviour. Most sediment fractions have low Stk values. Only the largest fraction  $D_{90}$  has a Stk of 2.8. This gives the expectation that the suspended sediment will mainly follow the path of the surrounding flow. Only the largest sediment fraction  $D_{90}$  is expected to move more towards the outside of the cyclone as the Stk value is higher than 1. The sediment diameter with  $Stk = 1$  is equal to  $31.9 \mu\text{m}$ . According to graph 2.3, 73% of the total sediment volume has a value of  $Stk < 1$ .

As depicted in table 4.4, the smallest nodules have a  $Re_p$  value of 250. This means an appropriate timescale ratio needs to be found for these particles. An average, or other combinations, of Stk and r to obtain an accurate prediction are difficult to determine as Stk values rapidly increase where r quickly reaches its maximum. Therefore, it is found best for the lowest timescale ratio to be used for indication of the particle response in the transition regime. In this case r has lower value than Stk and is therefore the relevant ratio. As a result, all the nodule responses can best be described by timescale ratio r and the responses of all the sediment fractions are best described by Stk.

Table 4.4 shows all nodule r values are 2.04 or higher. In theory, this suggest their trajectory is dominated by their own inertia rather than the surrounding fluid. Which means these particles should move toward the edges of the cyclone directly. However in reality this remains to be seen for the smaller nodules. For larger nodules it can be assumed with more certainty that their movement is governed by its own inertia. In the graphs from figure 4.7  $C_d$  is taken as a constant of 0.4 [54], however in reality  $C_d$  is not constant for high  $Re_p$  values. The  $C_d$  decreases around  $Re_p = 10^5$  to 0.1 or 0.2 depending on the roughness of the particle[19]. Therefore, the r values for larger nodules are higher than illustrated above.

# 5

## Experimental setup

The previous chapters explained the design of this cyclone, what the possibilities of a hydrocyclone are and what the particle behaviour is expected to be. However, for a full feasibility analysis, further investigation is required. Not only the performance of this cyclone should be measured, the factors determining this performance are equally as important. For this research, experiments will be used as means of gaining further insight in the feasibility of a hydrocyclone.

### 5.1. Setup

In order to be able to gain insight in the performance of the cyclone and its influencing factors, the experimental setup needs to imitate the actual deep-sea nodule collection process while enabling analyses and measurements. Therefore, the setup should be a controlled environment that can generate a large flow rate, while transporting a low concentration of particles without air getting into the system. Figures 5.1 and 5.2 schematically illustrate the setup that is used for the experimentation process.

To illustrate the separation purpose of the settling tank, figure 5.1 displays a filled settling tank and figure 5.2 displays an empty tank in order to illustrate the different compartments inside the settling tank. For more detailed information about individual components or parts appendix A can be consulted. Table 5.1 shows the components corresponding with the numbers in figures 5.1 & 5.2

Number	Component
1	Centrifugal pump
2	Inlet pipe
3	Hopper system
4	Cyclone separator
5	Overflow pipe
6	Underflow pipe
7	Settling tank
8	Overflow measuring container
9	Underflow measuring container
10	Buffer to pump connection pipe
11	Flow regulating valves
12	Flow meters

Table 5.1: Setup components

Side view

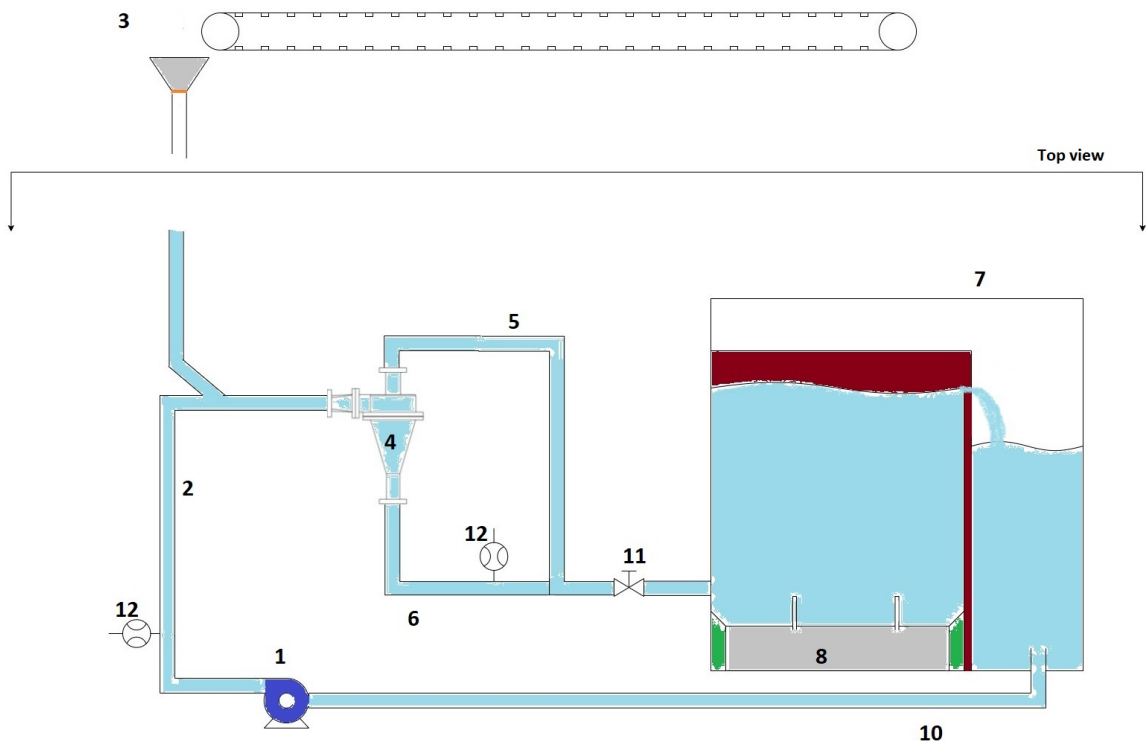


Figure 5.1: Side view of the experimental setup

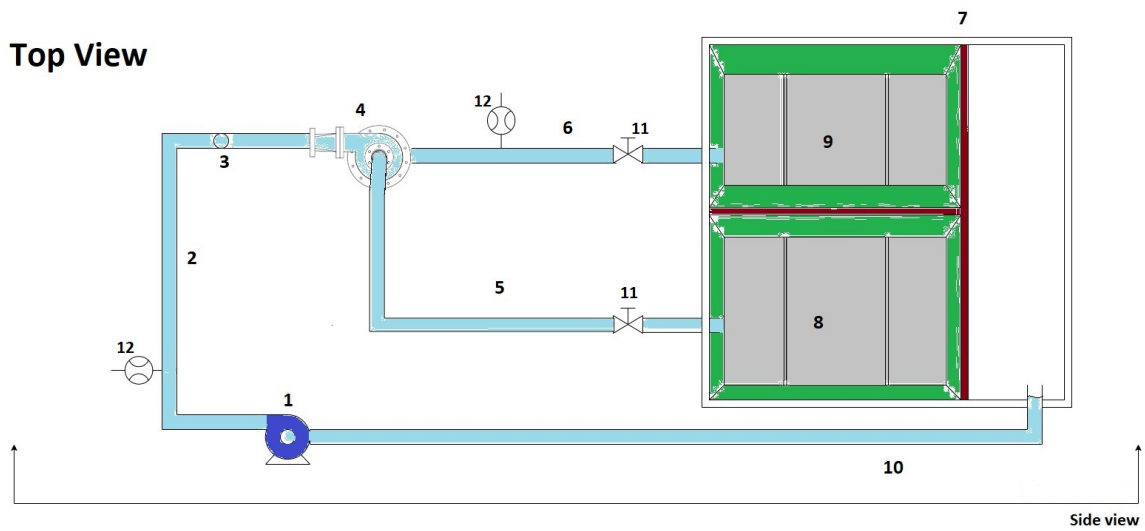


Figure 5.2: Top view of the experimental setup

**1. Centrifugal pump**

The flow is created by the centrifugal pump. This pump is able to deliver sufficient power and a specific capacity. Because the setup, and especially the cyclone, generates a high resistance while pumping a large volume of water and particles, a pump with a high capacity is preferred. Smaller particles can pass through the centrifugal pump. However, larger particles cannot as they will damage the pump. Therefore the larger particles need to be removed from the flow before entering the pump. The pump is operated by a frequency converter. This converter ensures that the pump runs on predetermined and constant RPM delivering a constant volume flow.

## 2. Inlet pipe

All the pipes used in this setup have an internal diameter of 5 cm. Because all internal diameters are known, the flow velocities in the entire system are known as well. When the flow velocity is determined in the inlet pipe, the cyclone inlet velocity is found by using the ratio of the cross areas of the inlet pipe and the cyclone's square inlet. Because the average flow velocity in the hopper system is equal to 0 during the experiment, the flow velocity into the cyclone can be controlled accurately.

The pipe runs from the pump to the cyclone with the inlet of the hopper system fitted in between. Therefore, the particles can be inserted into the stream without passing through the pump. For larger particles this is essential as they can damage the pump if they pass through it.

## 3. Hopper system

The hopper system consists of several individual parts. A conveyor belt that can deliver a constant supply of particles, a hopper to collect the particles from the conveyor belt and a transporting pipe connecting the hopper with the inlet pipe. The system is designed to insert particles into the flow without passing through the centrifugal pump.

The conveyor belt is used for a constant supply of particles. With the known velocity and the length of the conveyor belt the mass flow rate is accurately determined. For large particles with a high settling velocity the desired concentration in the flow can be simulated. For smaller particles however, this turns out to be not as straightforward. Because the particle settling velocity of smaller particles is low, and the mass flow of fines is too high, a plug is created. This interrupts the constant flow of particles.

Because the cyclone and rest of the pipes generate a resistance during operation, the pressure increases. As the hopper system is an open system, the water level in the pipe rises due to the pressure differences. Therefore, the vertical pipe connecting the hopper to the flow needs to reach as high as possible. This elevation is limited by the height of the facility, and the hopper is mounted at an elevation of 4 meters above the ground. This results in a maximum flow rate when carrying out experiments with the hopper system. If the flow rate exceeds its limit, the pressure created by the resistance becomes too large leading the hopper system to overflow.

Smaller particles are difficult to deliver into the flow because of their low settling velocity. Inserting these smaller particles into the system as a slurry helps the settling process and prevents the formation of a plug. When inserting the particles with a slurry a minimum volume has to be used for the particles to reach the inlet pipe. Because the particles settle so slow, they have to be forced downward. This is done by inserting a slurry excess. This surplus needs to be at least equal to the volume of the pipe. With a length of 310 cm and an inner diameter of 5 cm this surplus equals 6 liters.

## 4. Cyclone separator

This model cyclone separator is the scaled down version of the real cyclone that has been designed in the previous chapters. It has been made modular so different conical sections can be tested. Further information about cyclone is found in section 5.2

## 5. Overflow pipe

The overflow pipe is attached to the vortex-finder and transports water and the smaller particles to the overflow compartment in the settling tank. The overflow pipe enters the settling tank at the same height as the underflow pipe. Therefore the pressures at the underflow and the overflow ends are equal. Because the pressure is equal, the resistances generated by both the underflow and overflow pipe are similar, which is required when investigating the cyclones behaviour.

## 6. Underflow pipe

The underflow pipe is attached to the apex and guides the larger particles and the by-passed particles to the underflow compartment inside the settling tank. Depending in the split ratio, particles can accumulate inside this pipe when the flow velocity is too low.

## 7. Settling tank

The particles flowing out of the overflow and underflow pipe need to be captured. The particles have to be removed from the flow as the pump can be damaged by solids passing through it. Capturing the particles after separation is needed for the analysis of the partition curve of the cyclone. Due to the low concentrations of solids, concentration measurement devices are not suitable for this task.

The two streams will enter the settling tank in separate compartments. One for the overflow and one for the underflow. In these compartments particle settling occurs, leaving clean water at the water surface. These compartments both flow over a barrier, into a buffer section. This buffer section is needed for a constant supply of water into the pump. These areas of the sections have different sizes. The settling compartments sizes are determined with the terminal settling velocities of the smallest particle sizes that are used and the volume flow of the pump. If the particles settle

faster than the water column rises, the particles will not flow over the barrier. For the settling tank to do its work, the following requirement must be met:

$$v_{\text{watercolumn}} < w_0 \quad (5.1)$$

With requirement 5.1, the minimal particle size per compartment can be found. The compartment in which the overflow pipe ends has an area of  $0.42 \text{ m}^2$ , and the maximum inflow is equal to  $Q_i$  because several experiments will take place with a closed underflow. The underflow compartment has a surface area of  $0.29 \text{ m}^2$ , however the maximum inflow is smaller. The underflow only varies from the natural flow to zero because the underflow will be closed off during some experiments while the overflow will not. With  $v_{\text{watercolumn}}$  the minimal particle diameter is found by substituting equation 5.2 and the standard terminal settling velocity  $w_0$  into requirement 5.1.

$$v_{\text{watercolumn}} = \frac{Q_{\text{max}}}{A_{\text{container}}} \quad (5.2)$$

Both compartments have different surface areas and incoming flow. Therefore, both have a different minimal particle diameter that the settling tank can filter out. The largest particle diameter value found with requirement 5.1, is the minimal particle diameter the settling tank can handle. With the maximum flow of 228 liters per minute, this diameter is equal to  $100 \text{ }\mu\text{m}$ .

If the particles have a lower  $w_0$  than  $v_{\text{watercolumn}}$  of the compartment, there is a limited time an experiment can take before the particles will flow over the barrier. The velocity of the rising particle will be equal to  $v_{\text{watercolumn}} - w_0$ . This can be calculated for each individual particle size that is tested. However, this makes things unnecessarily complicated when experimenting with multiple ranges of smaller particle sizes for each experiment. Therefore, the time an experiment can take utilizing particle settling for smaller particles is equal to the time it takes for the water column to rise from the height of the inlet to the water surface.

$$t_{\text{experiment}} = \frac{H_{\text{barrier}} - H_{\text{inlet}}}{v_{\text{watercolumn}}} \quad (5.3)$$

The third compartment where the filtered flows of both the the settling compartments comes together, acts as a buffer. This is needed to provide a constant supply of water for the system. This minimal volume depends on the maximum volume flow created by the pump, and the volume of the entire system. Because the hopper is the only open section that can contain varying amounts of water, only a little volume is removed from the circulating flow.

Air can get into the pump when pumping water through the system. A sufficient supply and a pressure at the entrance of the pump will prevent this. Therefore, the pump is placed at the lowest possible point. When pumping an average of 228 liters per minute, a buffer of 300 liters is sufficient. Even when experiment requires twice the volume flow, and the flow to the buffer would somehow be blocked, the buffer can provide the pump with water for more than half a minute.

### 8 & 9. Measurement containers

To determine the partition of different particle sizes the particles need to be collected from both the overflow and underflow. Fitting containers inside the compartments have been constructed for this purpose. Number 8 represents the container in the overflow compartment whereas number 9 represents the container in the underflow compartment. Figure 5.3 illustrates the design of these containers. On the walls of the settling compartments steep edges have been placed, illustrated by the green areas in figures 5.1 & 5.2, to guide all the particles toward the containers to ensure optimal collection.

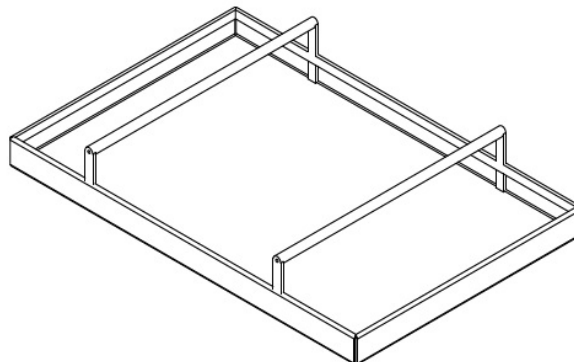


Figure 5.3: Schematic design of a measuring container

### 10. Buffer to pump connection pipe

A constant, clean and sufficient water supply must be available for the centrifugal pump. In order to close the loop, a pipe connects the clean buffer with the centrifugal pump.

### 11. Valves

Valves are installed to control the over and underflow. The valve at the underflow can be closed to change alter the split ratio to zero. The overflow valve however, is not used for the control of the flow directions, but rather for the cleaning of the cyclone and the underflow pipe when particles are hard to remove.

### 12. Flow sensors

The inlet pipe and the underflow pipe both have a flow meter equipped. Based on conservation of mass, the flow leaving through the vortex-finder is known when the other flows are known. With the volume flows of the underflow and overflow, the split ratio is determined precisely.

## 5.2. Hydrocyclone separator

The cyclone described in the previous chapters, which is designed for deep-sea operation, will be referred to as the 'prototype' cyclone. The cyclone used for the experimental purposes will be referred to as the 'model' cyclone. The model needs to be as comparable as possible to the prototype. However, limitations of the facility makes this hard to accomplish. In order to gain the most valuable information from the experiments, the model separator is designed as large as possible.

Scaling of the cyclone is done with limiting factors keeping the size of the model to a maximum. The first limiting factor is the pump, which has a maximum flow rate. Where normally a volume flow  $Q_i$  of  $0.5 \text{ m}^3/\text{s}$  is expected to flow through the cyclone, the pump used for the experiments has a maximum volume flow  $Q_{pump}$  of  $0.0042 \text{ m}^3/\text{s}$ . Another factor is the cost of construction. Therefore the dimensions of the cyclone are adjusted in order to use as many standardized parts as possible.

The main scaling principle of the cyclone used for this research is keeping the accelerations constant for the model and the prototype cyclone. For the cyclone to have the have the same shape, the conical angle needs to be equal. This angle is calculated with equations 4.5 & 4.4. Therefore,  $\frac{v_i^2}{g \cdot r}$  is constant for the model and the real cyclone. This results in the following equation:

$$\frac{v_i^2}{g \cdot r_c} = \frac{v_{model}^2}{g \cdot r_{model}} \quad (5.4)$$

Where  $v_i = Q_i / A_{inlet}$  and  $A_{inlet} = (0.35D_c)^2 = (0.7r_c)^2$

$$v_{model} = \sqrt{\frac{v_i^2 \cdot r_{model}}{r_c}} \quad (5.5)$$

As  $v_{model}$  can also be found with formula 5.6:

$$v_{model} < Q_{pump} / A_{inlet_{model}} \quad (5.6)$$

Combining equation 5.5 and 5.6 results in a maximum radius of the model cyclone. Implementing standard manufacturing sizes of  $r_{model}$  results in a maximum radius of 0.071m. Because the angles of the real cyclone and the model remain equal, the rest of the model cyclone dimensions can now be easily obtained. The same can be done for the second cyclone with the larger conical angle. The final designs of the two conical sections and the topside are illustrated in figures 5.4 and 5.5. Figure 5.6 shows the assembled cyclone with both cones. The  $v_{mod}$ , that results in the same angle as the prototype cyclone, is found with equation 5.4 and has a value of  $1.538 \text{ m/s}$ .

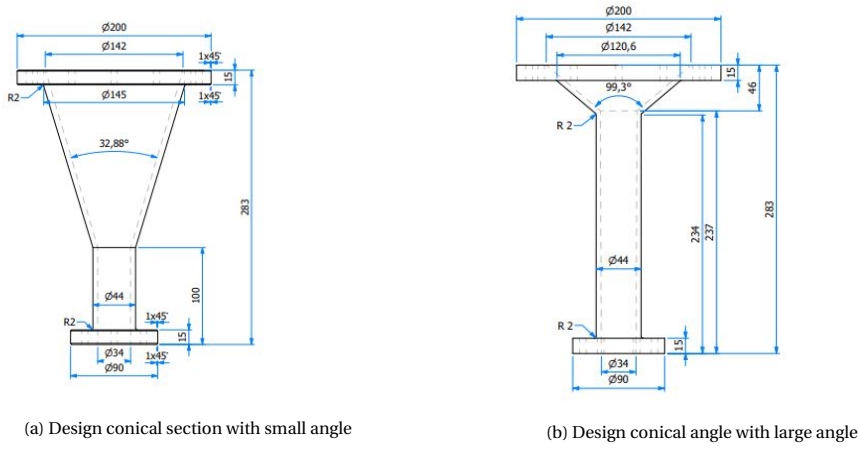


Figure 5.4: Model dimensions

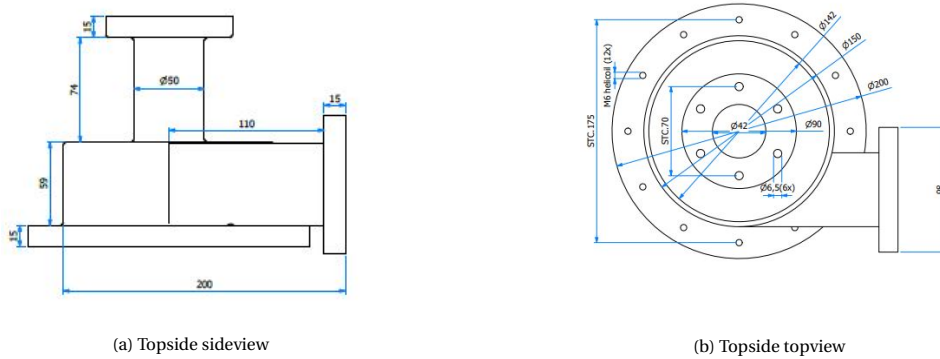


Figure 5.5: Topside dimensions

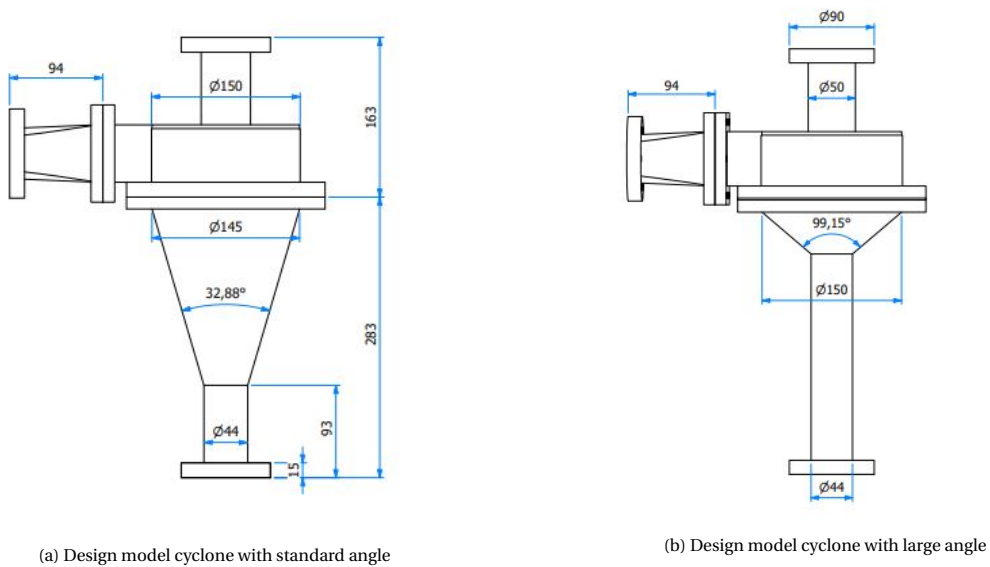


Figure 5.6: Assembled cyclone dimensions

This cyclone is made from PMMA which is a strong and transparent material that enables observation of the process inside this cyclone. PMMA has an optical breaking index of 1.49, which is close to water's 1.33[33]. Therefore, wear and damage sustained during usage does not obstruct the view of the inside of the cyclone when filled with water.

### 5.3. Particles

All the available particles have been separated into defined compact fractions and investigated for their relevant properties in order to accurately predict the prototypes' performance. More information about the separation method, measurements and particles properties can be found in appendix B. The density tests confirmed that the density of the particles used for the experiments is equal to the theoretically density of  $2650 \text{ kg/m}^3$  of quartz particles. And the settling tests give an accurate terminal settling velocity of all the individual fractions. However, these test have been carried out under normal gravity. Because settling in the cyclone takes place under centripetal conditions, the measured  $w_0$  is converted to the conditions under which the model cyclone operates. This is achieved by multiplying the the original  $w_0$  with  $g$  as the only acceleration coefficient, by the relative increase due to the centripetal acceleration as shown in equation 4.11:

$$w_{0c} = w_0 \cdot \frac{\frac{\Delta d^2 \sqrt{g^2 + a_c^2}}{18\nu + \sqrt{0.75\Delta d^3 \sqrt{g^2 + a_c^2}}}}{\frac{\Delta d^2 g}{18\nu + \sqrt{0.75\Delta d^3 g}}} \quad (5.7)$$

With the other known particle properties the Particle Reynolds number and the corresponding timescale ratios are calculated. Table 5.2 shows the tested particle ranges, the measured and converted settling velocities, the Particle Reynolds numbers and the corresponding timescale ratios.

$d_p$ range ( $d_0 - d_{100}$ ) [mm]	$\frac{d_0 + d_{100}}{2}$ [mm]	$w_0$ [m/s]	$w_{0c}$ [m/s]	$Re_p$	$Stk$	$r$
0.005 - 0.02	0.013	0.0005	0.0007	0.01	0.34	0.001
0.040-0.070	0.055	0.0021	0.0030	0.16	3.10	0.02
0.065-0.105	0.085	0.0051	0.0073	0.62	5.96	0.07
0.18-0.25	0.215	0.0327	0.0465	10.0	24.0	0.72
0.25-0.35	0.300	0.0424	0.0603	18.1	39.5	1.12
0.35-0.5	0.425	0.0634	0.0902	38.3	66.6	1.83
0.5-0.71	0.6050	0.0787	0.119	67.7	114	2.50
0.71-0.8	0.755	0.1034	0.1471	111	158	3.15
0.8-1.4	1.10	0.1134	0.1613	177	277	3.78
1.4-2.0	1.70	0.1886	0.2682	456	533	4.97
2.0-2.4	2.20	0.2124	0.3021	664	785	5.38
4.0-6.0.	5.00	0.4810	0.6841	3420	2689	6.63
8.0-12.0	10.0	0.6520	0.9273	9273	7605	6.63

Table 5.2: Particle properties and timescale ratios

### 5.4. Experimental protocol

Obtaining reliable data from the experiments is crucial for a scientific research. Therefore, consistent and accurate measurements must be made using the setup explained section 5.1. The way in which the measurements are done and how the setup is operated are explained in the following section. The extensive experimental protocol is presented in appendix C.

With the known particle, water and container properties, the particle weight gathered by each container can be found by weighing the filled containers. Because the mass conservation rule needs to be validated, the contents of both containers need to be compared with the total added particles in the flow. Besides measurement data, visual data is also collected. The transparent model cyclone is filmed using a high speed camera. This way the separation processes inside the cyclone can be researched and other findings can be observed. Investigating the filmed footage helps to understand the inner phenomena.

# 6

## Experiments

### 6.1. Parameters

In order to obtain information about the feasibility of a hydrocyclone varying setup settings need to be tested. For this research these parameters are: particle diameter, split ratio, and conical angle. Varying the particle concentration and adjusting the volume flow rate is helpful for a more extensive analysis. However, due to the restrictions explained in sections 5.1 & 5.1 these are difficult to regulate or measure.

#### 6.1.1. Particle diameter

A variety of particle diameters needs to be tested to be able to analyze the feasibility of the cyclone. Not only does the use of the specific particle sizes allow the creation of a partition curve, it also gives an insight in the particle- and flow-behaviour as well as the particle interaction inside the cyclone. Not all particle sizes are used for all settings of the setup because this would result in carrying out more experiments than necessary. Therefore, only several sizes are selected for experimentation.

The interesting particle diameters are those where the cutsize is expected, i.e. particles with timescale ratios around 1. However, even though the nodules and larger sediment are expected to leave through the underflow, several larger particles need to be tested as well. This helps to understand the particle behaviour of the larger particles even if their timescale ratio is much larger. During the tuning phase of the setup, the particles sizes of interest were identified. Table 6.1 shows the particles that were selected from table 5.2 and extensively tested.

$d_p$ range ( $d_0 - d_{100}$ ) [mm]	$\frac{d_0+d_{100}}{2}$ [mm]	$w_0$ [m/s]	$w_{0c}$ [m/s]	$Re_p$	$Stk$	$r$
0.005 - 0.02	0.013	0.0005	0.0007	0.01	0.34	0.001
0.040-0.070	0.055	0.0021	0.0030	0.16	3.10	0.02
0.065-0.105	0.085	0.0051	0.0073	0.62	5.96	0.07
0.18 - 0.25	0.215	0.033	0.0465	10.0	24.0	0.72
0.35 - 0.5	0.425	0.063	0.11	38.3	66.6	1.83
0.5-0.71	0.605	0.0787	0.119	67.7	114	2.50
8.0-12.0	10.0	0.6520	0.9273	9273	7605	6.63

Table 6.1: Particle properties and timescale ratios selected for research

#### 6.1.2. Split ratio

Because the feasibility of the cyclone does not only depend on the particles it can separate, but also on the amount of water that can be removed, a low split ratio,  $\frac{Q_u}{Q_{vf}}$ , is beneficial. In theory, particles with timescale ratios lower than 1 will remain distributed over the flow. Therefore, directing more water toward the vortex-finder will also remove more fine particles. Two different split ratios have been tested: the natural split ratio that occurs when both vortex-finder pipe and underflow have roughly equal resistance, and a split ratio of 0, where the underflow is totally closed.

#### 6.1.3. Conical angle

The third parameter that is researched is the conical angle. Sections 4.1 and 4.2 explain how the two conical angles were determined. By testing both cones the theory for the maximal conical angle explained in section 4.1 can be tested. But also the results of trapped particles due to an excessively large conical angle are relevant findings. Because both cones are transparent, the consequences of alternating angles can clearly be observed.

### 6.1.4. Flow rate

The flow rate of the original design is impossible to obtain with this setup. Depending on the conical angle and the split ratio, different flow rates are obtained due to resistance differences. For the original conical section, the flow rate decreased when the split ratio was reduced. However, for the large angled cyclone, the inflow velocity did not change when the underflow was cut off. Because the flow rates can be accurately measured and are important for further investigation, they are considered a variable parameter. Therefore, the different flow rates, which are converted to inlet velocities, are represented in the experimental matrix.

### 6.1.5. Experimental matrix

For an overview of the performed experiments, an experimental matrix has been composed. This matrix is illustrated in table 6.2. The density and settling tests of the particles are not indicated in this matrix. Neither are the experiments that have previously been conducted during the configuration of the setup and the determination of the specific particle sizes.

Experiment nr.	$\frac{d_0+d_{100}}{2}$ [mm]	Split ratio [-]	$v_i$ [m/s]	Conical angle [°]
1	0.013	0	1.03	32.9
2	0.055	0	1.03	32.9
3	0.085	0	1.03	32.9
4	0.215	0	1.03	32.9
5	0.425	0	1.03	32.9
6	0.605	0	1.03	32.9
7	10.00	0	1.03	32.9
8	0.013	0.54	1.11	32.9
9	0.055	0.54	1.11	32.9
10	0.085	0.54	1.11	32.9
11	0.215	0.54	1.11	32.9
12	0.425	0.54	1.11	32.9
13	0.605	0.54	1.11	32.9
14	10.00	0.54	1.11	32.9
15	0.013	0	0.99	99.3
16	0.055	0	0.99	99.3
17	0.085	0	0.99	99.3
18	0.215	0	0.99	99.3
19	0.425	0	0.99	99.3
20	0.605	0	0.99	99.3
21	10.00	0	0.99	99.3
22	0.013	0.41	0.99	99.3
23	0.055	0.41	0.99	99.3
24	0.085	0.41	0.99	99.3
25	0.215	0.41	0.99	99.3
26	0.425	0.41	0.99	99.3
27	0.605	0.41	0.99	99.3
28	10.00	0.41	0.99	99.3

Table 6.2: Experimental matrix

The experimental matrix indicates the different natural split ratios and the inlet velocities for both conical angles. These values have been determined during the calibration of the setup and the different cones. A different inlet velocity means a different maximum volume flow. The flow resistance of the original cone resulted in a maximum inflow of  $0.0028 \text{ m}^3/\text{s}$ , which corresponds with 72% of the designed flow rate. The wide angled cone, however, has a higher flow resistance and can only be tested up to  $0.0025 \text{ m}^3/\text{s}$ , which is equivalent to 65% of the originally designed flow rate. These flow rates are close enough to the original designed volume flow in order to predict the performance [22]. According to equation 4.8 both are still highly turbulent.

The mass concentration is not shown in figure 6.2. It has been attempted to reach the concentrations shown in table 2.2. However, only with the largest particles this concentration could be reached. Because all the other particles experienced settling hindrance in the hopper system, the desired concentrations were never consistently recreated. Because the original designed concentration is considered too low to influence the performance, an even lower concentration will not do so either.

## 6.2. Experimental observations

All the conducted experiments have been documented in an excel file. This way all the data is organized, and the outputs are easily converted to usable information files and stored. The experiments are reviewed here, using illustrations to display the relevant phenomena. A partition curve is introduced for both conical angles with a natural split ratio and a split ratio of 0. Because the partition of the smaller particles has been conducted with visual observation only, an error range has been implemented in the curve. Hence, a minimal, average and maximum partition is illustrated in the graphs. For further detailed information about the occurrences, the film footage and excel file can be consulted.

### 6.2.1. Original model

The original model cyclone is analysed here. The displayed observations are categorised per particle diameter. If different observations are made for different conditions they are schematically illustrated, side by side.

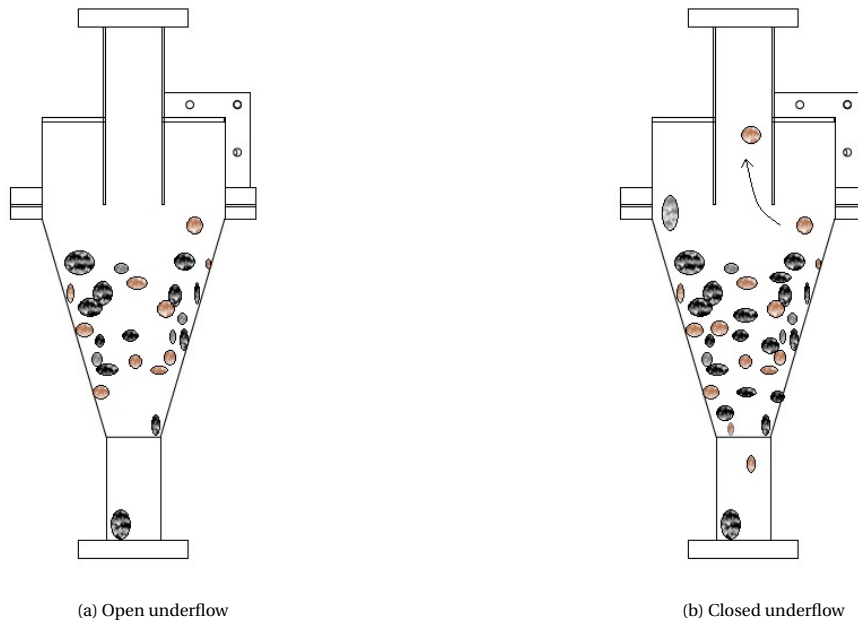


Figure 6.1: Original cyclone separation of 8-12 mm particles

Figure	$\theta$ [degrees]	Average $d_p$ [mm]	$v_i$ [m/s]	$c_m$	Split ratio	Stk	r	Partition [%]
6.1a	33.2	10	1.11	0.053	0.54	7605	6.63	100
6.1b	33.2	10	1.03	0.053	0	7605	6.63	97

Table 6.3: Parameters of original cyclone separation of 8-12 mm particles

**Figure 6.1a** Most particles keep rotating halfway through the conical section. This results in a crowded cyclone. The particles can be seen colliding with each other, mainly pushing each other downward in the direction of the underflow. All particles leave through the underflow when the underflow is open.

**Figure 6.1b** When the underflow is closed off, there is no flow that helps drag the particles toward the apex. Therefore, more particles accumulate inside the cyclone, called the crowding effect[34], until the point where some large particles are bounced toward the centre of the cyclone. This is where the inner vortex in the direction of the vortex-finder is located. Therefore, some large particles are captured by the vortex-finder and lost in the separation process. It is clear that without these collisions the large particles would all still leave through the underflow.

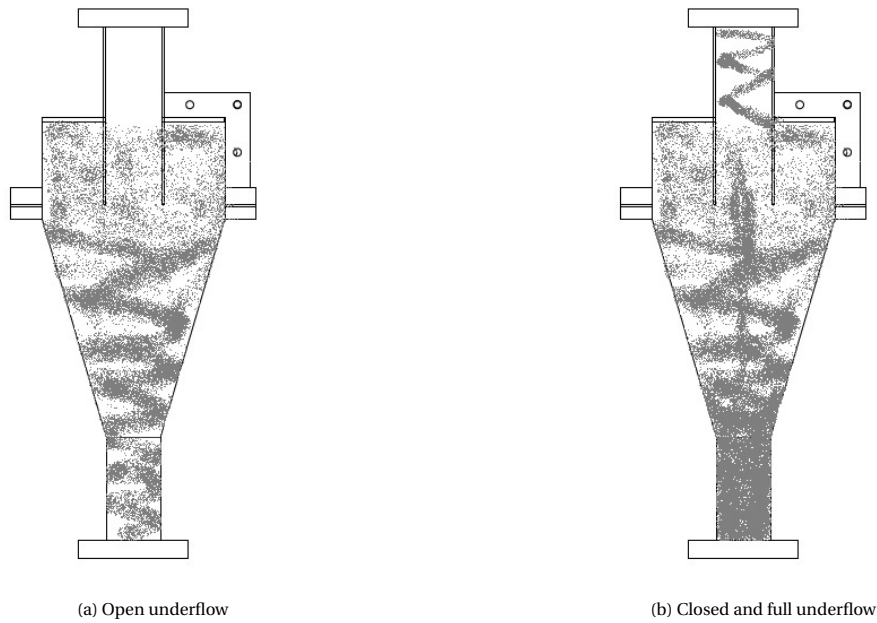


Figure 6.2: Original cyclone separation of 0.5-0.7 mm particles

Figure	$\theta$ [degrees]	Average $d_p$ [mm]	$v_i$ [m/s]	$c_m$	Split ratio	Stk	r	Partition [%]
6.2a	33.2	0.6	1.11	< 0.053	0.54	114	2.50	100
6.2b	33.2	0.6	1.03	< 0.053	0	114	2.50	100

Table 6.4: Parameters of original cyclone separation of 0.5-0.7 mm particles

**Figure 6.2a** This specific particle diameter is expected to roughly corresponds with the smallest nodules in reality. As expected all the particles report to the underflow. The particles can clearly be seen moving in a swirl.

**Figure 6.2b** All particles report to the underflow. It is clearly observed that all the particles move to the edge immediately. Therefore, this figure might be misleading. Because all the particles reported to the underflow, the underflow pipe filled up very fast leaving no space for other particles. However, the cyclone itself didn't fill up completely because all the particles that got close to the central vortex were captured by this flow. Therefore, the process inside the cyclone can still clearly be seen instead of just a moving bed of particles.

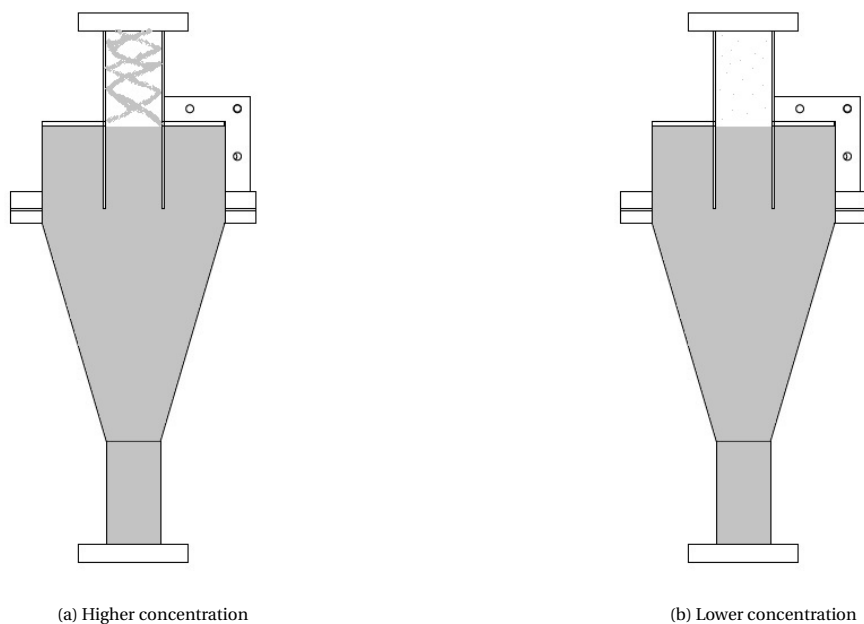
Figure 6.3: Original cyclone separation 65-105  $\mu\text{m}$  particles

Figure	$\theta$ [degrees]	Average $d_p$ [mm]	$v_i$ [m/s]	$c_m$	Split ratio	Stk	r	Partition [%]
6.3a	33.2	0.085	1.11	> 0.053	0 & 0.54	5.96	0.07	$70 \pm 10$
6.3b	33.2	0.085	1.03	< 0.053	0 & 0.54	5.96	0.07	$85 \pm 5$

Table 6.5: Parameters of original cyclone separation of 65-105  $\mu\text{m}$  particles

**Figure 6.3a** This specific particle diameter will roughly corresponds with the largest sediment grains in reality. The particles report to the underflow mostly. The particles can not be individually distinguished and there is no path the particles follow. Only when an increase in concentration can be observed, streams of particles can be seen leaving through the overflow.

**Figure 6.3b** Almost all particles report to the underflow. However, unlike the larger fractions, these particles do not move toward the cyclone wall directly. However, it appears to be sufficient to mainly stay out of the central vortex,

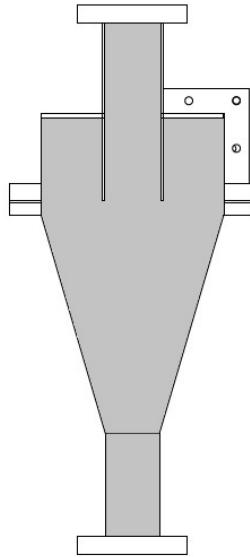
Figure 6.4: Original cyclone separation of 40-70  $\mu\text{m}$  particles

Figure	$\theta$ [degrees]	Average $d_p$ [mm]	$v_i$ [m/s]	$c_m$	Split ratio	Stk	r	Partition [%]
6.4	33.2	0.055	1.11	< 0.053	0.54	3.10	0.02	35
6.4	33.2	0.055	1.03	< 0.053	0	3.10	0.02	5

Table 6.6: Parameters of original cyclone separation of 40-70  $\mu\text{m}$  particles

**Figure 6.4** The smallest fraction that was tested clearly is not separated by the cyclone. The particles inside of the cyclone are equally distributed over the entire flow. The flows leaving through the apex and vortex-finder look similar. When the underflow was cut, a very small amount of particles precipitated in the underflow pipe. This is probably due to the bypass effect. When cleaning the underflow pipe after the experiment, these particles were transported into the overflow separation section of the settling tank where they clearly settled more than in the overflow section.

### 6.2.2. Partition curves original model

The partition curves of the original model, that have been constructed from the visuals, are illustrated below.

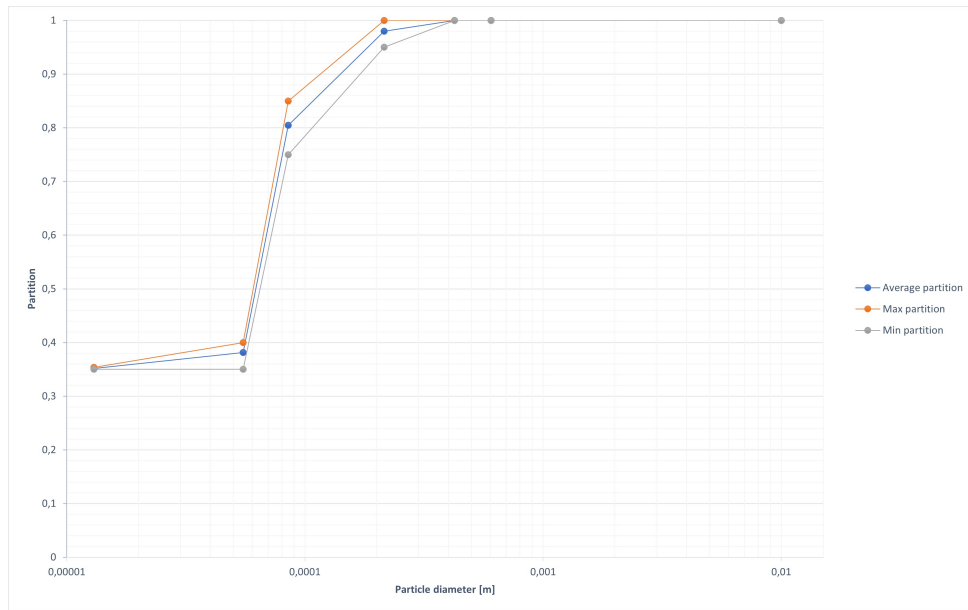


Figure 6.5: Partition curve original model with open underflow and low concentration

$\theta$ [degrees]	$\rho_s$ [ $kg/m^3$ ]	$v_i$ [m/s]	$c_m$ [-]	Split ratio [-]	$d_{50}$ [ $\mu m$ ]
33.2	2650	1.11	< 0.053	0.54	$\approx 65$

Table 6.7: Original cyclone with closed underflow partition curve parameters

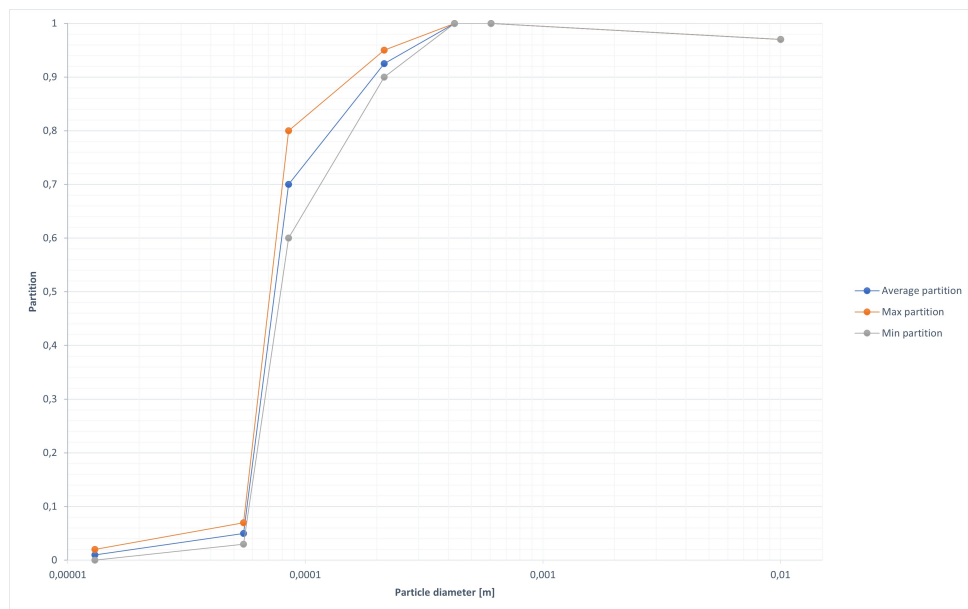


Figure 6.6: Partition curve original model with closed underflow and low concentration

$\theta$ [degrees]	$\rho_s$ [ $kg/m^3$ ]	$v_i$ [m/s]	$c_m$ [-]	Split ratio [-]	$d_{50}$ [ $\mu m$ ]
33.2	2650	1.03	< 0.053	0	$\approx 65$

Table 6.8: Original cyclone with closed underflow partition curve parameters

### 6.2.3. Large angled model

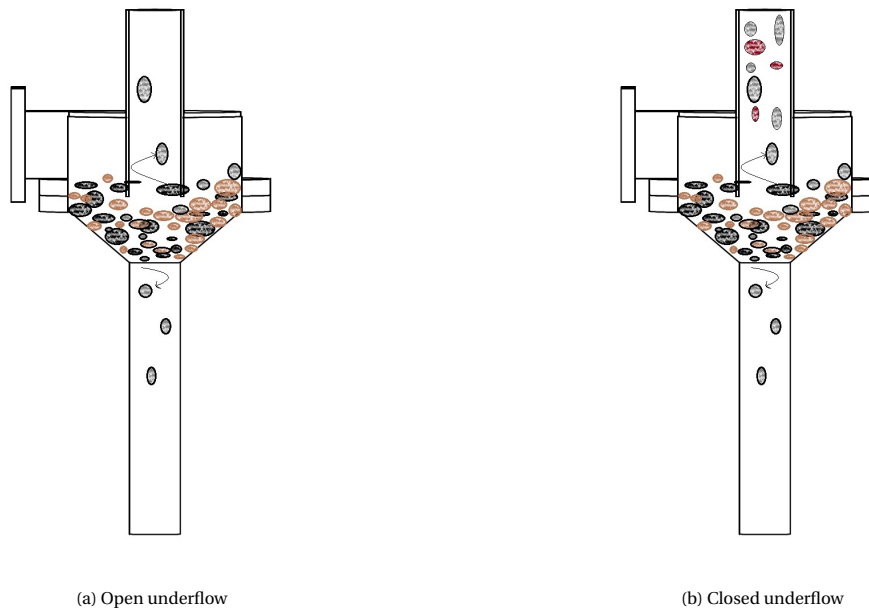


Figure 6.7: Large angled cyclone separation of 8-12 mm particles

Figure	$\theta$ [degrees]	Average $d_p$ [mm]	$v_i$ [m/s]	$c_m$	Split ratio	Stk	r	Partition [%]
6.7a	99.3	10	0.99	0.053	0.40	7605	6.63	$50 \pm 10$
6.7b	99.3	10	0.99	0.053	0	7605	6.63	$25 \pm 5$

Table 6.9: Parameters of large angled cyclone separation of 8-12 mm particles

**6.7a** No particle leaves the cyclone without being forced through particle interaction. Particles keep rotating inside the cyclone if nothing obstructs them. The vortex-finder entrance is close to the apex which causes particles to move in both directions. Around half of the all the particles leaves through the vortex-finder.

**6.7b** All particles keep circling around the centre at outer wall of the cyclone. Only the pushing of other particles cause circulating particles to move toward the centre. Because the flow through the apex is blocked, the particles that get pushed to the centre are most likely to leave through the overflow. 3 out of 4 particles are lost due to the suction of the vortex-finder and the lack of flow through the apex.

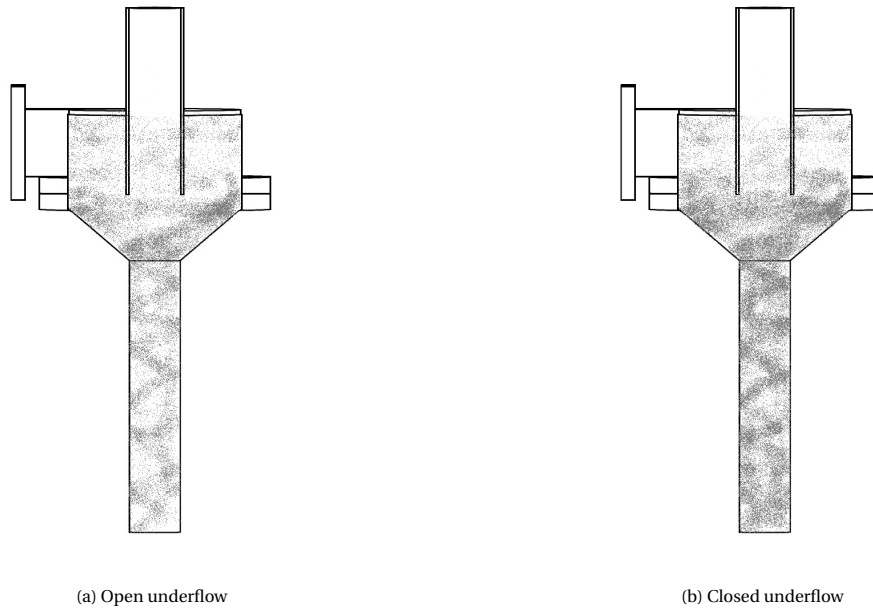


Figure 6.8: Large angled cyclone separation of 0.5-0.7 mm particles

Figure	$\theta$ [degrees]	Average $d_p$ [mm]	$v_i$ [m/s]	$c_m$	Split ratio	Stk	r	Partition [%]
6.8a	99.3	0.6	0.99	< 0.053	0.40	114	2.50	100
6.8b	99.3	0.6	0.99	< 0.053	0	114	2.50	100

Table 6.10: Parameters of large angled cyclone separation of 0.5-0.7 mm particles

**6.8a** The particles all report to the underflow. There is no visual difference between the partition for both cones.

**6.8b** More particles remain inside the cyclone which causes the concentration to go up inside the cyclone. Even though all particles still report to the underflow, the lack of underflow does have an affect on the residence time of the particles inside the cyclone.

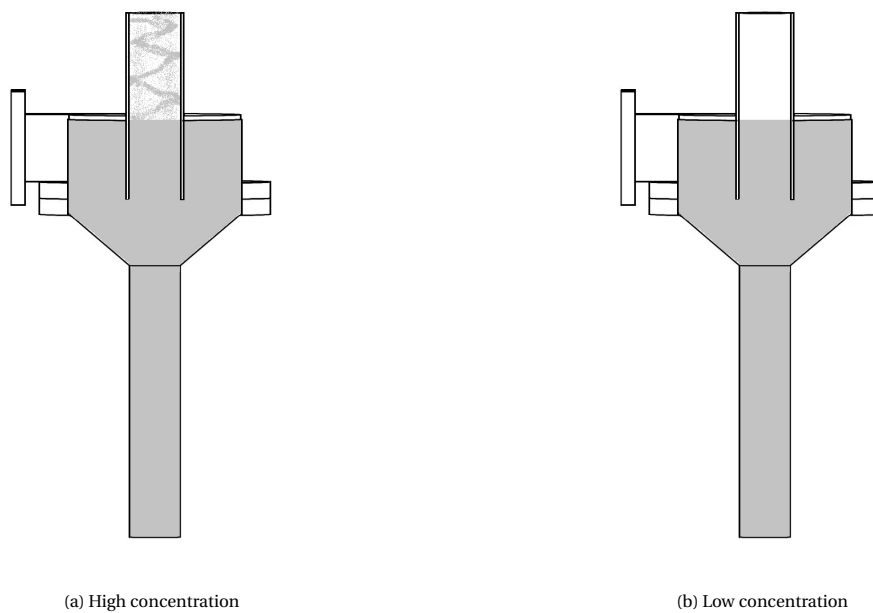
Figure 6.9: Large angled cyclone separation of 65-105  $\mu\text{m}$  particles

Figure	$\theta$ [degrees]	Average $d_p$ [mm]	$v_i$ [m/s]	$c_m$	Split ratio	Stk	r	Partition [%]
6.9a	99.3	0.6	0.99	> 0.053	0 & 0.40	5.96	0.07	60-80
6.9b	99.3	0.6	0.99	< 0.053	0 & 0.40	5.96	0.07	80-90

Table 6.11: Parameters of large angled cyclone separation of 65-105  $\mu\text{m}$  particles

**6.9a** Most particles report to the underflow. However, when the concentration fluctuates the partition changes. When a higher concentration enters the cyclone, the particles are clearly more likely to leave through the overflow than when the concentration is lower.

**6.9b** When the concentration is low, most particles report to the underflow. This is similar to the other cone.

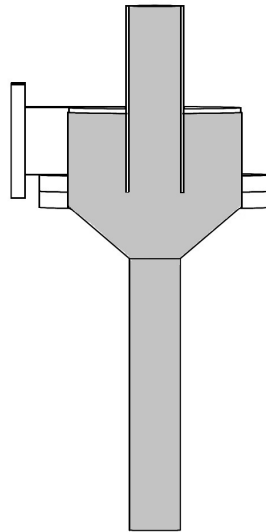
Figure 6.10: Large angled cyclone separation of 40-70  $\mu\text{m}$  particles

Figure	$\theta$ [degrees]	Average $d_p$ [mm]	$v_i$ [m/s]	$c_m$	Split ratio	Stk	r	Partition [%]
6.10	99.3	0.6	0.99	< 0.053	0.40	3.10	0.02	30
6.10	99.3	0.6	0.99	< 0.053	0	3.10	0.02	5

Table 6.12: Parameters of large angled cyclone separation of 40-70  $\mu\text{m}$  particles

**6.10** Clearly the particles do not separate from the flow. They are still evenly distributed. These particle sizes cannot be separated by the cyclone. The change of split ratio does not influence this.

### 6.2.4. Partition curves large angled model

The partition curves of the large angled model, that have been constructed from the visuals, are illustrated below.

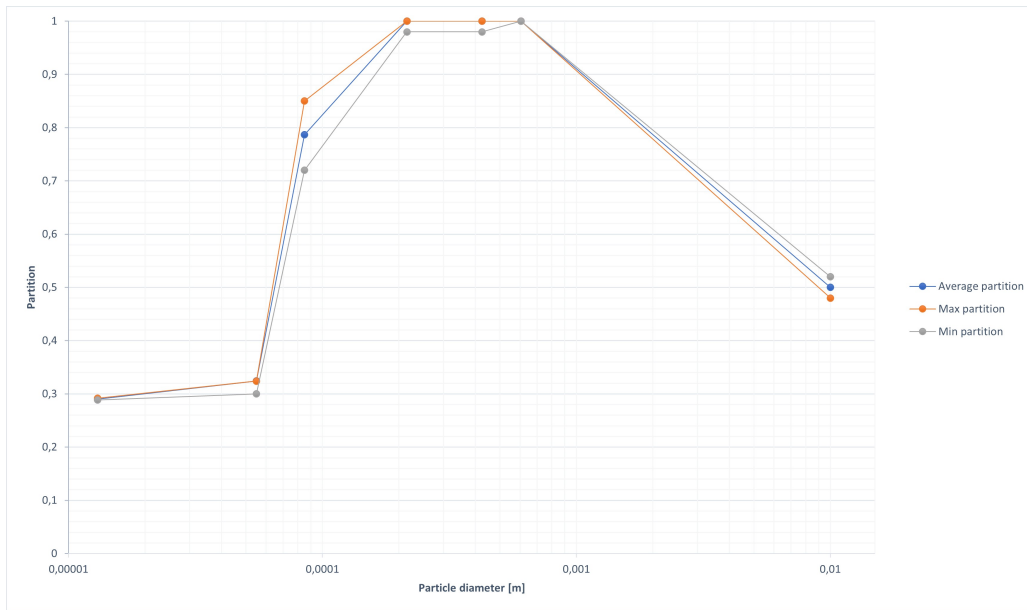


Figure 6.11: Partition curve large angled cyclone with open underflow and low concentration

$\theta$ [degrees]	$\rho_s$ [ $kg/m^3$ ]	$v_i$ [m/s]	$c_m$ [-]	Split ratio [-]	$d_{50}$ [ $\mu m$ ]
99.3	2650	0.99	< 0.053	0.4	$\approx 65$

Table 6.13: Large angled cyclone with open underflow partition curve parameters

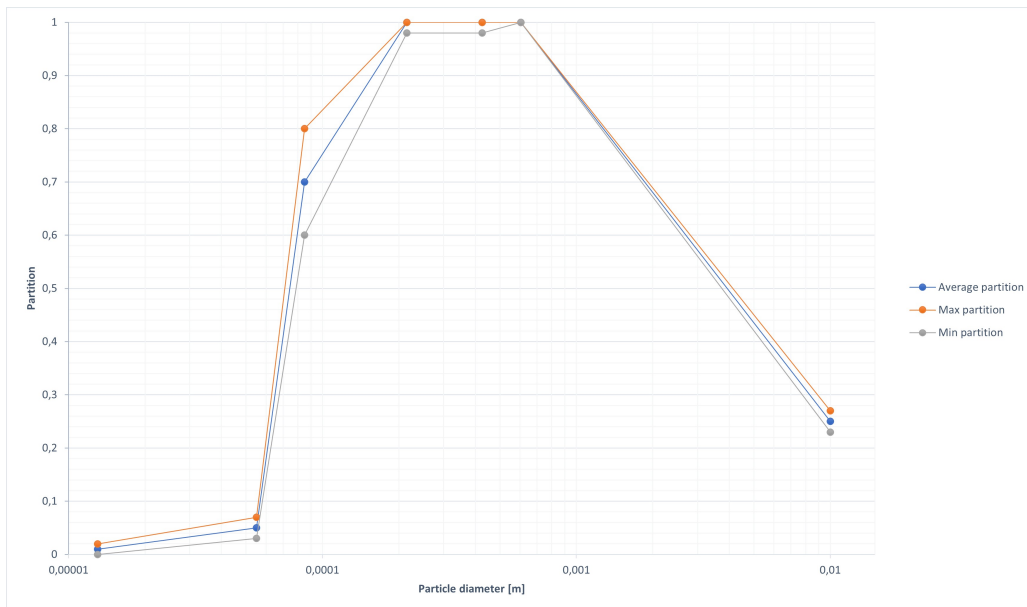


Figure 6.12: Partition curve large angled cyclone with closed underflow and low concentration

$\theta$ [degrees]	$\rho_s$ [ $kg/m^3$ ]	$v_i$ [m/s]	$c_m$ [-]	Split ratio [-]	$d_{50}$ [ $\mu m$ ]
99.3	2650	0.99	< 0.053	0	$\approx 65$

Table 6.14: Large angled cyclone with closed underflow partition curve parameters

# 7

## Analysis

Capacity, cut size, sharpness of separation and split ratio have been identified as the important performance parameters in this research. For the determination of the performance of the prototype cyclone, the findings of the model experiments need to be analyzed and scaled to represent prototype data. This data is compared to a performance prediction with the information from chapters 3 & 4. If the theoretical performance and the experimental data vary, a possible explanation is given. Besides the partition curve and split ratio, other experimental phenomena are analyzed, for a more complete overview of the cyclones' performance.

### 7.1. Predicted performance

When the primary goal of the device is separating sediment and surrounding water from the nodules as efficient as possible, the cyclone's performance is estimated by constructing a projected partition curve and finding the split ratio. The partition curve is a function of the split ratio. Smaller particles with lower Stokes numbers are assumed to remain suspended in the fluid which leads to the assumption that the bypass of fine material is equal to the percentage of the flow leaving through the underflow which is directly related to the split ratio.

#### 7.1.1. Cut size

The cut size is assumed to be the particle size where the timescale ratio is close to 1. Particles with high  $Stk$  &  $r$  values move toward the edge more quickly than the other particles. These particles will have maneuvered toward the outer edge of the swirl quickly enough to exit through the underflow pipe. For the prediction of the partition curve these particles with higher timescale ratios can be assumed to all leave through the underflow. This size varies for nodules and sediment because of density and shape differences.

With the assumed cut sizes a performance curve for both sediment and nodules is drawn up in figure 7.1. Both horizontal axes range from  $0.32 \mu m$  to 1 cm with logarithmic scale. It can clearly be seen that the diameters of the particles where the timescale ratio is equal to 1 is larger for nodules than that of the sediment.

Graph 7.1a indicates that not all the sediment is larger than the cutsize, which means not all the sediment is separated from the nodules. This gives reason to suspect that the large sediment fraction will mainly leave through the underflow. However, the particles smaller than the assumed cut size of  $31.9 \mu m$  take up to 73% of the total volume according to figure 2.3. Notably, all nodule sizes lie underneath the curve in graph 7.1b, indicating a large separation efficiency.

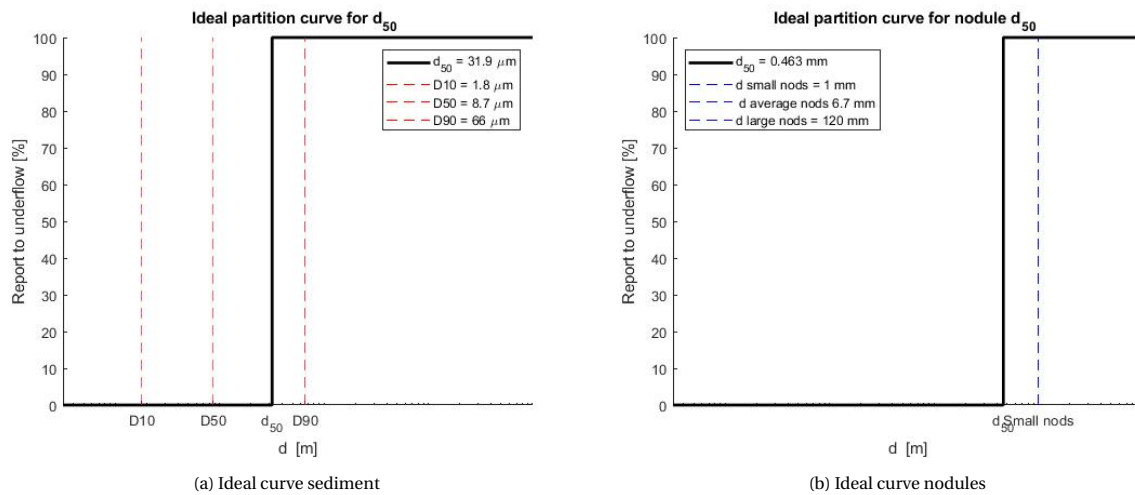


Figure 7.1: Ideal performance curves when sharpness of separation is neglected

### 7.1.2. Separation sharpness

As explained in chapter 3 an ideal partition curve does not exist. In order to obtain a more realistic curve, firstly, the separation sharpness is implemented. The sharpness of separation is complicated to predict theoretically. Because the proposed separation process lies outside the extremes of previous experimental data, the cyclones performance is uncertain due to the unconventional geometry and operating conditions of the cyclone and little is known about the particle behaviour in these flow conditions. M. Narasimha et al. say that a decrease in apex diameter and an increase of inlet velocity enhance the separation sharpness[34]. Because this cyclone has a relatively large apex and low inlet velocity, a sharp separation is not expected.

For this case a very sharp separation might not be essential. Figure 7.2a shows that a lower separation sharpness does not increase the amount of sediment particles below the line because the  $D_{90}$  is larger than the cut size. For the nodules only a very low separation sharpness would be disadvantageous. A decrease in sharpness would result in a fraction leaving through the overflow. This is illustrated in figure 7.2b.

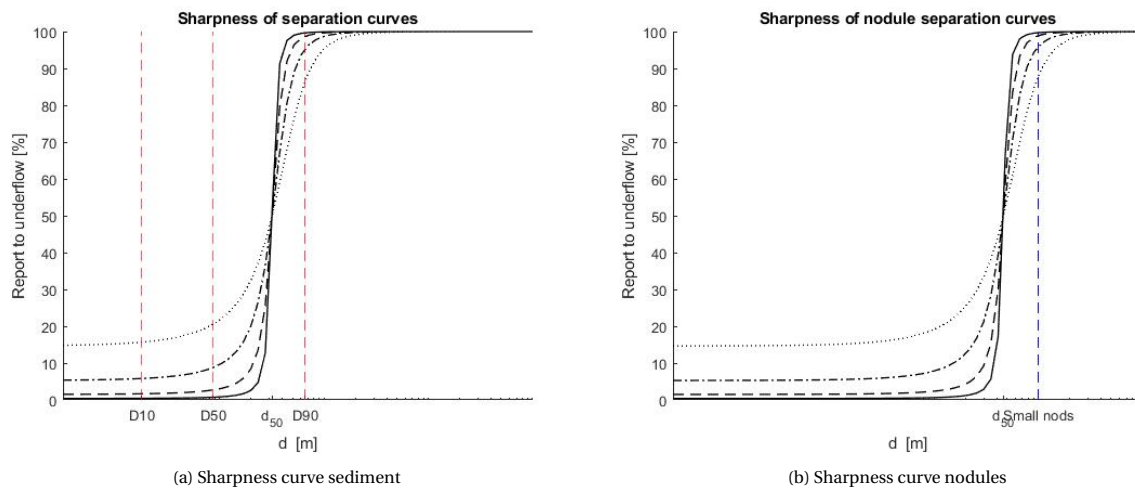


Figure 7.2: Sharpness curve

### 7.1.3. Bypass

Approximations of the 'actual' curves, as illustrated in figure 3.5, are obtained by substitution of the bypass in graphs 7.2a & 7.2b. However, the bypass depends on multiple factors. E.g. cyclone dimensions, flow characteristics, concentration and split ratio all have an influence on the bypass. It is assumed that the lighter particles with low timescale ratios remain evenly distributed over the flow. This automatically leads to the assumption that the bypass is approximately equal to the underflow. .

### 7.1.4. Split ratio

If the hydrocyclone would behave as a simple pipe section that splits the flow into two streams with different diameters with known resistances, the split ratio could easily be calculated. Figure 7.1 shows what the volume flow and flow velocities would be if resistances of both exits would be equal and other effects like static head, flow behaviour inside the cyclone and the presence of particles were neglected.

$Q_i$ [ $m^3/s$ ]	$Q_u$ [ $m^3/s$ ]	$Q_{vf}$ [ $m^3/s$ ]	$v_i$ [ $m/s$ ]	$v_u$ [ $m/s$ ]	$v_{vf}$ [ $m/s$ ]
0.50	0.20	0.30	4.08	4.31	4.31

Table 7.1: Expected flows and velocities

Particle	$D_{10}$	$D_{50}$	$D_{90}$	smallest nodules	average nodules	largest nodules
$w_0$ [ $m/s$ ]	0.014	0.030	0.083	0.79	1.21	2.03

Table 7.2: Terminal settling velocities different fractions

Figure 7.2 illustrates the terminal settling velocities of all different fractions expected when harvesting the CCZ. It is observed that when a particle is headed toward the vortex-finder it will leave through the vortex-finder as terminal velocities are far lower than the predicted flow velocity through the vortex-finder.

Unfortunately, an accurate theoretical prediction of the natural split ratio is complicated. Research by Narasimha et al. indicates that the split ratio is not resembled by the ratio of the the surfaces of the vortex-finder and the apex  $A_u/A_{vf}$  [34]. In their research  $Q_u$  is 20% less than when the the ratios of the surface areas are taken to approximate the split ratio. However, their research also suggests that lowering the flow velocity and increasing the  $A_u/A_{vf}$  ratio, quickly increases split ratio. As the inflow velocity of the designed cyclone is 1.5 lower and  $A_u/A_{vf}$  is 2 times higher than they researched, the split ratio is expected to be larger than was found by Narasimha et al. Therefore the prediction of the percentage of fluid leaving through the underflow without influencing resistances lies between the 39% ,obtained from the ratio of the surface areas, and the 26% found by Narasimha et al.

Depending on the harvester's possibilities and the desired flow characteristics after separation, the bypass can be adjusted to a preferred split ratio. A split ratio of 0 would mean the process behind the cyclone is no longer continuous and other mechanisms need to be implemented for particle transportation after separation. Therefore 10% is found a more realistic percentage. Figures 7.3a & 7.3b illustrate two approximated 'actual' partition curves for sediment and nodules with a bypass varying between 10% and 40%

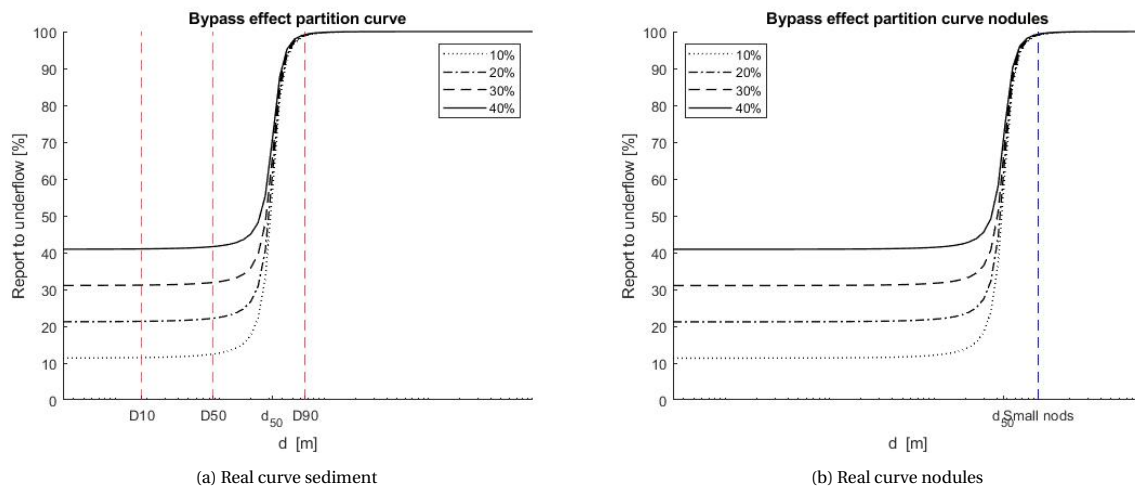


Figure 7.3: Predicted 'actual' partition curves

## 7.2. Particle scaling

The experimental data is obtained from investigation of the model cyclone. This data needs to be converted to data that represents the prototype. Before a partition curve can be constructed, the particles need to be scaled from particles used for the experiment to particles harvested in the CCZ. Before the results from the experiments can be compared to the expected results, the particles need to be scaled. If particle reaction to the surrounding flow is equal for particles used in the model and the prototype they are assumed to behave in a similar manner. Therefore, a particle

that passes through the prototype cyclone, will have the same partition as a particle that passes through the model, when the timescale ratio is equal.

Because the particle behaviour is predicted with the timescale ratios  $Stk$  &  $r$ , these are considered equal when scaling. Particles with  $Re_p < 1$  scale with a equal  $Stk$  value as the laminar regime is most accurately predicted by this value. For higher  $Re_p$  values  $r$  is considered constant. Before scaling the particles, the conditions under which the separation takes place need to be changed. Because the experimental setup does not allow for the designed volume flow to be tested, the centripetal acceleration has a lower value. Not only is this important for the determination of the timescale ratio's of the particles used in the experiments. This needs to be considered for the prototype as well.

The experimental setup reaches 72% of the original designed volume flow due to the resistance of the cyclone. This will be used in calculating a new centripetal acceleration for both the model and the prototype. Table 4.1 indicates that the original inflow velocity is 4,08 m/s resulting in a velocity of 2.94 m/s that is simulated by the experiments. The newly obtained centripetal accelerations are:

$$a_{c_p} = \frac{v_{i_p}^2}{0.5D_{c_p}} = \frac{2.94^2}{0.5} = 17,29 m/s^2 \quad (7.1)$$

With  $a_{c_p}$  as the centripetal acceleration of the prototype,  $v_{i_p}^2$  is the inlet flow velocity of the prototype and  $D_{c_p}$  is the prototype cyclone diameter. The same is done using the model dimensions and parameters.

$$a_{c_m} = \frac{v_{i_m}^2}{0.5D_{c_m}} = \frac{1.11^2}{0.071} = 17.35 m/s^2 \quad (7.2)$$

With  $a_{c_p}$  as the centripetal acceleration of the model,  $v_{i_p}^2$  is the inlet flow velocity of the model and  $D_{c_p}$  is the diameter of the model cyclone.

### 7.2.1. Scaling $Stk$

For  $0 < Re_p < 1$  the stokes number is considered the appropriate timescale ratio. Because nodules have a diameter larger than 1 mm they do not fall under the laminar regime, the scaling of the particles with low  $Re_p$  values is not needed for different densities.

$$Stk_m = Stk_p \quad (7.3)$$

Where  $Stk_m$  is the Stokesnumber of a specific particle used in the model experiments and  $Stk_p$  is the Stokes number of the particle with an equivalent reaction to the surrounding flow in the prototype. Rewriting  $Stk$  from equation 4.19 and incorporating equation 4.20 with the adjusted centripetal acceleration results in the following  $Stk$  equation.

$$Stk = d_p^{\frac{2}{3}} \cdot \frac{\sqrt{\frac{2}{3} \cdot \rho_p \cdot (\rho_p - \rho_f) \cdot \sqrt{g^2 + a_c^2}}}{\eta} \quad (7.4)$$

Substituting equation 7.4 with both model and prototype values into equation 7.3 results in equation 7.5 that describes the particles scaling from model to prototype. Equation 7.5 reveals that scaling in the laminar regime is constant for every diameter because all parameters are constant too and independent of the particle diameter. For these scaling conditions the prototype particles are 1.754 times larger than the model particles.

$$d_{p_p} = d_{p_m} \cdot \left( \frac{\frac{\sqrt{\frac{2}{3} \cdot \rho_{p_m} \cdot (\rho_{p_m} - \rho_{f_m}) \cdot \sqrt{g^2 + a_{c_m}^2}}}{\eta_m}}{\frac{\sqrt{\frac{2}{3} \cdot \rho_{p_p} \cdot (\rho_{p_p} - \rho_{f_p}) \cdot \sqrt{g^2 + a_{c_p}^2}}}{\eta_p}} \right)^{\frac{2}{3}} \quad (7.5)$$

### 7.2.2. Scaling $r$

For higher  $Re_p$  values, the preferred timescale ratio is  $r$ . As indicated in equation 4.17, the  $r$  value depends on the drag coefficient and the relative density between the particle and the surrounding fluid. Figure 4.7 indicates that the sediment found in the CCZ only contains particles with  $Re_p$  values lower than unity. Therefore the scaling of particles with higher  $Re_p$  values will be done by making use of nodule characteristics.

The same principle as described earlier is used for the scaling of the individual particle sizes. If the  $r$  value is equal for a particle in the model setup and a particle in the prototype, the particles are expected to behave in a similar manner. Therefore, to find the comparable particle values, the  $r$  values are considered equal.

$$r_m = r_p \quad (7.6)$$

With  $r$  defined in equation 4.17 as:

$$r = \frac{\rho_p}{\rho_f C_d} \quad (7.7)$$

Because scaling of the  $r$  value essentially comes down to  $C_d$  scaling, it can only be done for the transition regime. Equation 4.13 shows the definition for the  $C_d$  in the transition regime. Turbulent particles can definitely be scaled using different methods. However, because particles with turbulent  $Re_p$  values will all report to the underflow under normal circumstances, there is no need to scale them.

The scaling of  $r$  for the transition regime ( $1 < Re_p < 2000$ ), is done by finding the definition of the  $r$  value as a function of known properties.

$$C_d = \frac{24}{Re_p} + \frac{3}{\sqrt{Re_p}} + 0.34 \quad (7.8)$$

Writing out  $C_d$  with equations 4.11 & 4.12, and substituting it into equation 4.17, results in the following definitions of the  $r$  values of the particles for both the prototype and the model cyclone.

$$r_p = \frac{\rho_{p_p}}{\rho_{f_p}} \cdot \left( \frac{24}{\frac{\Delta_p d_{p_p}^3 \sqrt{g^2 + a_{c_p}^2}}{18v_p^2 + v_p \sqrt{0.75\Delta_p d_{p_p}^3 \sqrt{g^2 + a_{c_p}^2}}}} + \frac{3}{\sqrt{\frac{\Delta_p d_{p_p}^3 \sqrt{g^2 + a_{c_p}^2}}{18v_p^2 + v_p \sqrt{0.75\Delta_p d_{p_p}^3 \sqrt{g^2 + a_{c_p}^2}}}}} + 0.34 \right)^{-1} \quad (7.9)$$

$$r_m = \frac{\rho_{p_m}}{\rho_{f_m}} \cdot \left( \frac{24}{\frac{\Delta_m d_{p_m}^3 \sqrt{g^2 + a_{c_m}^2}}{18v_m^2 + v_m \sqrt{0.75\Delta_m d_{p_m}^3 \sqrt{g^2 + a_{c_m}^2}}}} + \frac{3}{\sqrt{\frac{\Delta_m d_{p_m}^3 \sqrt{g^2 + a_{c_m}^2}}{18v_m^2 + v_m \sqrt{0.75\Delta_m d_{p_m}^3 \sqrt{g^2 + a_{c_m}^2}}}}} + 0.34 \right)^{-1} \quad (7.10)$$

symbol	meaning	unit
$r_m$	$r$ value of specific particle passing through model	[-]
$r_p$	$r$ value of specific particle passing through prototype	[-]
$\rho_{p_m}$	Density particle passing through model	[kg/m <sup>3</sup> ]
$\rho_{p_p}$	Density particle passing through prototype	[kg/m <sup>3</sup> ]
$\rho_{f_m}$	Density fluid passing through model	[kg/m <sup>3</sup> ]
$\rho_{f_p}$	Density fluid passing through prototype	[kg/m <sup>3</sup> ]
$d_{p_m}$	Diameter of particle passing through model	[m]
$d_{p_p}$	Diameter of particle passing through prototype	[m]
$\Delta_m$	Specific density of particle passing through model	[-]
$\Delta_p$	Specific density of particle passing through prototype	[-]
$g$	Gravitational acceleration	[m/s <sup>2</sup> ]
$a_{c_m}$	Centripetal acceleration created by model cyclone	[m/s <sup>2</sup> ]
$a_{c_p}$	Centripetal acceleration created by prototype cyclone	[m/s <sup>2</sup> ]
$\nu_m$	Kinematic viscosity of the fluid passing through model	[m <sup>2</sup> /s]
$\nu_p$	Kinematic viscosity of the fluid passing through prototype	[m <sup>2</sup> /s]

Table 7.3:  $r$  scaling units

Substituting equations 7.9 & 7.10 into equation 7.6 gives the possibility to scale between model and prototype particles, if these particles have  $Re_p$  values between 1 and 2000. Table 7.4 illustrates the values that have been used for scaling  $r$  in the experiments.

symbol	value	unit
$\rho_{p_m}$	2650	$[kg/m^3]$
$\rho_{p_p}$	2000	$[kg/m^3]$
$\rho_{f_m}$	1000	$[kg/m^3]$
$\rho_{f_p}$	1050	$[kg/m^3]$
$\Delta_m$	1.65	[-]
$\Delta_p$	0.90	[-]
$g$	9.81	$[m/s^2]$
$a_{c_m}$	17.29	$[m/s^2]$
$a_{c_p}$	17.35	$[m/s^2]$
$\nu_m$	$1.0 \cdot 10^{-7}$	$[m^2/s]$
$\nu_p$	$1.7 \cdot 10^{-7}$	$[m^2/s]$

Table 7.4: r scaling values

Scaling these particles is less complicated, and more accurate, when the Stokes value and r number are empirically determined for the model cyclone.

### 7.2.3. Implementing scaling principles

Graph 7.4 implements both Stokes scaling and r scaling. The vertical lines represent the regime changes where different scaling methods are used. The blue lines represent the theoretical Stk and r values for the model cyclone as a function of the particle diameters. The prototype Stk and r values have been illustrated with a red line. This graph clarifies the scaling process which essentially is a horizontal transfer from the blue line to the red for both laminar and transition regime.

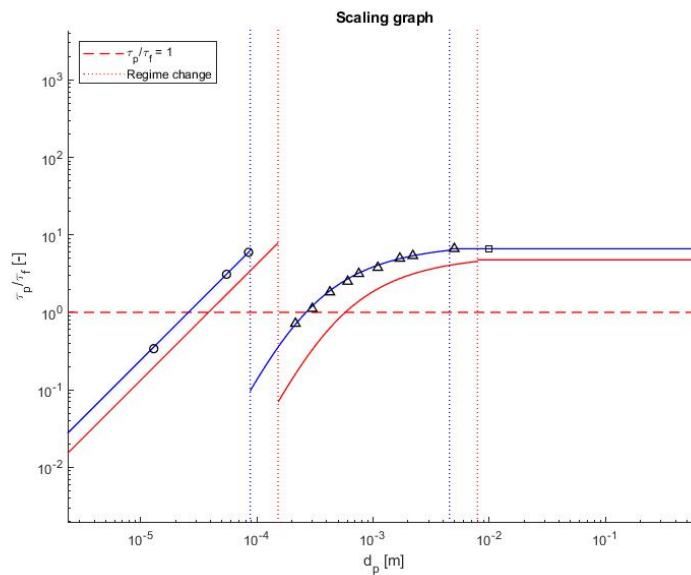


Figure 7.4: Scaling particle diameter from model to equivalent prototype diameter

The individual fractions that were studied and defined in table 5.2 are indicated in this graph with individual shapes. Circles represent the laminar particles, triangles the transition regime particles and the squares represent the turbulent particles. The Stk and r values that were determined in the settling experiments correspond quite accurately with the theoretical graph. The scaling of the individual model particle diameters leads to individual prototype particle diameters shown in table 7.5

$\frac{d_{m0} + d_{m100}}{2}$ [mm]	$Re_p$	$d_{pp}$ Stk scaled [mm]	$d_{pp}$ r scaled [mm]
0.013	0.01	0.0219	[-]
0.055	0.16	0.097	[-]
0.085	0.62	0.149	[-]
0.215	10.0	[-]	0.461
0.300	18.1	[-]	0.627
0.425	38.3	[-]	0.983
0.605	67.7	[-]	1.47
0.755	111	[-]	2.23
1.10	177	[-]	3.58
1.70	456	[-]	16.2
2.20	664	[-]	66.6
5.00	3420	[-]	[-]
10.0	9273	[-]	[-]

Table 7.5: Corresponding particle diameters

The graph is horizontally separated into different regimes where the graph is vertically separated. The laminar particles only show the Stokes scales particles and the particles in the transition regime only show the r scaled particles.

### 7.3. Performance

For a final feasibility analysis, the key performance parameters are examined. With the constructed scaling methods, the partition curve of the prototype can be predicted. Besides the partition curve, the split ratio, capacity and energy consumption are all relevant parameters that determine the feasibility of the cyclone.

#### 7.3.1. Partition curve prototype cyclone

##### Cutsizes

Depending on the concentration, the 65-105  $\mu\text{m}$  particles mostly report to the underflow. However, the smaller fraction does not see any separation at all. The assumed cut size of the model is therefore in the lower region of the 65-105  $\mu\text{m}$  fraction. The partition curves in sections 6.2.2 & 6.2.4 illustrate a cutsizes of approximately 65  $\mu\text{m}$ . Stk scaling 65  $\mu\text{m}$  to its prototype equivalent results in a prototype cut size of 114  $\mu\text{m}$ . This difference with the theoretically determined cutsizes, 31.9  $\mu\text{m}$ , can have several causes.

The first is the reduced maximum  $Q_i$  that was able for the setup. A reduced volume flow results in a reduced velocity, which causes a reduced centripetal force. A velocity reduction to 72.8 % reduces the the total acceleration force that is caused by gravity and the centripetal force,  $\sqrt{g^2 + a_c^2}$ , with 42%. This causes the diameter of the particle to increase to have an equal Stk value. However, this only increases the particle diameter with 20% which does not come close to the 114  $\mu\text{m}$  that is obtained from the experiments.

Another reason for the large cutsizes can be an unpredictable response to particle presence. The hindered settling of particles and equivalent liquid model have been investigated in section 2.1.3 and did not seem important influencing factors due to the low concentration of particles. Potentially this can play a role when particles are moved toward the outer edge of the flow. This increases the concentration on the outside of the circulating flow making it harder for particles to settle. If the volume concentration of particles with 65  $\mu\text{m}$  increases to 5%,  $\frac{w_s}{w_0}$  is equal to 0.8 and quickly decreases even further for higher concentrations. Due to the higher concentration of solids at the outer edges of the flow, it acts as a fluid with a higher density as well.

Also, the approximation of the time scale ratio might not be the most accurate when using Stk and r in this case. Stk and r indicate the timescale ratio accurately when the particles are either laminar or turbulent. Therefore one or the other has to be chosen to determine the appropriate timescale ratio. Due to the forced accelerated settling inside the cyclone, the particle diameters with a timescale ratio close to 1 are located close to the regime change from laminar to the transition regime. This makes either Stk or r a less accurate indication for the timescale ratio. Figure 7.5 shows a proposed curve with a smooth transition between Stokes and r.

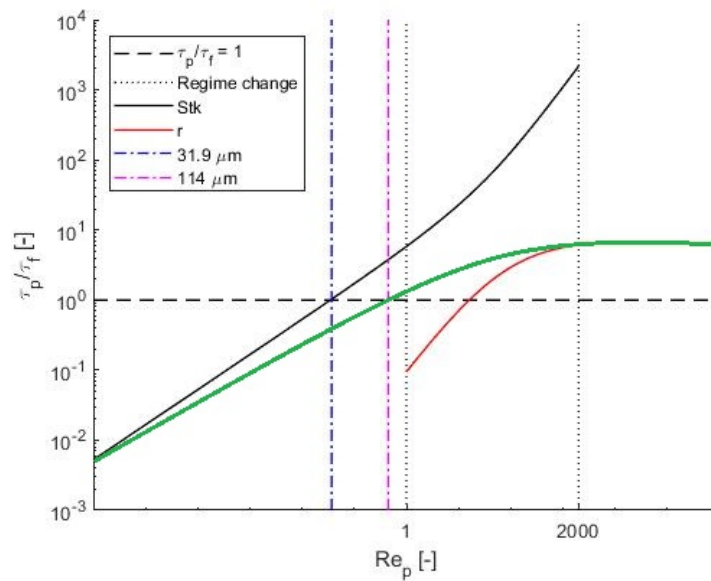


Figure 7.5: Alternative timescale curve

This function is shown in green and creates a smooth transition from Stk to r. This function is not verified and can have a different shape. However, it does show that the original particle diameter with a Stk value of 1 is larger than  $31.9 \mu\text{m}$ . The regime change occurs when particles become larger than  $152 \mu\text{m}$ . This leads to the conclusion that  $114 \mu\text{m}$  is a reasonable cut size.

Besides the explanations for the inexact theory, it must be considered that the measurements have inaccuracies too. The diverse values obtained from the theory and the data analysis can also be a result of imprecise measurements or different shape factors that influence the drag coefficient.

### Bypass

Some by-passed fine material has been observed in the underflow pipe with a closed underflow. Therefore this cyclone has a minimum by-pass rate. However, these were small quantities of around 5%. This did not increase for a wider conical angle which could prove to be beneficial when a shorter cyclone is needed.

### Split ratio

The split ratio visibly has an effect on the separating performance of particles. The cyclones accumulated more particles when the underflow was closed off than when it was open. However, for most particle sizes it did not influence the partition. This is a mayor benefit for the overall performance of the cyclone. However, it should still be assumed that a minimal amount of water needs to leave through the underflow to prevent an overcrowded cyclone as seen in figure 6.1b and a smooth particle transport after leaving the cyclone.

Figure 7.6 illustrates the partition curves of the model cyclone and the prototype cyclone. Because the separation sharpness cannot be determined, they look similar. However, the model cut size is scaled to the prototype size. The cut size is located inside the laminar regime and is therefore scaled using constant Stk values.

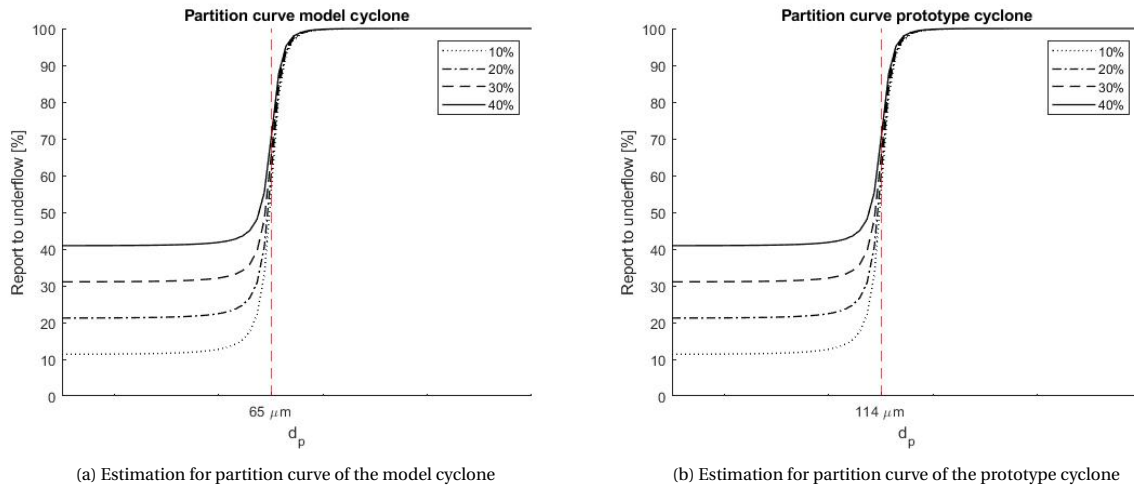


Figure 7.6: Model &amp; prototype partition curves

If this cut size is compared the average particle size distribution in graph 2.3, it is expected that a separation of 98% of the particles is attainable. This is significantly higher than was expected in section 4.3.4 and considerably increase the cyclone's performance.

### 7.3.2. Split ratio

The split ratio has little effect on the cut size. However, one phenomenon affecting the cyclones feasibility is losing large particles through the vortex-finder. This only happened with the largest particles and when the underflow is closed. A split ratio of 0 removes the downward flow resulting in more rotating particles inside the cyclone. Video footage shows particles occasionally colliding and bouncing toward the centre of the cyclone when there is an abundance of large particles. If this effect can be mitigated, lowering the split ratio as much as possible shows high potential for enhancing nodule separation from sediment and water.

### 7.3.3. Capacity

The experiments resulted in several insights regarding the capacity. When  $Q_i$  is increased,  $v_i$  is increased. Experiments showed that an increased velocity resulted in a higher orbit of circulating particles. Also, large particles are more susceptible to overcrowding when the flow velocity is higher.

Not only does an increase of velocity mean a higher concentration of large particles, it will also increase the resistance of the separator. The separator had a high resistance, which resulted in a limited volume flow. This resistance increases exponentially when the volume flow is increased. Because the prototype cyclone separator is driven by the same pumps that suck up the slurry, the pumps need to be very powerful if the separator would be implemented. power if that flow rate increases. These pumps must be able to create sufficient power when the separator would be implemented. If larger particles can be contained leaving through the vortex-finder and the the pumps deliver sufficient power, the cyclone has the capacity to separate the desired volume flows of approximately  $0.5 \text{ m}^3/\text{s}$ .

### 7.3.4. Energy consumption

At 72% of the original designed capacity, the inlet flow velocity is  $1.1 \text{ m/s}$ , and the static head is 2.55 m when the underflow is open. With the underflow closed, this static head rises by another 20 cm. Indicating there is a pressure drop of  $0.275 \cdot 10^5 \text{ Pa}$  created by the cyclone. The prototype has a far larger volume flow and higher flow velocity than the model used for these experiments. An approximation of the pressure difference caused by the resistance of the prototype cyclone is constructed with equation 7.11.

$$P = K0.5\rho_f v_i^2 \quad (7.11)$$

Where  $K$  is the shape factor of the cyclone,  $P$  is the pressure differences caused by the cyclone,  $\rho_f$  is the fluid density, and  $v_i$  is the inlet velocity. Substituting the model and prototype parameters into equation 7.11 gives the equation for the determination of the prototype pressure.

$$P_{proto} = P_{mod} \frac{\rho_{f_{proto}} v_{i_{proto}}^2}{\rho_{f_{mod}} v_{i_{mod}}^2} \quad (7.12)$$

The pressure drop caused by the prototype cyclone's resistance will be approximately  $4 \cdot 10^5$  Pa. To overcome this pressure drop, additional pump power is needed. With the pressure drop and the designed volume flow of  $0.5 \text{ m}^3/\text{s}$ , the minimal required power for one installed cyclone is found with equation 7.13

$$E_{proto} = Q_{i_{proto}} \cdot P_{proto} \quad (7.13)$$

The minimal required extra pump power,  $E_{proto}$ , would be 200 kW per cyclone. When 16 to 20 hydrocyclones are integrated into the harvester, the additional required power could rise to 4 MW.

The total power required by the VTS for transporting the total collected slurry by the harvester is expected to be 5 MW [55]. The power that the VTS saves by removing the smaller particles from the flow would only be a fraction of that 5 MW due to the low concentration of fines. Accompanied by costs of additional power installation inside the seafloor mining tool, it would be unfavourable to install this cyclone directly behind the collector.

## 7.4. Conical angle

### Original angle

Larger particles have been observed to stay in rotation in the cyclone, crowding the cyclone. The reason why this only happens for the largest particles, is because the surrounding current has a relative low effect on their behaviour compared to smaller particles. Larger particles are dominated more by their own inertia, than the finer particles. Because the current flows, parallel to the wall, in the direction of the underflow when near edge of the cyclone. Therefore, the smaller particles that do reach the outer wall, do not stay in orbit, but the larger particles do.

Because the particles mainly rotate halfway down the conical section, the first assumptions made in section 4.1 are correct. This is true for the top part of the conical section. No particles remain at the edge of the cone and the cylindrical section, unless the flow rate is increased or the conical angle is too large. This is clearly observed during experimentation. After examining the footage of the large particles, there clearly is a difference in angular velocity between the top part of the cyclone, and halfway down the conical section where the particles accumulate.

Halfway down the conical section, the particles have an angular velocity of at least two and a half that of the particles on top. Because the inlet velocity and the circumference of the cyclone are known, the centripetal acceleration was used for the calculation of the original conical angle. With the angular velocity in the middle of 2.5 times the angular velocity on top, and a diameter of 0.088 m in the middle, the velocity of the particles is equal to  $1.713 \text{ m/s}$ . Substituting the values for the topside of the flow into equation 7.14 and the values for the middle into equation 7.15 shows a large difference in centripetal acceleration.

$$a_{c_{top}} = \frac{v_{top}^2}{r_{top}} = \frac{1.106^2}{0.071} = 17.23 \text{ m/s}^2 \quad (7.14)$$

$$a_{c_{middle}} = \frac{v_{middle}^2}{r_{middle}} = \frac{1.713^2}{0.044} = 66.69 \text{ m/s}^2 \quad (7.15)$$

When implementing equations 4.5 & 4.4, an angle of  $33.2^\circ$  is needed for the top section of the cone, and an angle of  $16.7^\circ$  in the middle section. Both are still conservative assumptions. However, it shows that the further down the cone, the smaller the conical angle must be for a smooth transition toward the underflow. So, it is expected that large particles will always keep rotating at some location in the cyclone. However, they will force each other in the direction of the exit, when the concentration gets too high. Therefore, the cyclone will never be filled up with particles.

### Wide angle

Particles leaving through the vortex-finder occurs much more frequently with the large angled cone. With a split ratio of 0, approximately 3 out of 4 particles are collected by the vortex-finder. This is because the wide angled cone is always filled with large particles as they stay in rotation. Therefore, the particles are constantly colliding. The other reason for the losses of large particles, is that the opening of the vortex-finder is placed directly above the apex. Leaving little room for particles to escape the pull of the overflow, which can clearly be seen in figure 6.7. This loss of particles increases when split ratio is decreased to 0 where the underflow is closed. This is very disadvantageous for the performance of the cyclone.

A larger conical angle, and thus a shorter cyclone might be possible. Only the largest particles had a reduced partition when the concentration inside the cyclone got to high. If these particles could be prevented from entering the central vortex with e.g. a shorter vortex-finder, larger particles already removed from the flow or lower flow velocity, a wider conical angle could work as well.

# 8

## Discussion

### 8.1. Discussion

#### Airtight setup

Creating an environment that simulates deep-sea conditions above ground is complicated. Keeping air from entering the cyclone was not possible with the used setup. Air pockets arising inside the central vortex are difficult to remove due to the low pressure in the core of the cyclone. This may affect the motion of the particles in the centre of the cyclone due to the behaviour of the medium and the reaction of the particles to it. When the centre of the cyclone is filled with water, there is no area inside the cyclone where water does not move toward an exit. Now that unmoving air pockets occupy that core, the transportation of particles toward the exits is influenced.

#### Timescale ratio

Scaling the particle behaviour is done using  $Stk$  and  $r$ . However, both values are not completely accurate.  $Stk$  and  $r$  utilise a specific part of how the drag coefficient behaves towards the particle Reynolds number. This makes the Stokes number an overestimate for turbulent particle Reynolds numbers. And vice versa, for laminar  $Re_p$  values,  $r$  is very inaccurate. The particle diameter where the particle has a timescale ratio of unity, is estimated as the cutsize.

Because the particles with the estimated cut size as diameter have a Reynolds number close to the transition regime, neither  $Stk$  nor  $r$  gives an accurate prediction of the timescale ratio. The current cutsize is verified with a simple curve that transfers  $Stk$  into  $r$ . However, this function is merely an estimation which is not researched nor investigated. Therefore, this leaves the verification unsubstantiated. Theoretical or empirical research for an appropriate timescale ratio that describes the particle response to the surrounding flow in the transition regime could solve this predicament.

#### External factors

The cyclone has been designed with limited knowledge of the outside conditions. Therefore, the model inflow distribution might not reflect reality. The possibilities are limited due to the lack of information. For example, the way the flow enters the cyclone, which can greatly impact on the performance of the cyclone, is unknown. Also, the ability to adjust the split ratio and the required flow characteristics after separation are not known. However, they can be of importance for the feasibility of the hydrocyclone. For a more accurate performance prediction, the incoming flow and the required underflow characteristics are required.

#### Energy consumption

One of the most important key performance parameters of the hydrocyclone is energy consumption. The required power and energy consumption for the separation process can become a major issue when these turn out to unprofitable or even unattainable. The unexpectedly high static head created by the cyclone gives reason to suspect that this parameter might be decisive for the eventual feasibility.

### Residence time

Not just the timescale ratio is of importance when predicting the partition of the particles. The particle partition is expected to be a function of both the timescale ratio and the residence time. The timescale ratio describes how a particle reacts to the surrounding flow, where the residence time can determine the time a particle has to exercise that reaction.

If the residence time of the fluid is extended, it can be assumed particles have more time to move towards the wall. The average residence time of the fluid is computed with equation 8.1.

$$\frac{V_c}{Q_i} = T_{res} \quad (8.1)$$

The prototype residence time,  $T_{res,p}$ , is 1.42 seconds, where the residence time of the model,  $T_{res,m}$ , is 3.31 seconds. This gives particles in the model two times longer to exercise their reaction to the surrounding flow. Therefore, they might move toward the wall sufficiently to escape the pull of the central vortex. This would decrease the cut size and the separation sharpness of the cyclone.

### Nodule density

The average density of nodules has been used to determine the partition of the particles. However, the GSR data suggests a large difference between nodule densities. Lower density nodules are lost more easily in the separation process. For example, the smallest relevant nodule size of 1mm would have an  $r$  value of 0.14 if its density was  $1100 \text{ kg/m}^3$ , resulting in large losses of these particles. Therefore, more information about the minimal nodule density is required for a full feasibility analysis.

### Nodule shape

Only the largest particle fractions that were tested had varying shapes. All other particles consisted of quartz sand particles that have a rounder shape than most nodules. Both sediment and nodule terminal settling velocities have been theoretically approximated with 4.11, which takes the shape of sediment in account. Therefore, scaling sediment particles to nodules can give a slightly distorted view of the particle behaviour. However, due to the large timescale ratio and  $Re_p$  value of the nodules, it will not have a large impact on the results.

### Fluctuating concentration

Some experiments using fine particles experienced fluctuating concentrations inside the cyclone. Due to the restrictions of the setup, it is not possible to create a constant and predetermined concentration. Observations established that concentration has an impact on the separation performance. When a higher concentration was entering the cyclone, an relative increase of particles leaving through the vortex-finder was recorded. This is most likely due to density changes of the fluid or hindered settling of the particles. Although, the hindered settling and the equivalent liquid model have both been investigated, the impact might have been underestimated.

## 8.2. Alternative use case

This research provides evidence that a hydrocyclone is useful for separating nodules from sediment and water. However, large particles can accumulate inside the cyclone, which increases the chance of blockage and loss of nodules. Furthermore, investigation of the resistance created by the separator in section 7.3.4 determined that a cyclone designed for  $0.5 \text{ m}^3/\text{s}$  creates a pressure drop of approximately  $4 \cdot 10^5 \text{ Pa}$ . The pump power needed for a single cyclone would be 200 kW. With 16 to 20 cyclones required to separate the entire inflow of the harvester, the additional required power could rise to 4MW. The accompanying costs and technical challenges of installing this technology inside the seafloor mining tool are disadvantageous. Therefore, an alternative use case is proposed. Depending on the possibilities of the production support vessel, hydrocyclones can act as an effective dewatering installation before ship to ship transfer.

Topside utilisation of the cyclone mitigates the main disadvantages of the separation process. If the PSV has sufficient space, the cyclones' maximum dimensions would not be a restriction. Also, additional installation with the ability to capture the large particles from the incoming flow before entering a cyclone, prevents the loss of large nodules. Additionally, large vessels in the offshore and dredging industry often have no problem in generating an additional 4MW. Therefore, topside utilisation would be favorable over seafloor application.

# 9

## Conclusion & Recommendations

### 9.1. Conclusion

During this research, separation technologies have been investigated, a separator and an experimental setup have been designed and constructed, and the cyclones' performance has been analysed, This study concludes by answering the research question:

**'What is the feasibility of a hydrocyclone inspired machine designed to separate polymetallic nodules from surrounding water and sediment in deep-sea mining operations?'**

In order to do so, the sub-questions, as defined in section 1.5, will be elaborated upon.

#### 1. "When will the design be feasible?"

Multiple factors determine the feasibility of the separation device. These factors have been categorised under constraints and preferences. The seven vital requirements for utilisation in deep-sea mining operations are the following. The separation device needs to: 1) be able to separate solids from other solids and liquids, 2) be able to collect manganese nodules ranging from 0.1 cm to 12 cm, 3) have no moving parts, 4) have a continuous separation process, 5) be unable to get blocked, 6) be low maintenance, and 7) be energy efficient.

The preferences are the requirements that come with the implementations of the separator inside a specific harvester and determine that the maximum volume of the device is  $1 m^3$ , and that it must be capable of handling flow rates of  $0.5 m^3/s$ . If the separator does not comply with any of the constraints, the design is non-feasible. Failing to comply with the preferences however, does not automatically indicate that the separator is incapable of the suggested process.

#### 2. "What is the best method for this separation?"

From the literature it is evident that hydrocyclones are the best technology for separating manganese nodules from the carrier fluid in deep-sea conditions, when a sturdy mechanism that is capable of handling high flow rates with limited space is required. Unfortunately, this research indicates that larger particles can be difficult to separate and the energy consumption is high, which makes deep-sea utilisation impractical. However, there are opportunities for topside deployment.

#### 3. "What principles of a hydrocyclone can be used for the separation of the nodules?"

The fundamental principle on which the operation of the hydrocyclone is based is centrifugal sedimentation created by an inner downward vortex. Due to the geometry of the hydrocyclone a smaller central vortex is created, flowing in the opposite direction toward the vortex-finder. The motion of the coarser particles is dominated more by their own inertia than finer particles, allowing them to move toward the edge of the cyclone fast enough to escape the pull of this central vortex. Finer particles will not have time to move toward the edge and can be considered to follow the path of the flow. Reducing the split ratio by forcing the flow in the direction of the vortex-finder can therefore enhance nodule separation from the surrounding seawater and sediment.

#### 4. "What is the separation efficiency of this technique for the proposed operation?"

The efficiency of the cyclone is determined by its ability to separate the nodules from both sediment and carrier fluid. Investigation of the key performance parameters determined that 98% of the total volume of solids can be separated

from the nodules if a minimal bypass effect and a high separation sharpness can be achieved. Furthermore, analysis of the experimental results indicates that the cutsize is smaller than the smallest expected nodules, which suggests that all nodules can be collected. However, several large particles are lost due to crowding when reducing the split ratio and increasing the conical angle and volume flow.

The cyclone is capable of removing 100% of the unwanted fluid. Unfortunately, reducing the split ratio to 0 increases the loss of large particles and the resistance of the cyclone. However, as the flow requirements after separation and the possibilities within the harvester to control the underflow are unknown, a split ratio of 0 might not be desired. If the loss of large particles can be mitigated, a minimal split ratio increases the separation of the nodules from both sediment and fluid.

Because the cyclone complies with the rest of the restrictions and preferences, the capacity and the energy consumption determine if the separator is feasible. Experimentation suggests that the cyclone is capable of handling the requested flow rates. However, increasing the volume flow shows an increased accumulation of large particles. Therefore, exceeding the designed capacity is expected to limit the separation efficiency. Nonetheless, the results of the experiments indicate great potential for the performance of the cyclone for the original designed capacity.

Due to large resistances when operating at high flow rates, the energy consumption is excessive for deep-sea operation. Therefore, integrating the cyclone into the harvester is inefficient. Topside operation would be more beneficial for a hydrocyclone as the power supply costs are lower, and large particles can be removed from the flow before entering the cyclone.

## 9.2. Recommendations

### 9.2.1. Theory

#### Investigation of timescale ratio

Theoretically, particle behaviour of the flow is determined by the timescale ratios  $Stk$  and  $r$ . These have also been utilised for the scaling of the particles to determine the prototype cut size. The experimental results have been validated by creating a curve that transfers  $Stk$  into  $r$ . However, even though this validation is plausible, it is not substantiated. Research into a timescale ratio that accurately describes the particle reaction to the surrounding flow for the transition regime is recommended.

#### Effect residence time

Not only the reaction to the surrounding fluid determines the cyclone's performance. The time a particle has to carry out that reaction also plays a role. Investigating the effect can give an enhanced insight in the cyclone's separation and can help determine a more accurate cut size for the prototype cyclone.

### 9.2.2. Setup

#### Adjustable vortex-finder

The model cyclone was designed with the intention of testing alternative conical angles. The reason was the exceeding of the maximal length of the cyclone and the assumption that the conical angle had been determined too conservative. However, results of the experiments has given reason to assume that the vortex-finder length can affect the separation performance of the cyclone significantly. Customising the vortex-finder with an adjustable length would give more insight into the opportunities the cyclone has.

#### Redirection of the flow

The current setup was not able to bring fine particles into the flow with a consistent and predetermined concentration. Because the critical material to obtain the partition curve, consists of fine particles, this is a loss of valuable information. Creating an adjustable redirection between the buffer and the pump could improve the experiments considerably. The concentration could be controlled by creating a suspension in an external container. With this setup the original designed volume flow can be reached, which will lead to more reliable data. This extension to the setup is illustrated in figure A.36 in appendix A.

#### Fine particle measurement

Due to the current limitations of the setup, the partition of small particles cannot be measured accurately. Other methods of fine particle collection passing through the cyclone should be researched in order to construct an accurate partition curve. Permeable bags that retain the particles, or sufficiently large non-permeable bags that would take more than the whole experiment time to fill are viable options.

#### Increased flow rate

Experimentation of the cyclone performance was carried out with 70% of the original designed volume flow. Experimentation at 100% capacity would be beneficial, not only for the partition curve that comes with the originally designed flow rate, but also for the investigation of the large particle behaviour. Increasing the flow rate shall enhance

the accumulation of large particles inside the cyclone because of an increased angular velocity. Loss of large particles due to collisions when the concentration increases is an essential phenomenon that needs to be investigated to determine the feasibility of the cyclone.

### **9.2.3. Experiments**

#### **Mixture testing**

Large particles do not experience the presence of fine particles. However, large particles do experience the presence of slightly larger particles and vice versa. The experiments were all carried out with fractions of particles with roughly the same diameter. In doing so, a clear overview of the partition of specific particle diameters can be created. However, testing mixtures of particles could give other insights, for example, the loss of large particles through the vortex-finder. Due to heavy collisions with similar-sized particles, they can bounce toward the centre of the cyclone where they are captured by the central vortex. However, the presence of smaller particles might mitigate the effect of the collisions, which is favourable for the cyclone's feasibility.

### **9.2.4. Future research**

#### **CFD model**

Now that the model experiments have proven potential for the separation process, a CFD model can be constructed to determine if the cyclone is as efficient as the research concludes. The particle response to the surrounding flow, the partition curve, capacity and the energy consumption of the prototype cyclone can all be analysed in detail without high experimentation costs.

# Bibliography

- [1] International Seabed Authority. <https://www.isa.org.jm/es>, 2021.
- [2] V. Balaram. Rare earth elements: A review of applications, occurrence, exploration, analysis, recycling, and environmental impact. *Geoscience Frontiers*, 10(4):1285–1303, 2019.
- [3] The World Bank. Precautionary management of deep sea minerals. <https://openknowledge.worldbank.org/bitstream/handle/10986/28298/119106-WP-PUBLIC-114p-PPDSMbackgroundfinal.pdf?sequence=1&isAllowed=y>, 2017.
- [4] A. Barazi. Rohstoffrisikobewertung. [https://www.deutsche-rohstoffagentur.de/DE/Gemeinsames/Produkte/Downloads/DERA\\_Rohstoffinformationen/rohstoffinformationen-36.pdf?\\_\\_blob=publicationFile&v=2](https://www.deutsche-rohstoffagentur.de/DE/Gemeinsames/Produkte/Downloads/DERA_Rohstoffinformationen/rohstoffinformationen-36.pdf?__blob=publicationFile&v=2), 2018.
- [5] D. Bradley. *The Hydrocyclone*. International series of monographs in chemical engineering. Pergamon, 1965. ISBN 9781483155708.
- [6] L. Chu, W. Chen, and X. Lee. Effect of structural modification on hydrocyclone performance. *Separation and purification technology*, 21(1-2):71–86, 2000.
- [7] European Commission. Critical raw materials, 02 2020.
- [8] European Commission. Countries accounting for largest share of eu supply of crms, Sep 2020. URL [https://ec.europa.eu/growth/sectors/raw-materials/specific-interest/critical\\_en](https://ec.europa.eu/growth/sectors/raw-materials/specific-interest/critical_en).
- [9] D. Cronan. The geological society of london. <https://www.geolsoc.org.uk/Geoscientist/Archive/September-2015/Deep-sea-minerals>, 2012.
- [10] CRS. Critical minerals and u.s. public policy, Jun 2019. URL <https://www.everycrsreport.com/reports/R45810.html>.
- [11] M. Dlamini, M. Powell, and C. Meyer. A cfd simulation of a single phase hydrocyclone flow field, 2005. URL [https://www.researchgate.net/figure/A-hydrocyclone-flow-schematic\\_fig1\\_43498098](https://www.researchgate.net/figure/A-hydrocyclone-flow-schematic_fig1_43498098).
- [12] J. Dymond, M. Lyle, B. Finney, D.Z. Piper, K. Murphy, R. Conard, and N. Piasias. Ferromanganese nodules from manop sites h, s, and r—control of mineralogical and chemical composition by multiple accretionary processes. *Geochimica et Cosmochimica Acta*, 48(5):931–949, 1984.
- [13] E.K. Fallon, S Petersen, R.A. Brooker, and T.B. Scott. Oxidative dissolution of hydrothermal mixed-sulphide ore: An assessment of current knowledge in relation to seafloor massive sulphide mining. *Ore Geology Reviews*, 86: 309–337, 2017.
- [14] Y. Fan, J. Wang, Z. Bai, J. Wang, and H. Wang. Experimental investigation of various inlet section angles in mini-hydrocyclones using particle imaging velocimetry. *Separation and Purification Technology*, 149:156–164, 2015.
- [15] F.J. Fontein, J.G. Van Kooy, and H.A. Leniger. The influence of some variables upon hydrocyclone performance. *British Chemical Engineering*, 7(1):410–420, 1962.
- [16] M. B. Gallagher. Understanding the impact of deep-sea mining, 2019. URL <https://news.mit.edu/2019/understanding-impact-deep-sea-mining-1206>.
- [17] M. Ghodrati, S.B. Kuang, A.B. Yu, A. Vince, G.D. Barnett, and P.J. Barnett. Computational study of the multiphase flow and performance of hydrocyclones: effects of cyclone size and spigot diameter. *Industrial & Engineering Chemistry Research*, 52(45):16019–16031, 2013.
- [18] J.C. Goeree. Drift-flux modeling of hyper-concentrated solid-liquid flows in dredging applications. 1(1):45–51, 2018.
- [19] N. Hall. Drag of a sphere. <https://www.grc.nasa.gov/www/k-12/airplane/dragSphere.html>. (Accessed on 12/21/2020).

- [20] F. He, Y. Zhang, J. Wang, Q. Yang, H. Wang, and Y. Tan. Flow patterns in mini-hydrocyclones with different vortex finder depths. *Chemical Engineering & Technology*, 36(11):1935–1942, 2013.
- [21] J.R. Hein, A. Koschinsky, and T. Kuhn. Deep-ocean polymetallic nodules as a resource for critical materials. *Nature Reviews Earth & Environment*, pages 1–12, 2020.
- [22] R.L.J. Helmons, 2020-2021. Dr.ir. R.L.J. Helmons' consultation provided the information.
- [23] S. Hong, H. Kim, T. Yeu, J. Choi, T. Lee, and J. Lee. Technologies for safe and sustainable mining of deep-seabed minerals. In *Environmental Issues of Deep-Sea Mining*, pages 95–143. Springer, 2019.
- [24] C.Y. Hsu and R.M. Wu. Effect of overflow depth of a hydrocyclone on particle separation. *Drying Technology*, 28(7):916–921, 2010.
- [25] R. Israel and D.E. Rosner. Use of a generalized stokes number to determine the aerodynamic capture efficiency of non-stokesian particles from a compressible gas flow. *Aerosol Science and Technology*, 2(1):45–51, 1982.
- [26] A. Koschinsky, L. Heinrich, K. Boehnke, J.C. Cohrs, T. Markus, M. Shani, P. Singh, K. Smith Stegen, and W. Werner. Deep-sea mining: Interdisciplinary research on potential environmental, legal, economic, and societal implications. *Integrated Environmental Assessment and Management*, 14(6):672–691, 2018.
- [27] A.M. Lang, S. Dasselaar, K. Aasly, and E. Larsen. Blue nodules deliverable report d3.4 report describing the process flow overview. pages 1–23, 2019.
- [28] L.F. Martínez, A.G. Lavín, M.M. Mahamud, and J.L. Bueno. Vortex finder optimum length in hydrocyclone separation. *Chemical Engineering and Processing: Process Intensification*, 47(2):192–199, 2008.
- [29] V. Matoušek. Dredge pumps and slurry transport. 1(1), 2004.
- [30] J.L. Mero. Ocean-floor manganese nodules. *Economic Geology*, 57(5):747–767, 1962.
- [31] D. Michaud. Hydrocyclone working principle. <https://www.911metallurgist.com/blog/hydrocyclone-workingprinciple>, August 2015.
- [32] K.A. Miller, K.F. Thompson, P. Johnston, and D. Santillo. An overview of seabed mining including the current state of development, environmental impacts, and knowledge gaps. *Frontiers in Marine Science*, 4:418, 2018.
- [33] Naeff. Brekingsindex, 2021. URL <https://www.naeff.nl/nl/kunststoff-encyclopedie/brekingsindex>.
- [34] M. Narasimha, S. Rajendran, and P.K. Banerjee. Cfd modelling of hydrocyclone prediction of cut size. *International Journal of Mineral Processing*, 75:53–68, 01 2005. doi: 10.1016/j.minpro.2004.04.008.
- [35] United Nations. Preamble to the united nations convention on the law of the sea. [https://www.un.org/depts/los/convention\\_agreements/texts/unclos/part5.htm](https://www.un.org/depts/los/convention_agreements/texts/unclos/part5.htm).
- [36] L. Ni, J. Tian, and J. Zhao. Experimental study of the effect of underflow pipe diameter on separation performance of a novel de-foulant hydrocyclone with continuous underflow and reflux function. *Separation and Purification Technology*, 171:270–279, 2016.
- [37] L. Ni, J. Tian, and J. Zhao. Feasibility of a novel de-foulant hydrocyclone with reflux for flushing away foulant continuously. *Applied Thermal Engineering*, 103:695–704, 2016.
- [38] L. Ni, J. Tian, and J. Zhao. Experimental study of the relationship between separation performance and lengths of vortex finder of a novel de-foulant hydrocyclone with continuous underflow and reflux function. *Separation Science and Technology*, 52(1):142–154, 2017.
- [39] L. Ni, J. Tian, T. Song, Y. Jong, and J. Zhao. Optimizing geometric parameters in hydrocyclones for enhanced separations: a review and perspective. *Separation & Purification Reviews*, 48(1):30–51, 2019.
- [40] O. Ozcan. Performance comparison of a hydrocyclone and crossflow separator—a plant study. *Separation Science and Technology*, 55(4):799–810, 2020.
- [41] N.M. Ridgway. Temperature and salinity of sea water at the ocean floor in the new zealand region. *New Zealand Journal of Marine and Freshwater Research*, 1(1):57–72, 2010.
- [42] K. Rietema and Shell Internationale Research Maatschappij. Performance and design of hydrocyclones—i: General considerations. *Chemical Engineering Science*, 15(3-4):1–302, 1961.

- [43] C. Roche and S. Bice. Anticipating social and community impacts of deep sea mining. *Deep Sea Minerals and the Green Economy, Secretariat of the Pacific Community, Suva*, pages 59–80, 2013.
- [44] H. Shah, A.K. Majumder, and J.P. Barnwal. Development of water split model for a 76 mm hydrocyclone. *Minerals engineering*, 19(1):102–104, 2006.
- [45] R. Sharma. *Deep-sea mining: Resource potential, technical and environmental considerations*. Springer, 2017.
- [46] D.O. Silva, L.G.M. Vieira, and M.A.S. Barrozo. Optimization of design and performance of solid-liquid separators: a thickener hydrocyclone. *Chemical Engineering & Technology*, 38(2):319–326, 2015.
- [47] N.K.G. Silva, D.O. Silva, L.G.M. Vieira, and M.A.S. Barrozo. Effects of underflow diameter and vortex finder length on the performance of a newly designed filtering hydrocyclone. *Powder Technology*, 286:305–310, 2015.
- [48] L. Svarovsky. *Hydrocyclones*. Technomic Publishing Co: London., 1984.
- [49] L. Svarovsky. *Solid-liquid separation*. Elsevier, 2000.
- [50] B. Tang, Y. Xu, X. Song, Z. Sun, and J. Yu. Numerical study on the relationship between high sharpness and configurations of the vortex finder of a hydrocyclone by central composite design. *Chemical Engineering Journal*, 278:504–516, 2015.
- [51] S. Tarleton and R. Wakeman. *Solid/liquid separation: equipment selection and process design*. Elsevier, 2006.
- [52] Engineering ToolBox. Water - dynamic and kinematic viscosity. [https://www.engineeringtoolbox.com/water-dynamic-kinematic-viscosity-d\\_596.html](https://www.engineeringtoolbox.com/water-dynamic-kinematic-viscosity-d_596.html), 2004.
- [53] The Pew Charitable trusts. Deep-sea mining: The basics. [https://www.pewtrusts.org/-/media/assets/2018/07/deep-seabed-mining-basics\\_18-06-v3.pdf](https://www.pewtrusts.org/-/media/assets/2018/07/deep-seabed-mining-basics_18-06-v3.pdf), 2021.
- [54] C. Van Rhee. Lecture notes oe44045. 2.1(1), 2018.
- [55] J.M. Van Wijk. *Vertical hydraulic transport for deep sea mining: A study into flow assurance*. PhD thesis, Technical University of Delft, 2016.
- [56] L.G.M. Vieira, B.C. Silvério, J.J.R. Damasceno, and M.A.S. Barrozo. Performance of hydrocyclones with different geometries. *The Canadian Journal of Chemical Engineering*, 89(4):655–662, 2011.
- [57] L.G.M. Vieira, D. O. Silva, and M.A.S. Barrozo. Effect of inlet diameter on the performance of a filtering hydrocyclone separator, 2016. URL <https://onlinelibrary.wiley.com/doi/full/10.1002/ceat.201500724>.
- [58] L.G.M. Vieira, D.O. Silva, and M.A.S. Barrozo. Effect of inlet diameter on the performance of a filtering hydrocyclone separator. *Chemical Engineering & Technology*, 39(8):1406–1412, 2016.
- [59] U. Von Stackelberg. Growth history of manganese nodules and crusts of the peru basin. *Geological Society, London, Special Publications*, 119(1):153–176, 1997.
- [60] R.J. Wakeman. Classifiers. <http://www.thermopedia.com/content/635/>.
- [61] B. Wang and A.B. Yu. Numerical study of the gas-liquid-solid flow in hydrocyclones with different configuration of vortex finder. *Chemical Engineering Journal*, 135(1-2):33–42, 2008.
- [62] C.C. Wang and R.M. Wu. Experimental and simulation of a novel hydrocyclone-tubular membrane as overflow pipe. *Separation and Purification Technology*, 198:60–67, 2018.
- [63] J. Wright and A. Colling. Density of seawater and pressure. <https://www.britannica.com/science/seawater/Density-of-seawater-and-pressure>, 2007.
- [64] Q. Yang, H. Wang, Y. Liu, and Z. Li. Solid/liquid separation performance of hydrocyclones with different cone combinations. *Separation and Purification Technology*, 74(3):271–279, 2010.

# A

## Setup components

In this section the individual parts from the setup, that are worth mentioning, are shown. Figures A.2 & A.3 show the numbers of the components.



Figure A.1: Side view of setup in laboratory

### Side view

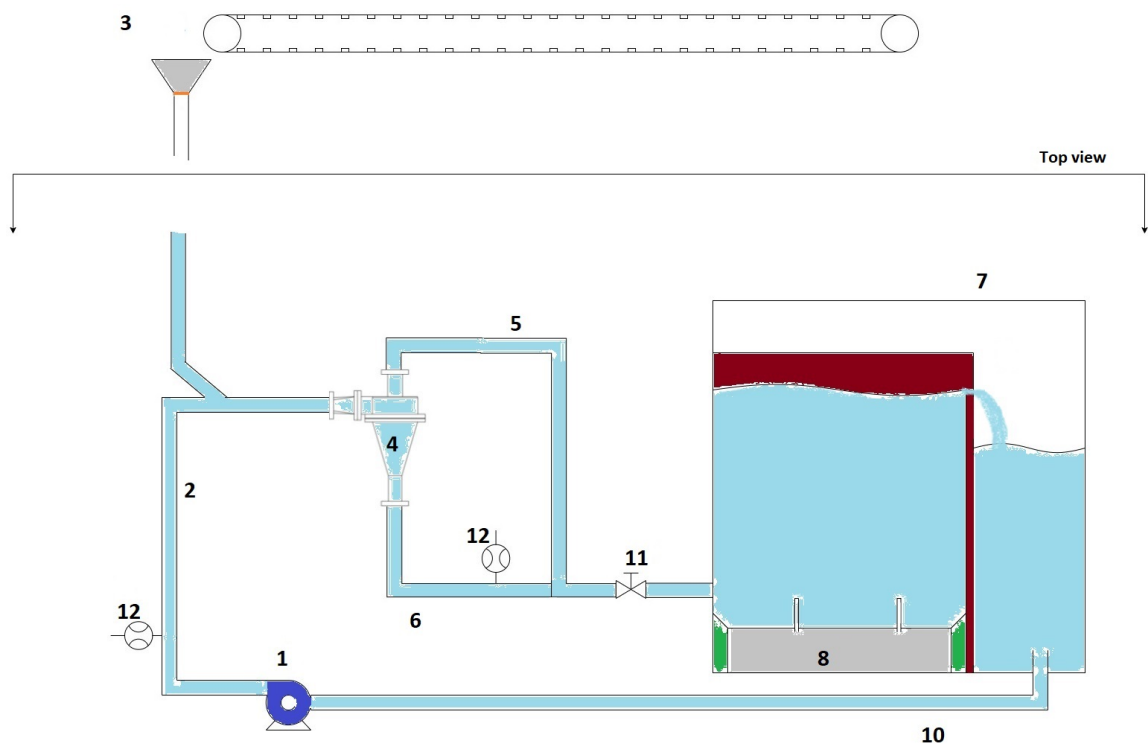


Figure A.2: Side view of the experimental setup

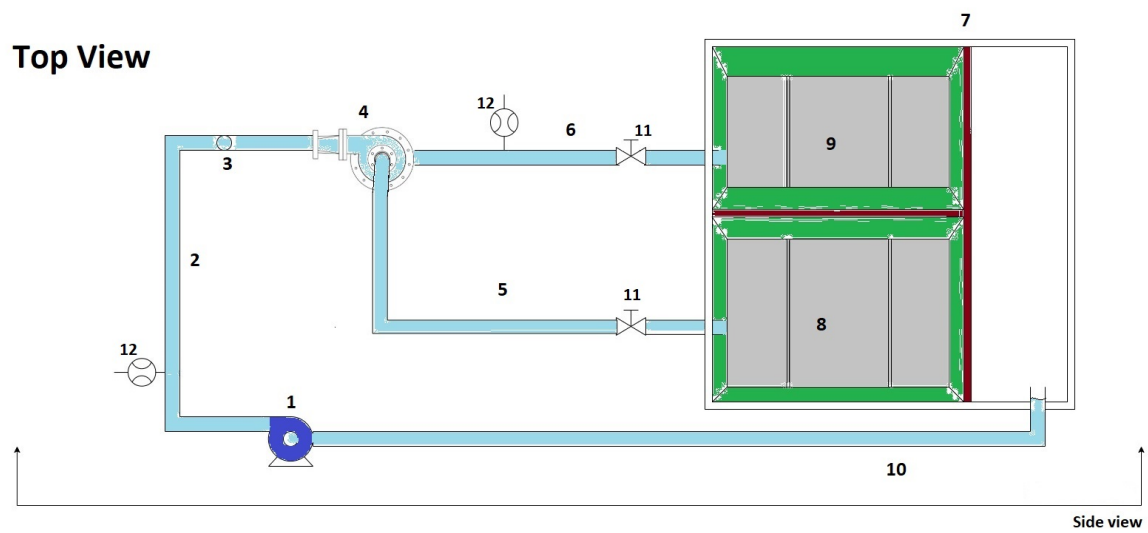


Figure A.3: Top view of the experimental setup

# 1. Centrifugal pump



Figure A.4: Topside of the centrifugal pump



Figure A.5: Centrifugal pump



Figure A.6: Frequency converter to control pump RPM

The centrifugal pump is controlled by a frequency converter shown in figure A.6.

### 3. Hopper system

#### Conveyor belt

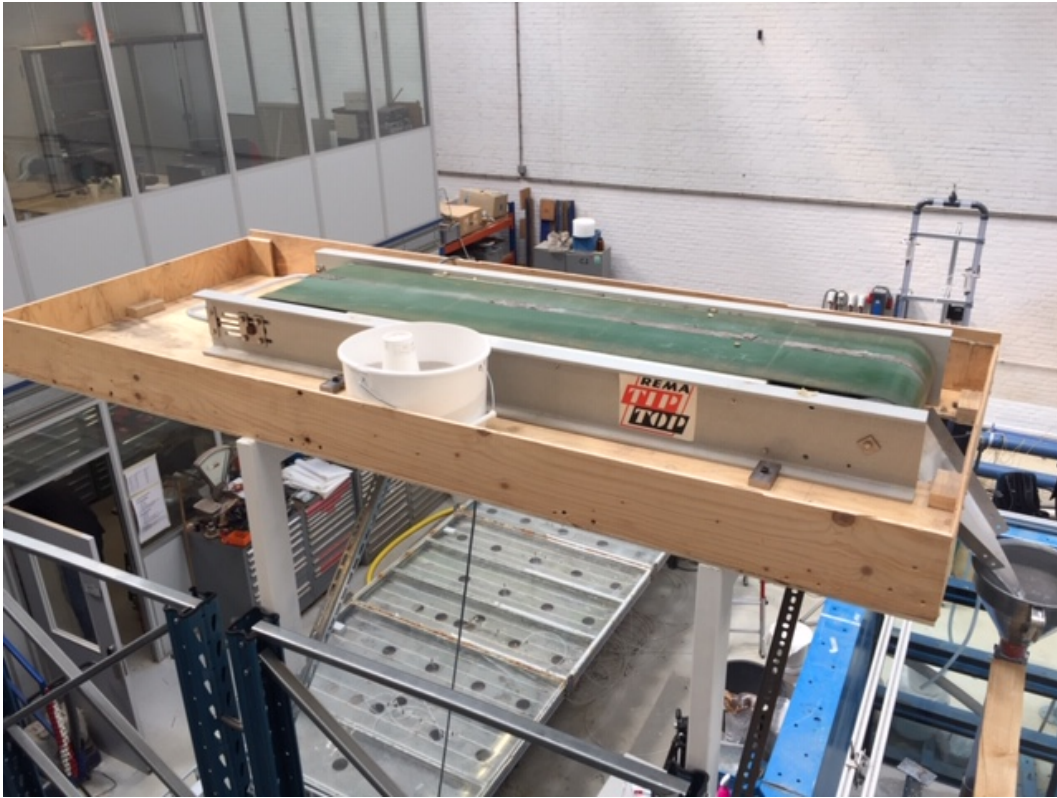


Figure A.7: Empty conveyor belt in position



Figure A.8: Partly filled conveyor belt in position

## Hopper



Figure A.9: Hopper used for guiding particles into stream

## 4. Cyclone separator model

The design of the cyclone separator is extensive. Therefore, all drawings are shown here.

### Topside of the model cyclone

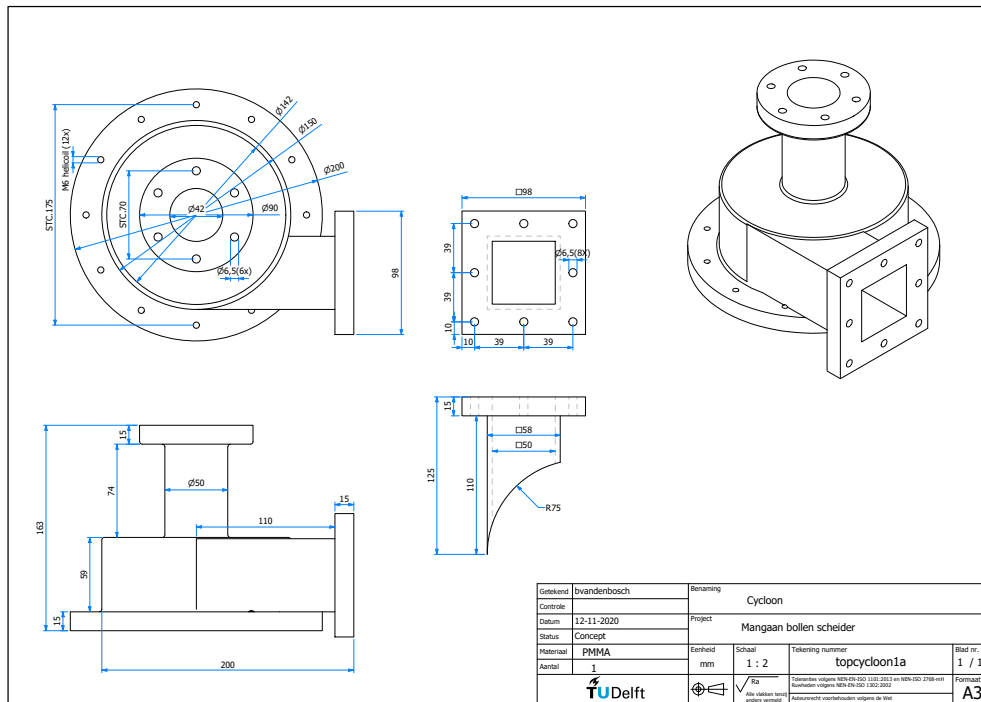


Figure A.10: Schematic design cyclone topside

### Original conical section

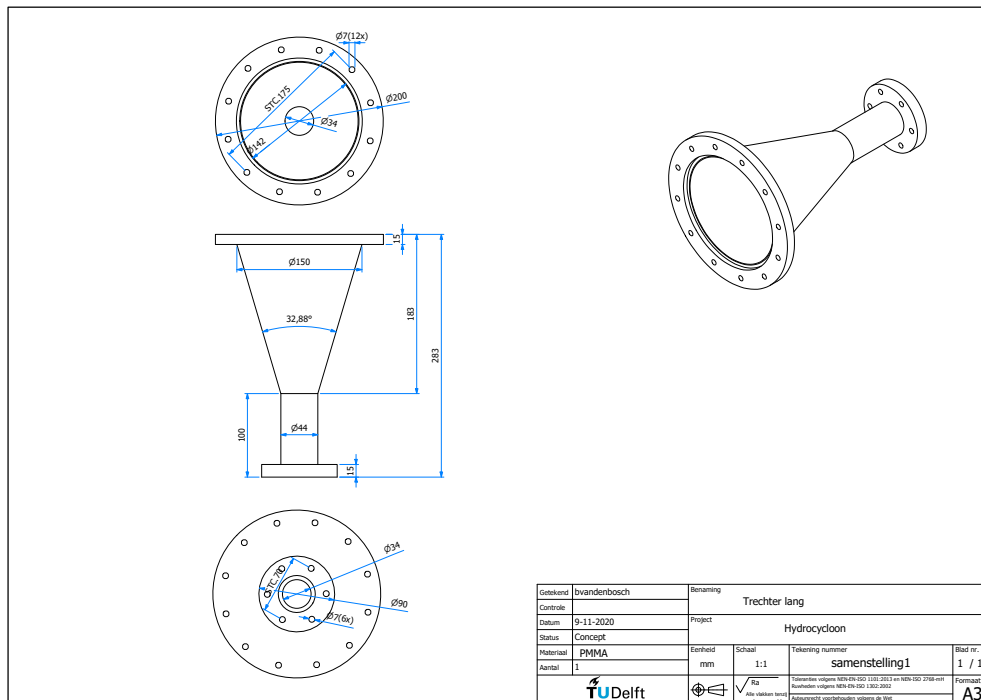


Figure A.11: Schematic design conical section

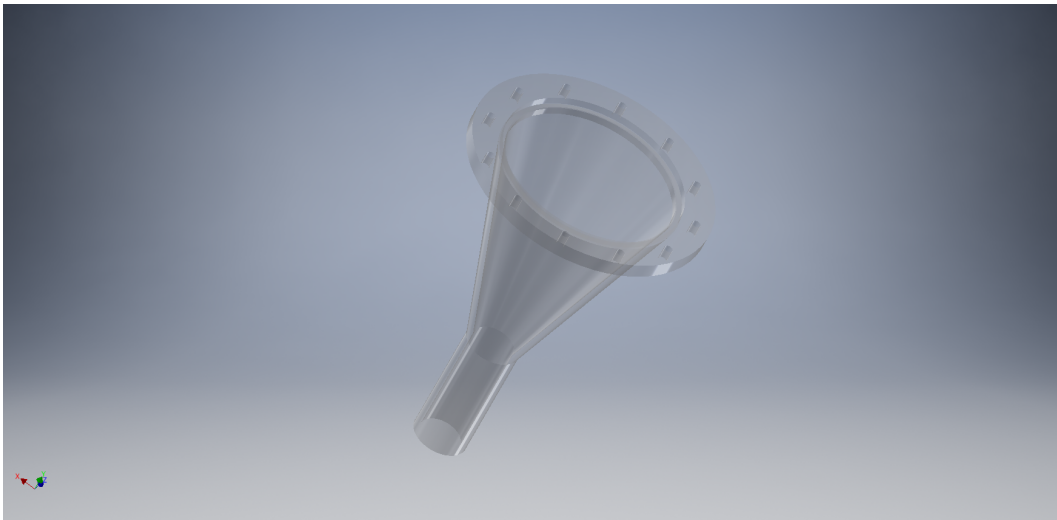


Figure A.12: 3D illustration conical section

### Large angle conical section

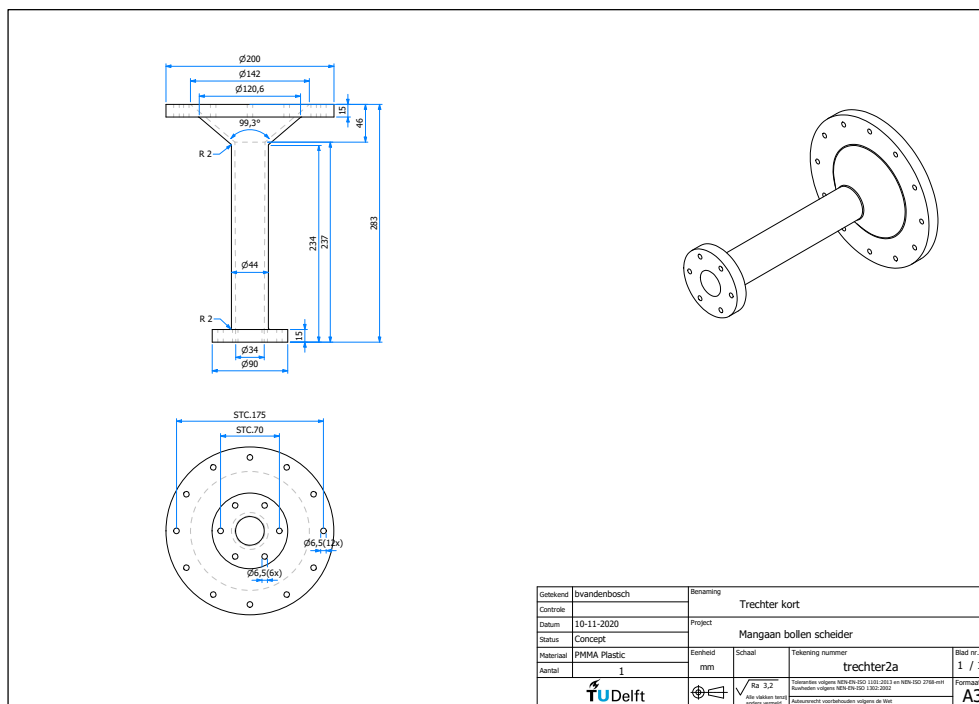


Figure A.13: Schematic design of Large angle conical section



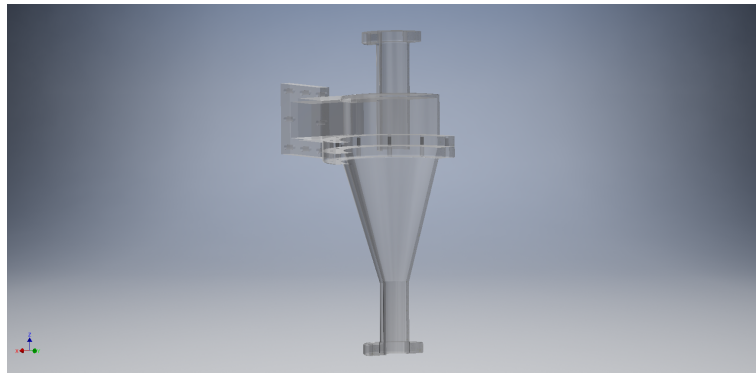
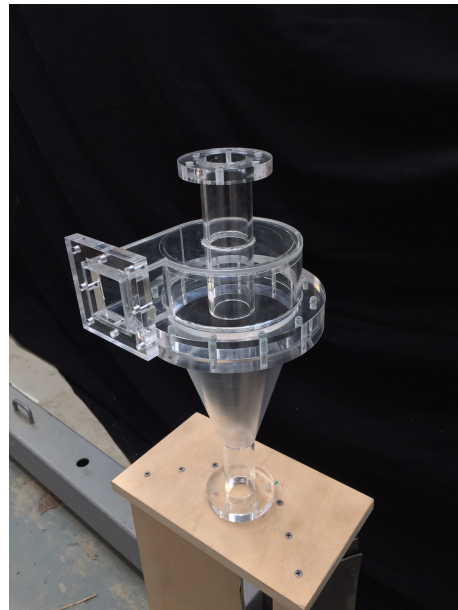


Figure A.16: 3D illustration assembled cyclone



(a) Front view cyclone



(b) Side view cyclone

Figure A.17: Pictures assembled cyclone

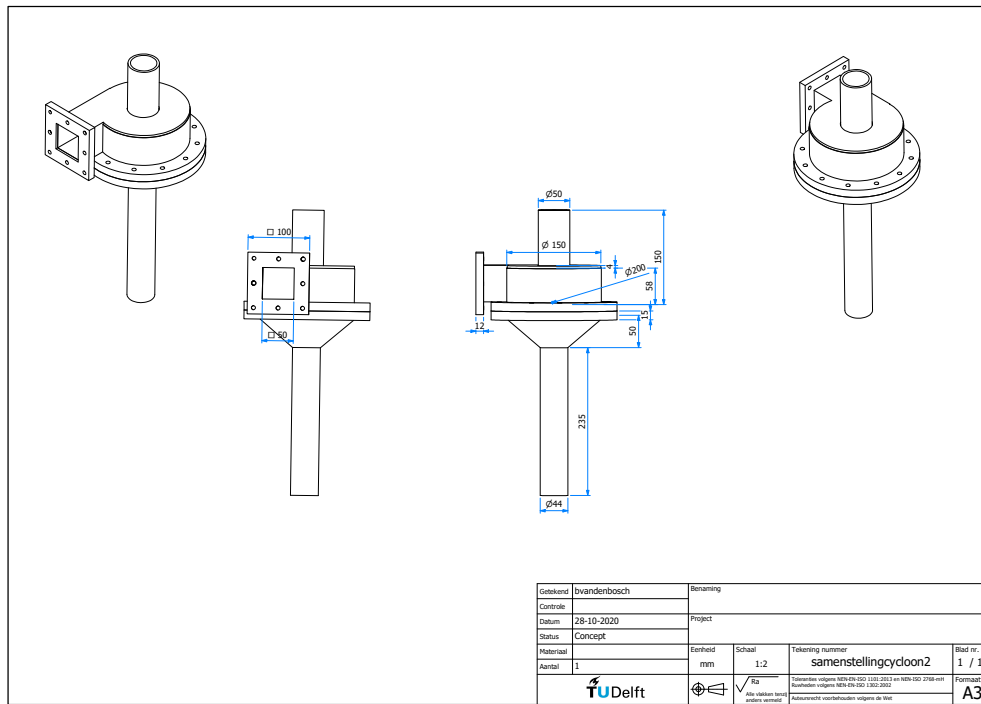


Figure A.18: Schematic design assembled large angle cyclone

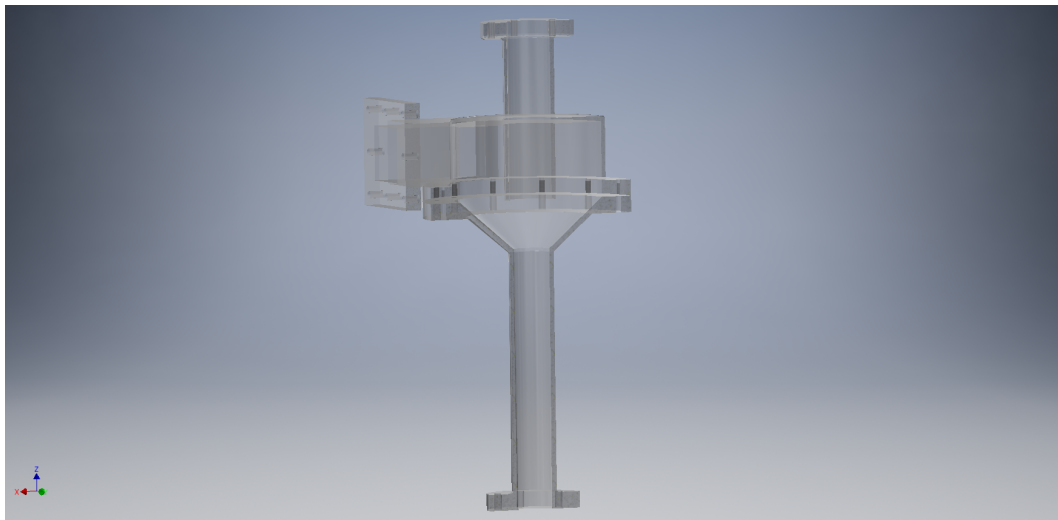


Figure A.19: 3D illustration of assembled cyclone with large conical angle



Figure A.20: Installed cyclone

**3D printed transition pieces** Individual 3D printed parts are illustrated below. These parts were needed to connect the separator to the rest of the setup.

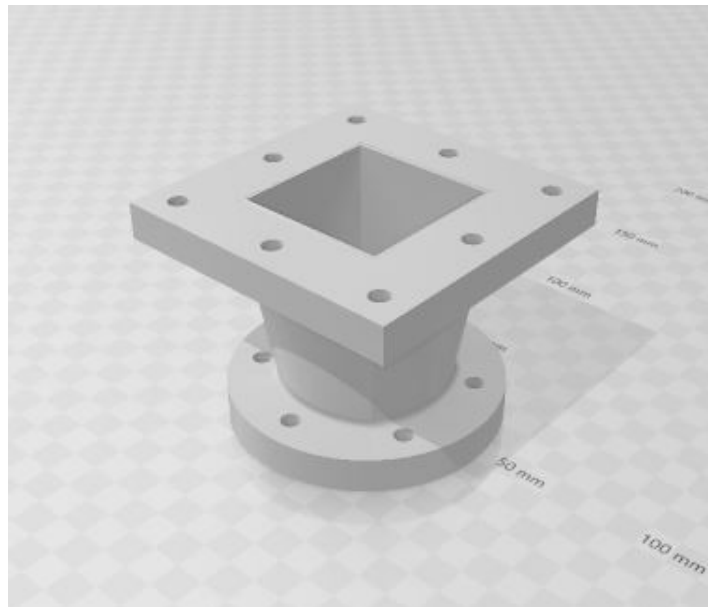
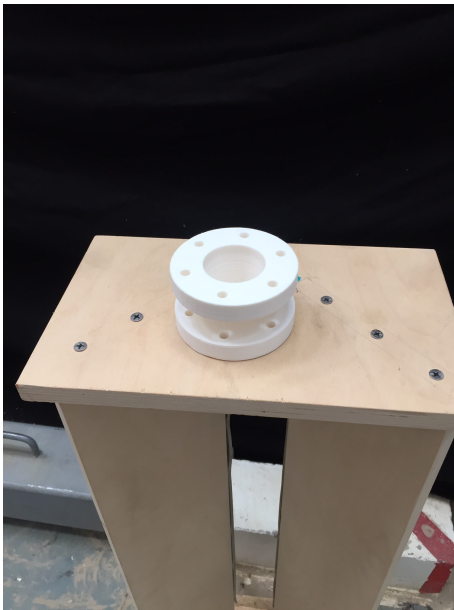
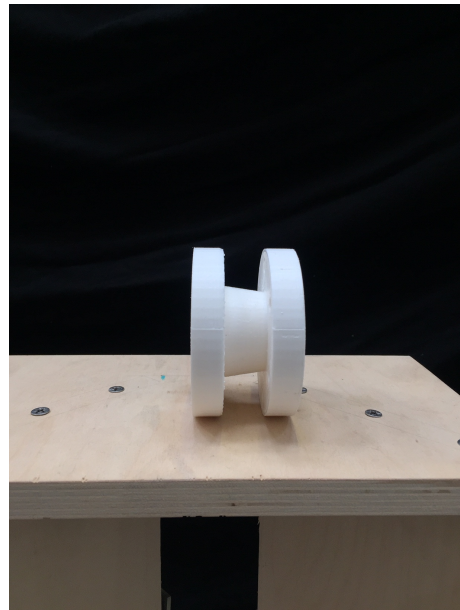


Figure A.21: 3D printed inlet transition piece design



(a) Top view underflow to pipe transition piece



(b) Side view underflow to pipe transition piece

Figure A.22: Photo's 3D printed transition piece for underflow to pipe

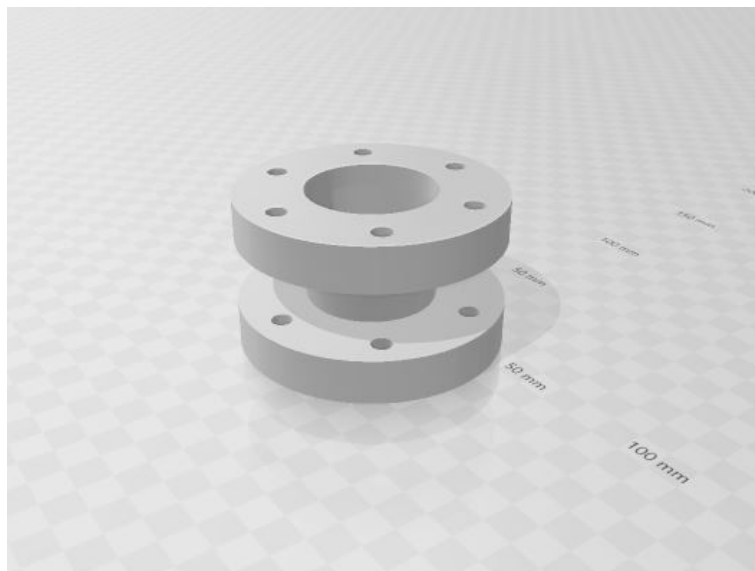
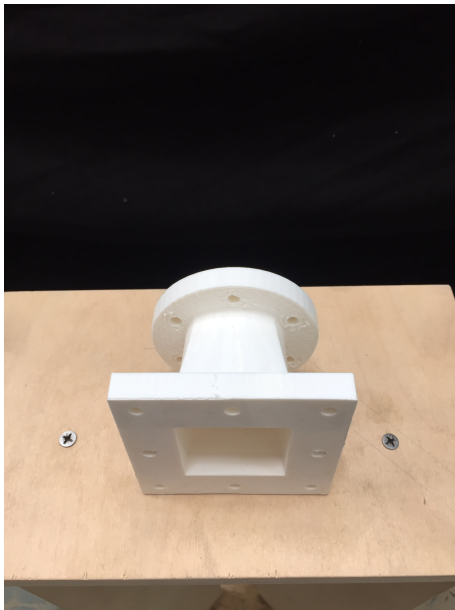
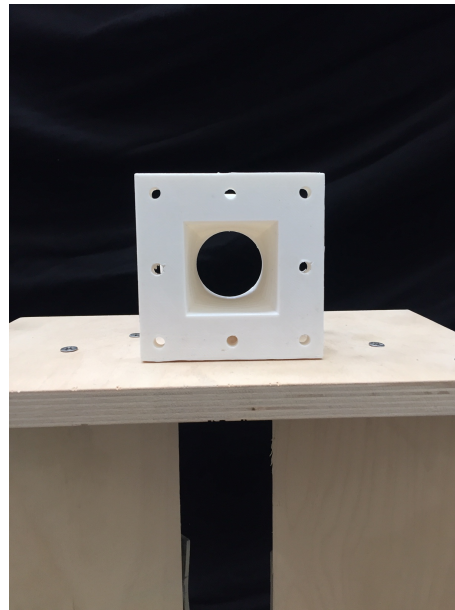


Figure A.23: 3D printed underflow to pipe transition piece



(a) Top view inlet transition piece



(b) View through inlet transition piece

Figure A.24: Photo's 3D printed inlet transition piece

## 7. Settling tank



Figure A.25: Empty settling tank



Figure A.26: Operating settling tank

## 8. Large measurement container



Figure A.27: Large measuring tank

## 9. Small measurement container



Figure A.28: Small measuring tank

## 11. Valves



Figure A.29: Valves used for altering split ratio of the cyclone.

## 12. Flow meters



Figure A.30: Flow meter attached to underflow



Figure A.31: Flow meter attached to the inflow

## Other components

Figure A.32 shows the scale used for the density tests and the weight measurements to determine the partition of the particles.



Figure A.32: Scale used for mass partition measurements

Figure A.33 illustrates the drill used to get the smaller particles in suspension before adding the slurry into the hopper.



Figure A.33: Drill used for mixing suspension

Figure A.34 shows the light panels used to enhance the video footage. This light panel was located next to the cyclone.



Figure A.34: Light panel used to illuminate the cyclone

The valves that were used for emergency drainage or to empty the setup completely after experimentation are shown in figure A.35. These valves open much faster than those that control the split ratio, but are less accurate in making a specific desired flow.



Figure A.35: Ball valves

### A.1. Suggested bypass

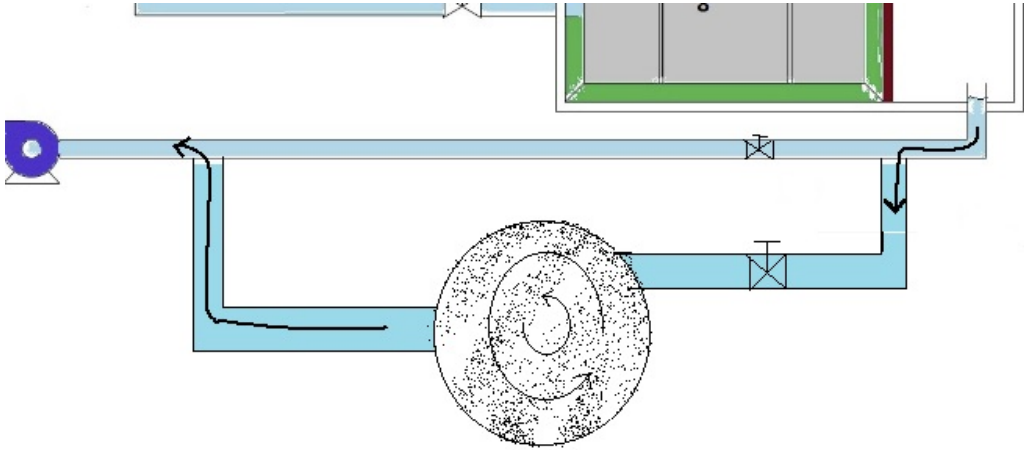


Figure A.36: Suggested redirected flow

# B

## Particle tests

### B.1. Separation into compact fractions

The available particles have been sorted and measured in order to determine the particle properties and their timescale ratios.

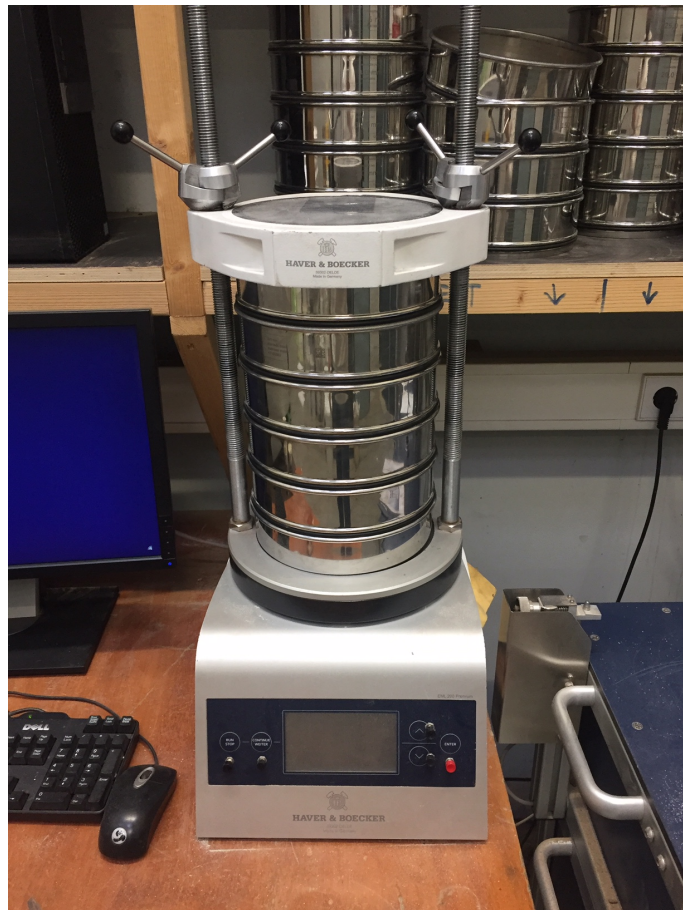


Figure B.1: Particle sorting device



Figure B.2: Sorted particle fractions

## B.2. Density tests



Figure B.3: Sand used for density tests



Figure B.4: Scale used density tests

### B.3. Settling tests

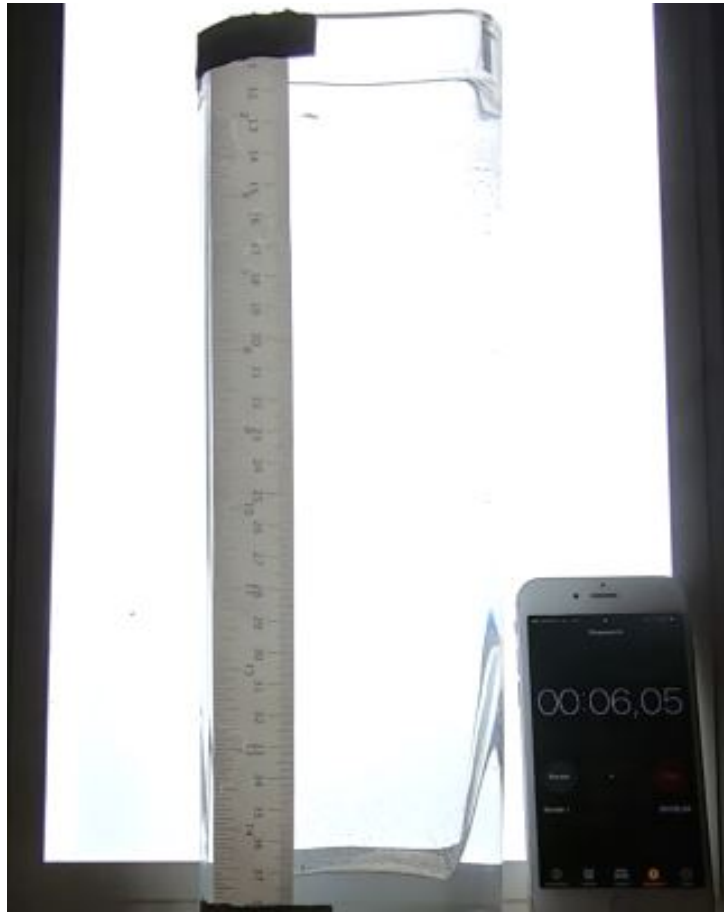


Figure B.5: Tank and timer used for settling tests

### B.4. Particles properties

$d_p$ range ( $d_0 - d_{100}$ ) [mm]	$\frac{d_0 + d_{100}}{2}$ [mm]	$\rho_s$ [ $kg/m^3$ ]	$w_0$ [m/s]	$w_{0c}$ [m/s]	$Re_p$	$Stk$	$r$
0.005 - 0.02	0.013	2650	0.0005	0.0007	0.01	0.34	0.001
0.040-0.070	0.055	2650	0.0021	0.0030	0.16	3.10	0.02
0.065-0.105	0.085	2650	0.0051	0.0073	0.62	5.96	0.07
0.18-0.25	0.215	2650	0.0327	0.0465	10.0	24.0	0.72
0.25-0.35	0.300	2650	0.0424	0.0603	18.1	39.5	1.12
0.35-0.5	0.425	2650	0.0634	0.0902	38.3	66.6	1.83
0.5-0.71	0.6050	2650	0.0787	0.119	67.7	114	2.50
0.71-0.8	0.755	2650	0.1034	0.1471	111	158	3.15
0.8-1.4	1.10	2650	0.1134	0.1613	177	277	3.78
1.4-2.0	1.70	2650	0.1886	0.2682	456	533	4.97
2.0-2.4	2.20	2650	0.2124	0.3021	664	785	5.38
4.0-6.0.	5.00	2650	0.4810	0.6841	3420	2689	6.63
8.0-12.0	10.0	2650	0.6520	0.9273	9273	7605	6.63

Table B.1: Particle properties and timescale ratios from sorted particles

# C

## Operational protocol

This operational protocol will act as a guide to prepare, operate and finishing up the setup in order to have successful experiments and get consistent measurements.

### C.1. Preparation

Before an experiment can take place, the setup needs to be clean, filled to the correct water level and it should not lose water. This can be accomplished by following the steps below.

1. Clean the setup with vacuum and water hose.
2. Let out all remaining water.
3. Close all the exits.
4. Open all valves that regulate water stream through the system.
5. Fill up with water until the required water level in the settling tank is reached.
6. Check for leakage and fix any problems.
7. Let out all the remaining air. (Creating a small flow can help.)

### C.2. Operation

Depending on the particle size, a different approach of operating the setup needs to be chosen. Large particles cannot be guided through the pump and are inserted through the hopper with the use of the conveyor belt. Smaller particles can flow through the pump and settle slowly in the hopper system. Therefore, a slurry can be submitted in the hopper or small particles can be mixed in the buffer.

#### C.2.1. Large particles

1. Turn power on.
2. Make sure the conveyor belt is not moving.
3. Turn on laptop and check flow meters.
4. Clear conveyor belt
5. Add required weight for the wanted concentration on the conveyor belt. The excel file can be used to determine the required weight.
6. Turn on pump (max 1140 RPM). And check leakage and other occurrences. Fix problems before filming and starting the experiment.
7. Check and start camera. Make sure the experiment number is visible.
8. Remove the created vortex from the cyclone by cutting of the underflow temporarily.
9. Start experiment by turning on conveyor.
10. Carry out experiments, while watching the setup. Look out for blockage of pipes, and hopper.

11. Turn off conveyor belt
12. When experiment is finished, first lower pump power before stopping it completely. Otherwise a reverse current occurs due to water level differences in settling tank.

### C.2.2. Small particles

1. Turn power on.
2. Make sure the conveyor belt is not moving.
3. Turn on laptop and check flow meters.
4. Clear conveyor belt
5. Make the required slurry in a large bucket. The excel file can be used to determine the required weight.
6. Turn on pump (max 1140 RPM). And check leakage and other occurrences. Fix problems before filming and starting the experiment.
7. Check and start camera. Make sure the experiment number is visible.
8. Remove the created vortex from the cyclone by cutting of the underflow temporarily.
9. Start experiment by adding slurry to the hopper. Or add slurry to the buffer section.
10. Carry out experiments, while watching the setup. Look out for blockage of pipes, and hopper.
11. Watch the underflow and overflow section of the particles are not overflowing into the buffer section. Preferably the particles are captured in their designed containers.
12. When experiment is finished, first lower pump power before stopping it completely. Otherwise a reverse current occurs due to water level differences in settling tank.

### C.3. After operation

1. Turn off camera
2. Turn off power
3. Let particles settle in the tanks.
4. Carry out measurements.
5. Empty hopper system
6. Empty setup.
7. Clean setup. Sometimes the setup needs to be filled a couple of times to remove all small particles.
8. Disconnect from power and remove laptop.

#### C.3.1. Other occurrences

**Blockage in pipes** This can happen when too much particles are transported through the system. Or when the velocity through the pipes is too low. WATCH OUT DURING EXPERIMENTS FOR ACCUMULATION OF PARTICLES IN PIPES. Prevention is always better than solving the blockage. The following can be done when the pipe is blocked:

1. Remove some of the water in the buffer tank. This will enhance the difference in water pressure for both sides.
2. Close valve in other direction to force water through the blocked section.
3. Start and stop the pump several times while shaking the pipe softly. The pump will push the particles toward the settling tank, and when the pump is stopped, the difference in water level will push the water in the other direction in the pipe.

#### **Blockage of hopper**

Stop conveyor immediately. When small particles create a plug, pour some water down the hopper. Adjusting the pump power helps unplugging the system. If large particles block the hopper, guide them through the pipe by hand.

## C.4. Measurement protocol

When the particle and water densities are known and the empty and full container weight are known, the weight of collected particles can easily be determined. First the volume of the containers is precisely measured by subtracting the empty container weight from the with water filled container weight and dividing it by the water density.

$$V_{container} = \frac{W_w - W_{empty}}{\rho_w} \quad (C.1)$$

When exact volume of the container is known, the density of the mixture inside the containers can be obtained by weighing the containers with the mixture and dividing it by the volume.

$$\rho_{mix} = \frac{W_{mix}}{V_{container}} \quad (C.2)$$

This leads to the following equation for the total particle weight per container:

$$W_p = W_{mix} \frac{\rho_{mix} - \rho_w}{\rho_p - \rho_w} \quad (C.3)$$

Both containers need to be measured and compared to the total amount added to the flow. If the total amount collected by the containers is not comparable to the total amount added, the measurements are inaccurate and the gathered data is incorrect.

Besides measurement data, visual data is also collected. The transparent model cyclone is filmed using a high speed camera. This way all separation process inside the cyclone can be investigated. If remarkable findings are observed, the video footage helps understanding the phenomena.